PNL-9003
UC-603

Comparison of Surface Energy Fluxes with Satellite-Derived Surface Energy Flux Estimates from a Shrub-Steppe

A dissertation submitted in partial fulfillment of the requirements for the degree of Doctor of Philosophy

University of Washington

R. R. Kirkham

December 1993

Prepared for
the U.S. Department of Energy
under Contract DE-AC06-76RLO 1830

Pacific Northwest Laboratory
Richland, Washington 99352

MASTER

DISTRIBUTION OF THIS DOCUMENT IS UNLIMITED

University of Washington

Abstract

Comparison of Surface Energy Fluxes with Satellite-Derived
Surface Energy Flux Estimates from a Shrub-Steppe

by Randy R. Kirkham

Chairperson of the Supervisor Committee: Professor L. J. Fritschen
Department of Forest Resources

This thesis relates the components of the surface energy balance (i.e., net radiation, sensible and latent heat flux densities, soil heat flow) to remotely sensed data for native vegetation in a semi-arid environment. Thermatic mapper data from Landsat 4 and 5 were used to estimate net radiation, sensible heat flux (H), and vegetation amount. Several sources of ground truth were employed. They included soil water balance using the neutron thermalization method and weighing lysimeters, and the measurement of energy fluxes with the Bowen ratio energy balance (BREB) technique.

Sensible and latent heat flux were measured at four sites on the U.S. Department of Energy's Hanford Site using a weighing lysimeter and/or BREB stations. The objective was to calibrate an aerodynamic transport equation that related H to radiant surface temperature. The transport equation was then used with Landsat thermal data to generate estimates of H and compare these estimates against H values obtained with BREB/lysimeters at the time of overflight.

Landsat and surface meteorologic data were used to estimate the radiation budget terms at the surface. Landsat estimates of short-wave radiation reflected from the surface correlate well with reflected radiation measured using inverted Eppley pyranometers. Correlation of net radiation estimates determined from satellite data, pyranometer, air temperature, and vapor pressure compared to net radiometer values obtained at time of overflight were excellent for a single image, but decrease for multiple images.

Soil heat flux, G_T, is a major component of the energy balance in arid systems and G_T generally decreases as vegetation cover increases. Normalized difference vegetation index (NDVI) values generated from Landsat thermatic mapper data were representative of field observations of the presence of green vegetation, but it was not possible to determine a single relationship between NDVI and G_T for all sites.

Data collected at two vegetated sites were used to calibrate the resistance term of a H transport equation for the two surface types. Data used to calibrate the equation were restricted to approximate Landsat overflight time. Radiant temperature was measured with infrared thermometers. This equation was then used with surface temperatures derived from Landsat overflights to estimate H. The H density estimates were similar to H density values determined at the time of overflight with BREB stations, but exhibited significant scatter.

Comparable evapotranspiration measurements were obtained with three independent methods. These evapotranspiration data sets were then used to calibrate a sensible heat transport equation with approximately the same amount of scatter as reported by other researchers. The resultant equations were used with site-specific pixel values from three satellite scenes to predict H. These satellite-derived estimates of H were similar in magnitude to the BREB estimates but poorly correlated. This approach was not accurate enough to detect the difference between sites. This lack of sensitivity is in part caused by the highly variable soil heat flux term. Soil heat flux could not be predicted from the available Landsat spectral bands.

TABLE OF CONTENTS

Page

List of Figures iii

List of Tables vi

Glossary of Symbols vii

Glossary of Terms viii

1.0 Introduction 1

2.0 Research Approach 5

3.0 Evaportranspiration Measurement Methodology 7
3.1 Hydrologic Category 9
3.2 Surface Atmospheric Flux Measurement 10

4.0 Modeling Evapotranspiration 13

5.0 Remote Sensing Methods 17

6.0 Experimental Design and Test Methods 23
6.1 Hanford Site Geology and Climate 23
6.2 Study Areas 24
6.2.1 Arid Lands Ecology Reserve Lysimeter and Water Balance Plots 24
6.2.2 Grass 300 Site 28
6.2.3 Buried Waste Test Facility 28
6.2.4 Field Lysimeter Test Facility 29
6.3 Lysimeter Design 29
6.4 Bowen Ratio 30
6.5 Satellite Data 31

7.0 Results 37
7.1 Direct Measurements of Energy Balance Components 38
7.2 Remote Estimates of Radiation Terms 43
7.2.1 Remote Estimates of $R_S\uparrow$ 43
7.2.2 Remote Estimates of $R_L\uparrow$ 46
7.2.3 Remote Estimates of Incoming Long-Wave Radiation 50
7.2.4 Field and Remote Estimates of Net Radiation 50
7.3 Normalized Difference Vegetation Index as a Predictor of Soil Heat Flux 57
7.4 Development of Resistance Term for Sensible Heat Transport 66
7.5 Comparison of Remote Energy Balance Results with Measured Values 72

8.0 Conclusions and Recommendations 85

Bibliography 89

Appendix A: Neutron Probe Sample Data Set and Calculations 97

Appendix B: Calculations of Sun Angle, Atmospheric Corrections to Landsat, NDVI, $R_S\uparrow$, and R_N 101

Appendix C: Calculations of Aerodynamic Resistance for Bunchgrass in 1988 109

Appendix D: Calculations of Aerodynamic Resistance for Sagebrush in 1988 117

LIST OF FIGURES

Number		*Page*
3.1	Cross Section of Typical Hanford Site Grass and Sagebrush Communities	8
6.1	a) Growing Degree Days for 1986 to 1990, b) Soil Profile Moisture at the G300 Site for 1986 to 1990	25
6.2	Landsat Subscene from 8-May-89 with Bands 4, 3, 2 Displayed as Red, Green, and Blue	26
6.3	Simulated False Color IR for Landsat Subscenes of the Hanford Site, a) 8-May-86, b) 11-May-87, c) 8-May-89, d) 1-Jun-89, e) 28-Feb-90, f) 1-Apr-90	33
6.4	Digital Elevation Map and Portion of USGS Snively Basin, Washington, 7.5 Quadrangle of the Hanford Site	35
7.1	Lysimeter Total Storage Values for 1987 Through 1990	39
7.2	Lysimeter and BREB Latent Heat Flux Values, and Lysimeter Weight for the Bunchgrass Site for April 19-21, 1988	41
7.3	Lysimeter and BREB Latent Heat Flux Values, and Lysimeter Weight for the Sagebrush Site for April 19-21, 1988	42
7.4	Landsat-Based Estimates and Measured Short-Wave Reflected Radiation for 8-May-89 and 1-Jun-89 Overflights	44
7.5	Landsat Bands 2, 3, 4, 5, 7 Combined to Estimate Reflected Short-Wave Radiation for Six Dates	45
7.6	Estimated $R_L\uparrow$ from Band 6 of Landsat Images for a) 8-May-86, b) 11-May-87, c) 8-May-89, d) 1-Jun-89, e) 28-Feb-90 not shown, f) 1-Apr-90	48
7.7	Bunchgrass and Sagebrush Site View by Landsat Thermal Band Subset 8-May-87 and Aircraft Daedalus Thermal Band	49
7.8	Measured and Estimated Incoming Long-Wave Radiation for the G300 Site on April 7, 10, and 21, 1988	51
7.9	Diurnal Air Temperature Cycle for Four BREB Systems on 8-May-89	52

7.10 Comparison of Air Temperatures Between a) Sagebrush and Bunchgrass, b) Bunchgrass and G300 Sites, April 1988 53

7.11 Incoming Short-Wave Radiation Compared to Net Radiation and the Estimate of Net Radiation Versus the Net Radiation for 1987 and 1988 54

7.12 Net Radiometer Values from Five Sites on 8-May-89 and 1-Jun-89 Compared to the Sum of Short- and Long-Wave Radiation from Landsat 56

7.13 Net Radiation for Lower Snively, Bunchgrass, Sagebrush and G300 at 15-min Intervals During 8-May-89 and 1-Jun-89 58

7.14 Estimate of R_N for 8-May-89 and 1-Jun-89 Using Landsat and Limited Ground-Station Measurements 59

7.15 NDVI Calculated with Four Different DN Treatments for Seven Field Sites on 8-May-89 and 1-Jun-89 61

7.16 Soil Heat Flux Density, 0-5 cm Storage and Their Sum for Four Sites on 8-May-89. 63

7.17 NDVI from Landsat Data Versus the Ratio of Soil Heat Flux to Net Radiation for 1986, 1987, and 1989 Data 65

7.18 NDVI Calculated from Reflectance Values for Six Subscenes of the Hanford Site 67

7.19 Weight Changes in Bunchgrass and Sagebrush Lysimeters Caused by Evapotranspiration and Precipitation During the Calibration Period in April 1988 69

7.20 Resistance Equation Used to Solve Plant Height and Example Plot with Varying Wind Speed and Temperature Difference 70

7.21 Resistance Equation Used to Solve for λ and Additional Fitted Term and Surface Plot with Varying Wind Speed and Temperature Difference 71

7.22 Estimated Sensible Heat Flux for Bunchgrass, 1988 73

7.23 Estimated Sensible Heat Transport for Sagebrush, 1988 74

7.24 Energy Balance for Bunchgrass Site on 8-May-89 and 1-Jun-89 75

7.25 Energy Balance for Sagebrush on 8-May-89 and 1-Jun-89 77

7.26 Energy Balance at Lower Snively on 8-May-89 and 1-Jun-89 78

7.27 Energy Balance at the G300 Site and Buried Waste Test Facility on 8-May-89 and 1-Jun-89 79

7.28 Sensible Heat Flux Density Determined with Landsat and Average Values of Incoming Short- and Long-Wave Radiation Compared to Sensible Heat Estimates Obtained with BREB Stations for Selected Sites in 1986 and 1989 83

LIST OF TABLES

Number *Page*

VI.1 Evapotranspiration Measurement Methods Used at Six Locations on the Hanford Site 27

VI.2 Gains and Offsets for Landsat TM Bands 1 Through 7 32

VI.3 Atmospheric Corrections and Columbia River Temperatures for Six Landsat Overpasses 34

VII.1 Average Daily Latent Heat Flux Determined from Weighing Lysimeters and Neutron Moisture Probes for the Bunchgrass and Sagebrush Sites 40

VII.2 Image Means and Variances of Reflected Short Wave, Long-Wave, and Net Radiation 46

VII.3 Daily Average G_T Density 64

VII.4 Statistic for Resistance Equation Development 68

VII.5 Surface Observations at Sagebrush Site on 8-May-89 and 1-Jun-89 80

VII.6 Surface Observations at Bunchgrass Site on 8-May-89 and 1-Jun-89 80

VII.7 Surface Energy Budget Values at G300 During 8-May-89 and 1-Jun-89 Landsat Overflights 81

VII.8 Surface Energy Budget Values at Lower Snively During 8-May-89 and 1-Jun-89 Landsat Overflights 81

VII.9 Surface Observations, Predicted Aerodynamic Resistance and Sensible Heat Flux, and Measure Sensible Heat Flux for Landsat Overflights 82

Appendix

A.1 Raw Neutron Probe Data for Sagebrush Site on 23-Mar-89 98

A.2 Soil Water Content for Sagebrush Site on 23-Mar-89 99

A.3 Soil Moisture Storage for Sagebrush Site on 23-Mar-89 100

GLOSSARY OF SYMBOLS

Symbol	Description	SI Units
β	Bowen ratio	---
C_p	Specific heat of air	$J\ kg^{-1}\ K^{-1}$
E	Latent heat*	W/m^2
e_a	Emissivity of atmosphere	
e_s	Emissivity of surface	
G	Soil heat flux at 5 cm	W/m^2
G_S	Soil heat storage*	W/m^2
G_T	Total soil heat flux*	W/m^2
H	Sensible heat*	W/m^2
K_m, K_v, K_h	Eddy transfer coefficients for momentum, vapor, and heat	---
ρ	Density of air	$kg\ m^{-3}$
ρ_v	Density of water vapor	$kg\ m^{-3}$
r_a	Aerodynamic resistance to sensible or latent heat flux	s/m
r_c	Canopy or soil resistance to latent heat flux	s/m
$R_L\downarrow$	Long-wave radiation incoming*	W/m^2
$R_L\uparrow$	Long-wave radiation outgoing*	W/m^2
R_N	Net radiation*	W/m^2
$R_S\downarrow$	Short-wave radiation incoming*	W/m^2
$R_S\uparrow$	Short-wave radiation outgoing*	W/m^2
T_a, T_1, T_2	Air temperature at various heights	°C or °K
T_S	Surface temperature	°C
vp	Vapor pressure	kPa

*Flux density.

GLOSSARY OF TERMS

BREB	Bowen ratio energy balance
DN	digital number
DOY	day of year
ET	evapotranspiration
HMS	Hanford Meteorological Station
IR	infrared
LAI	leaf area index
msl	mean sea level
NDVI	normalized difference vegetation index
	NDVI = (Near IR-Red)/(Near IR+Red)
PET	potential evapotranspiration

ACKNOWLEDGEMENTS

Sincere appreciation is extended to Drs. Leo Fritschen, John Adams, Terrance Cundy, Peter Schiess, and Frank Gruelich of the University of Washington and Dr. Glendon Gee of Pacific Northwest Laboratory for their guidance. Special thanks is extended to Dr. Fritschen who spent many days in the field with the author establishing the micro-meteorological field sites. Several Pacific Northwest Laboratory staff members also have helped collect and process many of the varied data sets and answered endless questions on computer procedures. These staff members include Janelle Downs (special thanks also goes to Janelle for being my wife and supporting me during this research), Guy McWethy, Diana Felmy, and Drs. Steve Link and Mike Fayer. The contributions of these colleagues are appreciated. The educational leave of absence from Pacific Northwest Laboratory and the financial support of the U.S. Department of Energy is also greatly appreciated.

1.0 Introduction

The study of evapotranspiration (ET) from natural communities has become more important during the past decade as concerns increase about the critical role of ET in diverse areas including waste management, pollution, deforestation, and global climate change. The semi-arid Hanford Site in southeastern Washington contains large areas of native vegetation with extensive areas of hazardous and radioactive contamination. Assessing the effectiveness of cleanup efforts designed to isolate buried waste material from the general environment must include model simulation of water balance over time periods ranging from decades to centuries. The purpose of this research is to determine ET rates (a component of water balance models) in major community types on the Hanford Site and determine if remotely sensed data can be used to estimate sensible (heating of the air) and latent (evaporation of water) heat fluxes from these same areas.

This dissertation reviews the ET measurement methods used at the Hanford Site, the theory of sensible and latent heat transport, and the use of simplified equations in ET models. The experimental sites are described and the results obtained from these sites are presented. Evapotranspiration measurements from the sites are compared and best fit equations of sensible heat flux are developed and applied to a Landsat image.

The theoretical basis for ET processes are well defined. Measurement and modeling studies have become routine in agricultural environments when describing a monoculture in relatively uniform fields under ideal growing conditions. As we increase the measurement scale and move away from these ideal conditions to model natural systems, the variation in several important driving variables (e.g., temperature, radiation) and state variables (e.g., vegetation, soil type) increases rapidly.

Predictions of ET are further complicated by the presence of multiple plant species with variable distributions and phenology. Incorporating all of the variability associated with all environmental processes rapidly overwhelms highly mechanistic process-based models. As the scale increases in both horizontal extent (regional- and global-scale atmospheric models, and watershed models) and vertical depths (hazardous waste modeling), the ET algorithms

become a small portion of the overall modeling effort and must be simplified to minimize computation time. Many of the processes affecting ET may be filtered by the scale of the simulation. For example, a watershed may have a north and south slope exposure with a greatly different energy balance and ET, but it may be adequately represented by an average value for the combined area. In such cases, stream outflow for the watershed provides an area-integrated boundary-flux parameter that can be used for comparison. In semi-arid regions, stream runoff may not occur and model validation efforts are usually focused on direct measurement of energy fluxes in key plant communities.

Arid sites with thick persistent unsaturated soil zones are generally considered ideal for shallow land burial of radioactive waste (Mercer et al. 1983). The Hanford Site is in a semi-arid environment, has a thick persistent unsaturated soil zone, and is one of the largest U.S. waste disposal sites both in terms of land area and waste inventory.

Evapotranspiration estimates are frequently used in water balance calculations to determine drainage of natural and disposal areas located on the Hanford Site. Drainage (or recharge) at such sites is calculated as the difference between incoming precipitation and water lost by ET (for one-dimensional simulations, it generally is assumed that there is no runoff and negligible annual changes in net storage). Early predictions of water balance at the semi-arid Hanford Site using numerical models assumed that each year's accumulation of precipitation was lost through ET (Brownell et al. 1975), and thus no water infiltrates into the waste zone. In actual fact, accurate estimates of ET are not available, and the amount of yearly precipitation not removed by ET and available to drain through waste sites at Hanford is reported for only a few sites (Gee et al. 1992). However, calculations made in the *Final Environmental Impact Statement, Disposal of Hanford Defense High-Level, Transuranic and Tank Waste, Hanford Site, Richland, Washington* (DOE 1987) indicate that only a small amount of water (<0.5 cm/yr over hundreds of years) can move through the waste without potentially transporting radionuclides through the vadose zone and into the ground water. Results of model simulations for a simple grass-covered community with a 3.5-m soil profile that showed end-of-the-year storage values differing from measured values by 2.5 cm (Gee and Kirkham 1984). Drainage estimates at this same site were 5 cm (estimated from below rooting depth soil profile water content changes) and 3.5 cm (model simulations).

Deficiencies in modeling are caused in part by inadequate estimates of time-dependent ET for specific soil/vegetation surfaces. Clearly, an improvement in water balance modeling is needed, and the requirement to validate the modeled effects of a vegetation cover on water balance requires that actual ET values be available to compare against model output.

Estimates of ET at the Hanford Site have been provided by neutron probe measurements (i.e., water storage values usually semi-monthly) combined with precipitation records or by a weighing lysimeter (box of soil whose weight is measured electronically over time). Water flux either by precipitation or ET loss can be directly measured by weighing lysimeters. Weighing lysimeters provide hourly measurements of water balance, but this may not be representative of the natural environment over seasonal time periods because of truncated rooting depth (Gee et al. 1991). This may not preclude the use of lysimeters for validation studies over short time intervals.

The lysimeter measurements are compared with estimates of latent heat flux determined with Bowen ratio energy balance (BREB) stations. The BREB stations measure the available energy and partition it into sensible and latent heat fluxes. Accurate temporal assignment of ET is critical when impacts associated with climatic change are being modeled or remotely sensed data is used to scale ET measurements onto similar land surfaces.

Remote sensing is often presented as the tool of choice for estimating ET over large areas. Estimates of latent heat flux for the Arid Lands Ecology Reserve (a portion of the Hanford Site) have been reported by Gibbons et al. (1991). In that work, a linear relationship was developed between lysimeter values of latent heat flux and an infrared thermometer viewing the lysimeter surface (a simple relationship adopted from irrigated agriculture). Unfortunately, as the growing season progresses, the surface temperature increases while ET is decreasing as water becomes limiting.

A more mechanistically correct approach (the approach adopted in this work) is to predict sensible heat flux directly from surface temperature (thermal band data). Then, develop relationships between visible and thermal bands, and radiation and soil heat flux terms. Next, determine latent heat flux as the residual term in the energy balance at the surface.

Only a few studies have been implemented at a large scale to acquire satellite imagery and ground truth data simultaneously. These include FIFE in Kansas (FIFE Special Issue 1992), HAPEX-MOBILHY in France (Andre et al. 1986), smaller studies in Owens Valley, California (Smith et al. 1990, Kustas et al. 1989), MONSOON 90 in the San Pedro basin in southern Arizona (Kustas et al. 1991), and BARFEX near Boardman, Oregon (Doran et al. 1992).

In estimating the energy balance of the earth's surface at scales ranging from hundreds to thousands of meters, remotely sensed data must be used. This data is most commonly a surface temperature and possibly a vegetation index (determined by measuring the vegetation absorbance of radiation in the visible red wavelengths as compared to increased reflectance of near-infrared radiation). To close the energy balance at the surface, other energy fluxes such as incoming long-wave ($R_L\downarrow$) and outgoing short-wave radiation ($R_S\uparrow$) must be estimated. In arid environments, soil heat flux also becomes a significant component of the energy balance equation and must also be estimated. Soil heat flux is not a constant fraction of net radiation as assumed in many models. It changes significantly over the diurnal cycle (Kustas and Daughtry 1990) and algorithms estimating total soil heat flux density (G_T) as a function of net radiation (R_N) must be restricted in application to a certain time interval or sensitive to the time of day.

For this investigation, the remote sensing data is limited to Landsat [other platforms lack thermal infrared (IR) or the resolution necessary for realistic comparisons with field measured energy fluxes]. This fixes the time of day of satellite data collection to approximately 1020 hours for the Hanford Site.

2.0 Research Approach

This research focuses on measuring ET at a semi-arid site using lysimeters and BREB stations. The intent is to develop simplified sensible heat flux relationships that can be used with remotely sensed data to predict surface energy fluxes. The low evaporation rates in this arid environment make collection of Bowen ratio data difficult and the equipment is often operating near the sensor noise level. Weighing lysimeters continue to function well at low ET rates but encompass a relatively small area. Whether weighing lysimeter data adequately represent the surrounding environment is assessed by examining the correlation in ET estimates between water balance and lysimetry, and between lysimetry and the Bowen ratio.

For this study, I obtained ET data from five study areas on the Hanford Site. For several of these study areas, data were gathered using at least two ET measurement methods during the primary growing season. Standard linear regression techniques were used to establish the relationships between similar measurements at different sites.

Selected data sets from a shrub-dominated and a grass-dominated site were used to set parameters for a resistance-based sensible heat flux equation for use with a net radiation map developed from a satellite image. Maps of short-wave reflectance and a qualitative estimate of vegetation cover were also developed. The relationship of soil heat flux (G_T) density to net radiation (R_N) is examined for each measurement site.

Specifically, to determine if remote sensing can be used to predict ET at the Hanford Site, various estimates of components of the energy balance were validated or calibrated. The terms estimated are as follows:

1. reflected short-wave radiation from satellite spectral data
2. net radiation as a function of short- and long-wave radiation components
3. soil heat flux as a function of satellite derive vegetation index or net radiation map
4. appropriate resistance values for use in sensible heat transport equations.

These steps were accomplished by collecting ET and energy balance information simultaneously with Landsat overpasses on 8-May-89 and 1-Jun-89. Additional, less complete data sets spanning 1986 through 1990 were also used to indicate variability associated with some of the satellite measurements. These data sets included water balance measurements with lysimeters and neutron probes, energy balance measurements with Bowen ratio stations, and spectral reflectance values obtained from Landsat.

Direct comparisons between satellite and ground truth measurements were limited because of the 2-week interval between satellite overpasses, cloud cover on overflight days, and the expense of the satellite data and associated ground truth measurements. Because of this limited data set, statistical evaluations were limited to simple regression and ANOVA analysis.

Also, it was necessary to determine if lysimeters, Bowen ratio, and water balance data were comparable. Lysimeters provide a continuous record but because of their small size may not be representative of the surrounding environment. Comparisons of latent heat flux between the methods were reported. The soil heat flux density component of the energy balance data collected on the Hanford Site was examined in conjunction with satellite-derived estimates of a vegetation index to determine if a predictive relationship exists.

3.0 Evapotranspiration Measurement Methodology

This section briefly reviews the methods applicable to measuring ET. The components of the near-surface environment and how various physical parameters affect ET are reviewed first. Major topographical features of the measurement site include the low elevation cataclysmic flood deposits of sandy soil overlaying flood deposited rock as well as the high elevation eolian soils overlying flood deposits and fractured basalt. The bunchgrass and sagebrush area have sparse cover with extensive areas of bare soil or cryptogram cover between plants (Figure 3.1). Water arrives at the surface as either rain or snow and in extremely rare cases as overland flow. This surface water is either immediately lost by evaporation (sublimation in the case of snow) or absorbed into the soil and surface litter. Evaporation of water from the surface requires the input of energy; the major portion of this energy is received from solar radiation, but small amounts come from energy stored in the soil and advection of warmer (drier) air from adjacent areas.

Evaporation is commonly viewed as occurring in two stages. The first stage occurs when the soil or vegetation surface is wet (i.e., after a rain shower) and is energy limited; the second stage occurs as the soil surface dries, soil hydraulic conductivity decreases, and evaporation becomes limited by soil properties.

Transpiration is controlled by both biotic and abiotic factors. Water is removed from the soil by plant roots, transported by the plant vascular system to the leaves, and lost to the atmosphere from stomatal openings in the leaves. The transport process is driven by the vapor pressure gradients between the leaf and the atmosphere. This gradient is a complex function of surface environmental variables (radiation, temperature, vapor density, wind speed) and subsurface variables (soil water, root distribution, soil temperature). Biological processes in the plant allow the rate at which water is lost to the atmosphere to be regulated to varying degrees. This regulation usually occurs at the expense of growth.

Several excellent reviews of ET measurement methods were written in soil physics and micro-climatology textbooks by Arya (1988); Campbell (1977); Hanks and Ashcroft (1980); Rosenberg et al. (1983); and Monteith (1975). Also, several symposia and workshops have

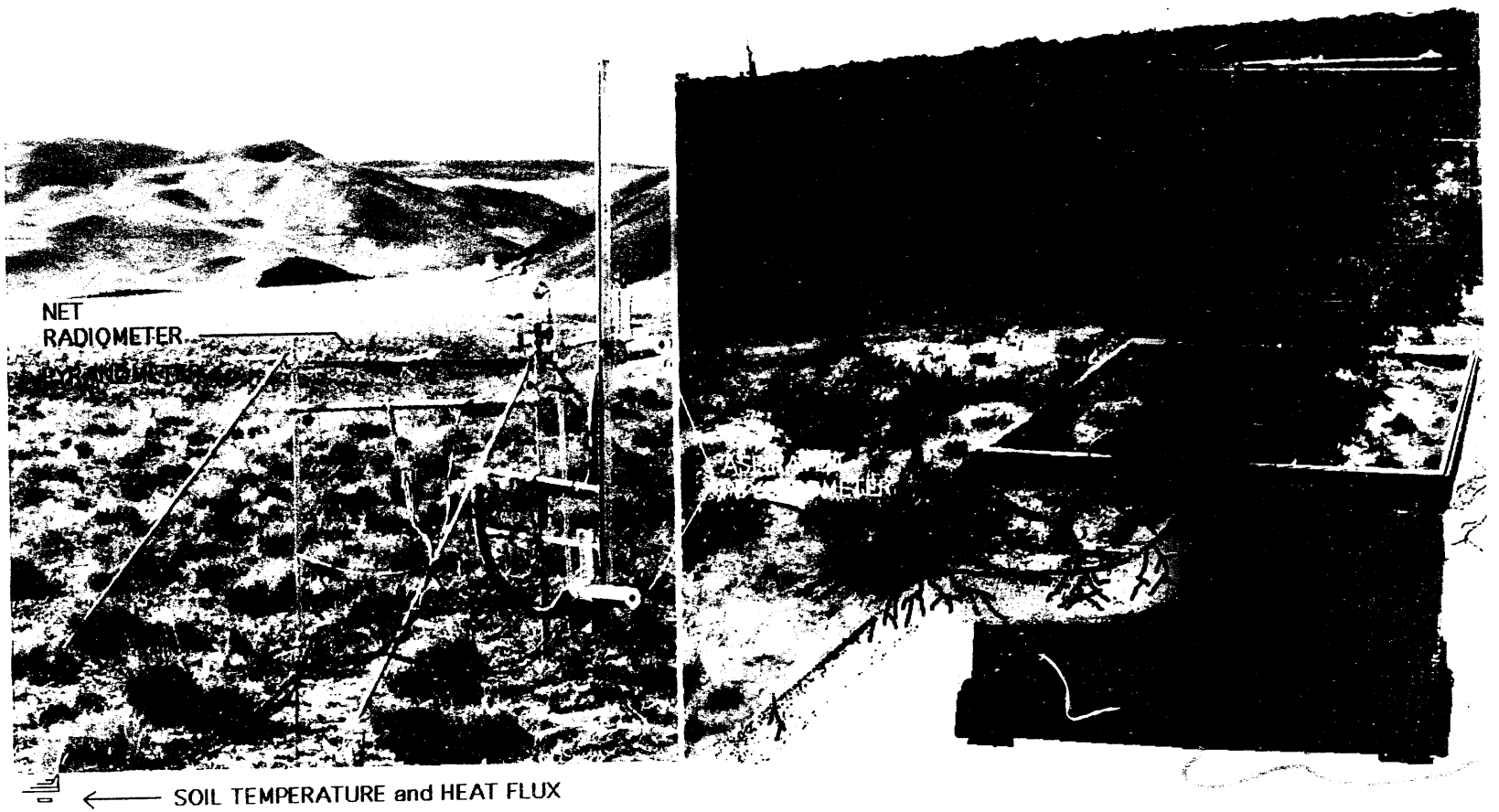

FIGURE 3.1. Cross Section of Typical Hanford Site Grass and Sagebrush Communities.

addressed ET methods including Sharma (1982), Allen et al. (1991), and FIFE Special Issue (1992). The results of water balance studies at the Hanford Site using lysimetry and soil profile storage from neutron probe measurements have been presented previously (Gee and Kirkham 1984; Gee 1987; Gee et al. 1989; Jones 1989; Reece 1991). The measurement methods discussed in detail in the previously mentioned soil physics and microclimatology text are separated into two categories and reviewed in the following section.

3.1 Hydrologic Category

Most methods within this category are based on an accounting that keeps track of the inventory of the water within a defined control volume. This inventory is represented by the following water balance equation

$$\Delta S = P - ET - D - Ro \tag{1}$$

where ΔS = change in soil water

P = precipitation

ET = evapotranspiration

D = drainage

Ro = runoff or runon to the control volume.

Generally, P is measured with a tipping bucket rain gauge, often at an official weather station or airport which may be several miles from the site under study. When precipitation falls as snow, the tipping bucket or weighing gauge should be heated. If a collection gauge is used, it should have antifreeze in the collection cylinder. More accurate rainfall amounts can be determined from weighing lysimeters if ET rates during the sampling interval remain low.

Soil water storage change can also be determined using lysimeters. Lysimeters are commonly used to quantify the amount of water that is stored or lost from a volume of soil (Howell 1957; Aboukhaled et al. 1982; Hillel 1982). Evaporation from a lysimeter may be measured by observing water table fluctuations (Van Hylckama 1968), by monitoring weight

changes using pressure changes (Fritschen et al. 1977), by mechanical scales (Harrold and Dreibelbis 1967), or by using strain-gage devices as a counterbalance or incorporated into platform scales (Kirkham et al. 1984). Soil water storage can also be measured by destructive soil sampling for gravimetric moisture or nondestructive nuclear methods discussed below. An extensive review of existing lysimeters was reported by Marek et al. (1988) and Howell et al. (1991). Criticism of lysimeters includes the limited areal surface, edge effects including heat loss or gain through metal side walls, and preferential water flow at the side walls. Also, the limited soil volume may limit rooting depth and water storage.

The neutron moisture probe is commonly used to measure soil moisture in lysimeters and in natural environmental settings. In operation, the neutron probe emits fast neutrons that are moderated (slowed down) by hydrogen atoms (Greacen 1981). These slow neutrons are then counted. The major source of hydrogen in soils is in water; so, the measurement primarily reflects water content. The required calibration removes secondary effects of pipe materials (in case plastics are used), soil organic matter, and soil density.

Runoff for water balance studies at the Hanford Site is usually assumed to be negligible. This may not be true during rapid snow melt into frozen soils on sloping surfaces (Gee and Hillel 1988).

At larger scales, ET is often determined as the difference between precipitation and catchment outflow. The Hanford Site does not have any catchments with surface drainage offsite. Recently, the U.S. Geological Survey began measuring outflows in catchment basins that terminate onsite. Seepage and overland flow contributions to catchment outflow do not need to be separated to estimate ET for annual or seasonal periods. However, accurate predictions of ET at daily time steps would require that the seepage and overland flow be separable.

3.2 Surface Atmospheric Flux Measurement

Evapotranspiration can be measured using the BREB method, which combines atmospheric transport equations for sensible and latent heat with the energy budget equation. These

equations also form the basis of modeling ET discussed in Chapter 4.0. The energy budget equation is

$$R_N - G - H - \lambda E = 0 \tag{2}$$

where R_N = net radiation (the difference between incoming and outgoing radiation)

G = soil heat flux

H = sensible heat flux

λE = latent heat flux.

The Bowen ratio method (Bowen 1926) was originally proposed for use over bodies of water (equation 3). The most commonly used BREB systems measure the air and wet bulb temperatures, net radiation, and soil heat flux. From these data, temperature and vapor pressure gradients are converted to common energy units and used to partition available energy (net radiation + soil heat flux) into sensible and latent heat fluxes. The Bowen ratio (β) is defined as

$$\beta = H/\lambda E = \frac{\rho C_p * K_h * \Delta T}{\lambda \varepsilon * K_v * \Delta \rho_v} \tag{3}$$

This method has been used by several investigators to estimate ET in both agriculture and natural environments ranging from forests to deserts (Fritschen and Simpson 1989). Fundamental to the method is the assumption that K_h and K_w, turbulent exchange coefficients for sensible and latent heat fluxs, are equal. The validity of this assumption may deteriorate in arid environments such as the Hanford Site. Combining and rearranging equations 2 and 3 gives equation 4, which we use to predict the latent heat flux.

$$\lambda E = \frac{R_N - G}{(1 + \beta)} \tag{4}$$

Another problem pointed out by Angus and Watts (1984) is related to the accuracy of the

air and wet bulb temperature gradient measurements. They indicate these temperature gradients must be measured to 0.0013°C when the Bowen ratio is 10 to keep the error below 10%. This accuracy is not required on the actual temperature measurement, only on the difference between the two measurements. Bowen ratio values less than 1 are typical for moist climate and 10 or higher for a summer-time desert climate.

4.0 Modeling Evapotranspiration

Evapotranspiration changes from a process primarily controlled by radiation and/or atmospheric demand in wet climates to a process controlled by soil and/or plant factors in arid climates. Whether the climate is wet or dry, determining the potential evapotranspiration (PET) is a common starting point for most models. A range of models from empirical to mechanistic are available to estimate PET. Several empirical methods exist relating PET or ET to one or more environmental variables. Models based on air temperature include the Thornthwaite, Blaney-Criddle, Hargreaves, and Linacre methods. Equations based on solar radiation and combination equations that consider energy supply and turbulent transport of water vapor are discussed in Rosenburg et al. (1983). Combination equations that include the Penman (1948) equation for evaporation from a saturated surface and the Penman-Monteith (Monteith 1963, 1964) equation for use when water is limited are used almost exclusively in models to determine PET. These equations are derived from gradient transport equations that assume turbulent mixing approximates diffusion processes. If eddy transfer coefficients K_m, K_v, and K_h for momentum, vapor, and heat, respectively, are known, these equations can be used to determine the flux of each quantity. For example, sensible heat flux density is represented as

$$H = \rho C_p * K_h \frac{T_2 - T_1}{z_2 - z_1} \tag{5}$$

where ρ = density of air (kg m^{-3})

C_p = specific heat at constant pressure (J kg^{-1} K^{-1})

T = temperature (°C) measured at two heights.

The Penman equation is used to estimate PET and is developed by assuming a linear approximation to the slope of the saturation vapor pressure curve, and the substitution of the gradient transport equations for sensible and latent heat into the energy balance equation. For wet surfaces, the following equation is used.

$$\lambda PET = \frac{sR_N + \left[\frac{\rho C_p (\acute{\rho}_v - \rho_v)}{r_h}\right]}{s + \gamma^*} \tag{6}$$

where s = saturation vapor pressure curve slope

γ^* = psychrometric constant times the r_v/r_h (resistance to vapor transport/resistance to sensible heat transport).

When both bare soil and plants are present, it may be necessary to partition PET into potential transpiration and potential evaporation. Partitioning is usually achieved by multiplying PET by some function of leaf area index (LAI). Evapotranspiration may also be modeled by some form of the Penman-Monteith equation that will reduce ET as plant water potential decreases in the leaf or soil. The modification of Penman's equation by Monteith introduced a resistance term that allows prediction of evaporation from non-wet surfaces. The revised equation (equation 7) introduces a canopy, or soil resistance, r_c in addition to r_a, the aerodynamic resistance above the canopy.

$$\lambda E = \frac{s(R_N + G) + \rho_a C_p \frac{\acute{\rho}_v - \rho_v}{r_a}}{(s + \gamma)\frac{r_a + r_c}{r_a}} \tag{7}$$

The use of this equation is still limited by the need to know aerodynamic and canopy resistances. The General Purpose Simulation Model (Buttler and Riha 1989) uses the Penman-Monteith equation to calculate plant and soil ET. Radiation is partitioned between the vegetation and soil by the LAI value in a similar approach to modeling by Shuttleworth and Wallace (1985). General Purpose Simulation Model also provides estimates of R_N, G_T, LAI, growing degree days, and water balance estimates. Soil properties can be used to

control the actual uptake of water by plant roots in each soil layer thereby limiting transpiration. Model results may be useful in filling in missing data and scaling bi-weekly values to hourly or daily ET values.

For this investigation where the primary driving force is surface temperature measured by satellite, we have the special case where z_1 is at the surface and the flux is more appropriately represented in terms of a bulk transport equation incorporating a dimensionless heat transfer coefficient.

$$H = -\rho C_p C_H U * (T_s - T_a) \tag{8}$$

where C_H = dimensionless heat transfer coefficient

U = mean wind speed at height z.

Recognizing that resistance to sensible heat transport (r_h) is the inverse of $C_H U$ and often assumed equal to r_a leads to the common formulation of sensible heat flux as

$$H = \rho C_p \frac{T_s - T_a}{r_a} \tag{9}$$

The resistance formulation is useful when the path characteristics change (i.e., soil-root-shoot-leaf-atmosphere) or when multiple paths exist (i.e., soil-root and soil-atmosphere).

The resistance terms in the Penman-Montieth method or the bulk transport equation can be expanded to include stability corrections (Hatfield et al. 1985). Specifically for sensible heat transport, the resistance to heat transfer (sm^{-1}) is

$$r_a = \frac{\ln\frac{z - d_o}{z_{om}} + \ln\frac{z_{om}}{z_{oh}} - \Psi_h * \ln\frac{z - d_o}{z_{om}} - \Psi_m}{\kappa^2 \mu} \tag{10}$$

where z = height at the top of the canopy

z_0 = roughness length for the soil or canopy

d_0 = zero plane displacement height

ψ_n = stability correction function of heat

ψ_m = stability correction function of momentum.

The terms ψ_n and ψ_m were derived from Monin-Obukhov surface layer similarity theory.

This resistance approach has been modified for sparse canopies in several recent models (Shuttleworth and Wallace 1985; Kustas 1990; Shuttleworth and Gurney 1990). Shuttleworth and Gurney (1990) partition R_N into soil and vegetation fractions based upon leaf area, and then determine separate resistance terms for the soil and vegetation surfaces. This is useful if separate measurements of canopy and soil temperatures are available.

Nichols (1992) applied this modeling approach to field measurements of energy budgets in sparse greasewood (*Sarcobatus spp.*). He found r_a for sensible heat flux on days when soil evaporation was assumed zero to be highly correlated to wind speed. He also observed a possible oasis effect for the individual shrubs. Ham and Heilman (1991) using the same approach in sparse cotton found aerodynamic resistances within and above the canopy highly variable and only partially explained by wind speed.

The term $\ln(z_{om}/z_{oh}) = kB^{-1}$ in equation 10 is included to account for the apparent source or sink of heat being located at a lower level than the apparent sink for momentum. Kustas et al. (1989) found $Kb^{-1} = 5.6$ in a sparse canopy located in Owens Valley, California. They also found Kb^{-1} was related to wind speed and surface temperature. Recent work by Kohsiek et al. (1993) indicated success in predicting sensible heat flux in a semi-arid area of France using $Kb^{-1} = 9.2$ provided the surface temperature was known to within 2°C.

5.0 Remote Sensing Methods

Two areas of application of remotely sensed data are

1. a direct estimate H or E, or parameters (i.e., net radiation, soil heat flux and amount of vegetation) used with aerodynamic transport equations to predict H and E

2. a classification of geographical areas into regions with similar characteristics to assign a point source measurement of ET taken within the region to all of the pixels of the image with similar characteristics. These characteristics include elevation, slope, aspect, vegetation type and cover, soil type, and incident radiation. Classification of the Hanford Site using remotely sensed data is being addressed in other investigations and is not considered here. Choudhury (1991) provides an excellent overview of the use of multispectral satellite data for estimating land surface energy balance.

The aerodynamic transport equations are often simplified for use with remotely sensed data. In wet environments, it may be possible to directly predict latent heat flux using simplifying assumptions. For example, turbulent transport equations describing latent heat flux can be simplified when information on the vapor pressure gradient (e_s - e_a) and resistance to vapor transport (r_v) are not available. Assume e_s and e_a are primarily a function of surface temperature (T_s) and air temperature (T_a), respectively. Also assume ρC_p to be constant. The resistance to vapor transport although dependent on wind speed is also assumed to be constant. A simplified equation (equation 11) results that relates latent heat flux to temperature difference and some statistically derived coefficients.

$$E = C_0 + C_1 * (T_s - T_a) \tag{11}$$

Because T_s is a function of incoming radiation and T_a is both a function of T_s through convective heating and the total energy stored within the local environment, the equation is often simplified even further to

$$E = C_0 + C_1 * T_s \tag{12}$$

with C_0 and C_1 being determined from statistical analysis of data sets. Using the diurnal temperature cycle as an analogue to daily temperature variations, and a regression of lysimeter weight loss against temperature, Gibbons et al. (1991) presents

$$ET = (b_0 + b_1 * T_s) * \left[\frac{LAI}{0.276} \right] \tag{13}$$

where T_s is determined from Landsat data, and LAI is a fraction of the normalized difference vegetation index (NDVI) until NDVI reaches 0.35 at which point LAI is set to a constant value of 0.32.

These simple equations are not suitable for the Hanford Site where resistance to vapor flow varies considerably because of stomatal control at the leaf surface, and soil conductivity decreases (or resistance increases) rapidly as the surface dries.

Estimating sensible heat transport through simple equations is not compounded by changes in the stomatal resistance or the soil surface resistance as found in latent heat transport. This equation combined with the energy balance equation and estimates or measurements of R_N and G provides the framework for predicting ET from remotely sensed data. Similar attempts to simplify the sensible heat transport equation are evident in the literature. As before, $\rho C_p/r_a$ is assumed constant resulting in a simple equation (equation 14) as proposed by Jackson et al. (1977).

$$E - R_N = 0.64 * (T_s - T_a) \tag{14}$$

where E and R_N are expressed in millimeters of water per day. A similar linear relationship (equation 15) was proposed for sensible heat flux by Brunel (1989).

$$H = -13.6 + 17.1 * (T_s - T_a) \tag{15}$$

Holwill and Stewart (1992) measure sensible heat transport (H), air, and surface temperature at one FIFE site to determine a transfer coefficient (equivalent to equation 13). This transfer coefficient is then used with surface temperatures obtained from aircraft-mounted scanners to predict sensible heat flux on a portion of the FIFE site. Hall et al. (1992) reports little success in predicting H from remotely sensed surface temperatures using equations in the form of 9 and 10.

To determine ET through completion of the energy balance equation, remotely sensed data must provide estimates of R_N, G_T, and H. An indicator of vegetation amount, such as the NDVI [NDVI = (Near IR-Red)/(Near IR+Red)], proposed by Rouse et al. (1974) can be used to scale soil heat flux and assign resistance values. Jackson et al. (1983) compared several vegetation indices and indicated that NDVI was the more sensitive index at low vegetation amounts. The NDVI calculations can be performed on raw digital numbers (DN), DNs minus atmospheric background determined from river or shaded areas, or from Dns converted to atmospherically corrected radiances. It is often not clear in the literature exactly which values are used to calculate NDVI making it difficult to compare values between investigation. A limited data set relating NDVI and LAI for the Hanford Site was presented by Gibbons et al. (1991). For the 8-May-89 image, they report LAIs of 0.21 and 0.36, and NDVIs of 0.2 and 0.35 (determined from atmospherically corrected radiances) for the bunchgrass and sagebrush sites, respectively (estimated from a report figure).

The calculation of net radiation follows the procedure described by Jackson et al. (1985). Net radiation is described as

$$R_N = R_{S\downarrow} - R_{S\uparrow} + \epsilon_a \sigma T_a^4 - \epsilon_s \sigma T_s^4 \tag{16}$$

where $R_{S\downarrow}$ = incoming short-wave radiation

$R_{S\uparrow}$ = outgoing short-wave radiation

ϵ_a = effective sky emissivity

σ = Stefan Boltzmann constant

T_a = air temperature (°K)

ϵ_s = surface emissivity

T_s = surface temperature (°K)

$\epsilon_a \sigma T_a^4$ = long-wave radiation down ($R_L\downarrow$).

Direct measurements of this term ($\epsilon_a \sigma T_a^4$) are seldom available, but it can be predicted using air temperature and vapor pressure as proposed by Brutsaert (1982). See equation 17.

$$R_L\downarrow = \epsilon_a * \left[\sigma * (Air_{wet}+273)^4\right] \tag{17}$$

where σ = Stefan-Boltzmann constant ($5.6697*10^{-12}$ W cm^{-2} °K^{-4}). Atmospheric emissivity is determined using the formula presented by Brutsaert (1975).

$$\epsilon_a = 1.24 * (vp/T_{air})^{(1/7)} \tag{18}$$

Values for T_{air} and vapor pressure (vp) are determined from BREB station sensors.

Also required for solution of the energy balance equation is an estimate of soil heat flux. Several empirical models of soil heat flux have been proposed. These models include

$$G/R_N = 0.583 * e^{-2.13NDVI} \tag{19}$$

by Moran et al. (1989),

$$G = 0.4 * \exp(-0.5 * LAI) * R_N \tag{20}$$

by Choudhury et al. (1987), and

$$G/R_N = 0.294 - 0.0164 * NDVI \tag{21}$$

by Kustas and Daughtry (1990).

The ratio of G/R_N changes significantly in agricultural crops where vegetation cover changes from 0 to full cover (Oliver et al. 1987). They also observed that in a short grass site the ratio changes 5 to 10% depending on prevailing weather and soil conditions. This relationship was created over a developing wheat canopy, but G was determined as a residual in the energy balance equation rather than measured directly. Fuchs and Hadas (1972) found the G/R_N ratio to be 0.34 in a bare loess soil. Camuffo and Bernardi (1982) recognize the diurnal cycle associated with R_N and propose that

$$G_T = a_1 * R_N(t) + a_2 \frac{\partial}{\partial t} R_N(t) + a_3 \tag{22}$$

This cycle is quite evident when plotting soil heat flux against net radiation; this emphasized the need to develop G/R_N ratio for specific time of the day corresponding to overflights (Landsat at 1100 hours). Alternatively, the time-based G_T equation could be used to adjust the relationships to other times of the day as might be required for satellite with non-uniform overpass times.

6.0 Experimental Design and Test Methods

6.1 Hanford Site Geology and Climate

The Hanford Site is located in southeastern Washington, with an areal extent of 1450 km^2 located from latitude 46° 18′ N to 49° 49′ N and longitude 119° 17′ W to 119° 52′ W. Geological features in the area consist of large flat areas with monoclinal escarpments and tilted basalt outcrops. Altitude ranges from a high of 1093 m at the top of Rattlesnake Mountain to a low of 92 m at the Columbia River. A summary of geologic history can be found in Chatters (1989).

The Hanford Site is primarily a shrub-steppe grassland. This class is the largest of the grassland classes and covers 644,716 km^2 in the western United States. Disturbances such as grazing in the 1800s, farming before 1943, and large-scale construction activities have allowed cheatgrass (*Bromus tectorum*) to become the dominant grass in the lower elevations. The silt loam soils are found on the slope and at the base of Rattlesnake Mountain, part of which is located in the Arid Lands Ecology Reserve. The reserve is a 33,500-hectare area set aside in 1967 by the U.S. Atomic Energy Commission for preservation and ecological research. The flat lower elevation areas of the Hanford Site contain soils classed as sandy loams and sands. The average annual rainfall is 15.2 cm, with precipitation occurring primarily in the cool season months. The Arid Lands Ecology Reserve, its climate, soils, water balance, plants, and animals are described in detail in Rickard et al. (1988).

The Hanford Meteorological Station (HMS) is situated on the Hanford Site approximately 40 km northwest of Richland, Washington. The HMS elevation is 223 m above mean sea level (msl) at latitude 46° 34′ and longitude 119° 36′. Meteorological data collected at the site from 1946 to 1980 are summarized in Stone et al. (1983). More recent data are obtained from the HMS directly from computer files. Variables measured include air and soil temperatures at multiple heights and depths, wind speed at multiple heights, solar radiation, and precipitation. Total precipitation for 1986 was 18.0 cm (normal = 15.8 cm), and the average temperature was above normal. The year 1987 was one of the warmest with 10 months warmer than normal. The maximum temperature of 38.9°C (102°F) on May 8, 1987, was

the hottest temperature ever recorded so early in the year. Precipitation for 1987 was 12.9 cm. The year 1988 was warmer than normal and the second driest year on record with precipitation of 10.6 cm. The year 1989 was also warmer than normal. The spring months of March, April, and May were much wetter than normal with 7.6 cm or 227% of normal precipitation. Total precipitation for 1989 was 17.57 cm. The average temperature in 1990 was also above normal but precipitation was only 12.9 cm, 81% of normal.

As previously described, considerable variation exists between observation years. Growing degree days is an indicator of the plant's growth and development; in Figure 6.1a, 1986 is shown to have an early growth season and 1989, delayed growing season. The growing degree day was calculated with a base temperature of 10°C. In arid environments, the amount of vegetation growth is not only controlled by temperature but by available moisture including precipitation and stored soil moisture. Total soil profile moisture for the study years is shown in Figure 6.1b.

6.2 Study Areas

The relative locations of the field sites are shown on the 8-May-89 Landsat image in Figure 6.2. Three key features visible in the Landsat image approximate the boundary of the Hanford Site; these are the Columbia River crossing the upper (north) and right sides (east), Rattlesnake Mountain at the bottom (south), and irrigated and dryland agriculture on all sides. Site abbreviations, elevations, and type of water balance measurement made at each site are listed in Table VI.1.

6.2.1 Arid Lands Ecology Reserve Lysimeter and Water Balance Plots. An extensive ET measurement site has been developed in a shrub-steppe community at the 300-m elevation on the southeast slope of Rattlesnake Mountain located on the Arid Lands Ecology Reserve. Vegetation at this site is primarily big sagebrush (*Artemisia tridentata*), bluebunch wheatgrass (*Agropyron spicatum*), and Sandberg's bluegrass (*Poa sandbergii*) (secunda). Two areas are being studied, both with natural vegetation (see Figure 3.1). A range fire in 1984 removed the sagebrush from one area. These two study sites are referred to as the sagebrush and bunchgrass sites, respectively. Continuous measurements of ET are made with monolith

(a)

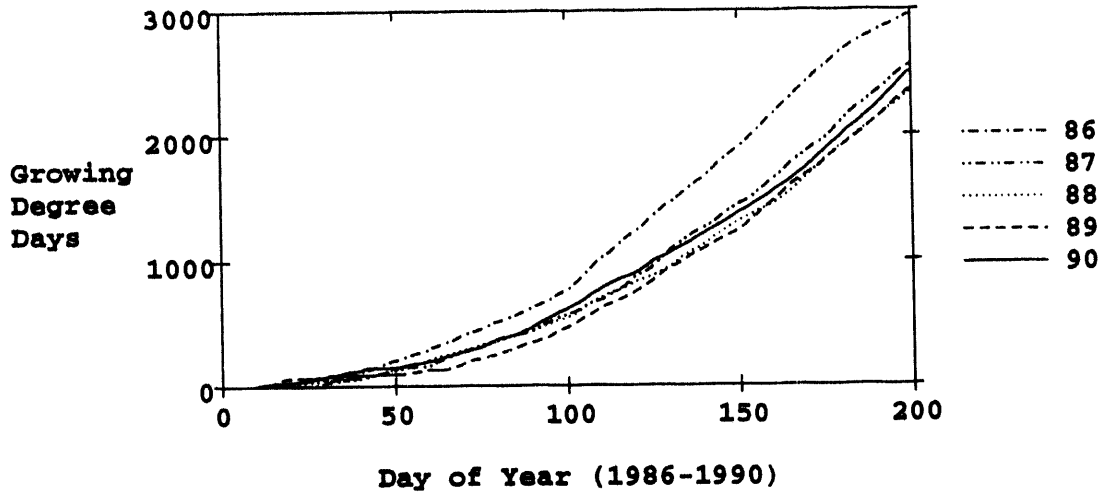

(b)

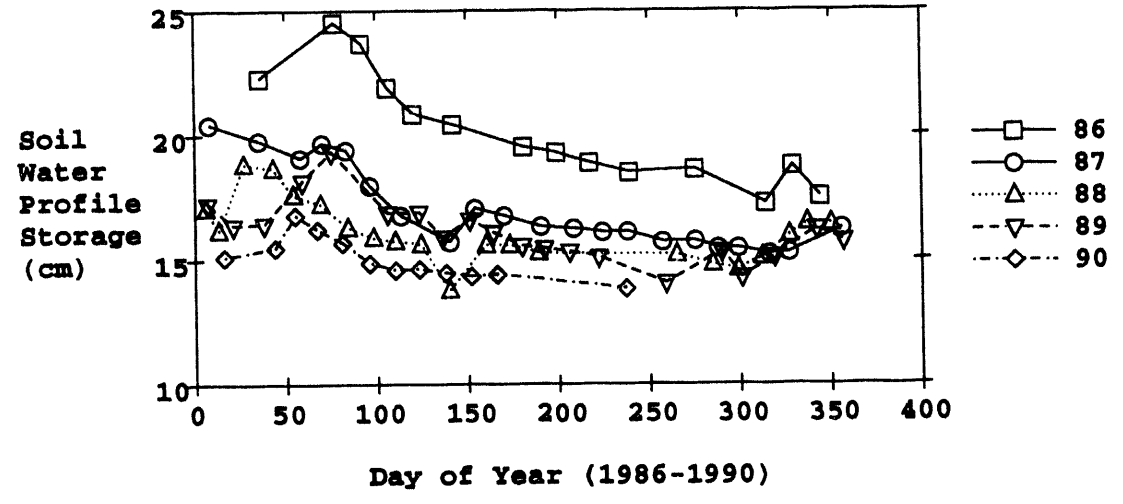

FIGURE 6.1. a) Growing Degree Days for 1986 to 1990, b) Soil Profile Moisture at the G300 Site for 1986 to 1990.

weighing lysimeters. Water balance measurements are made using a neutron moisture probe every three weeks, and BREB measurements are made during the spring and early summer months. Eight access tubes were randomly installed at each site. Neutron moisture probe measurements are taken at 30, 45, 125, 175, 225, and 275 cm in each access tube. Soils are classified as mesic Xerollic Camborthids with texture in the upper layers predominantly silt loams and loams.

FIGURE 6.2. Landsat Subscene from 8-May-89 with Bands 4,3,2 Displayed as Red, Green, and Blue (rectangle represents area processed in subsequent figures).

TABLE VI.1. Evapotranspiration Measurement Methods Used at Six Locations on the Hanford Site.

Year	Grass 300 (G300)	Buried Waste Test Facility (BWTF)	Bunchgrass (AC)	Sagebrush (AB)	Lower Snively (LS)	Upper Snively (US)	Field Lysimeter Test Facility (FLTF)
1986	NP	NP Lysim	NP	NP			
1987	NP	NP Lysim	NP Lysim	NP Lysim			
1988	NP	NP Lysim	NP Lysim IR	NP Lysm IR			
1989	NP BREB	NP Lysim	NP BREB Lysim	NP BREB Lysim	BREB	BREB limited	Lysim
1990	NP	Lysim	Lysim	Lysim			Lysim
Elevation (m)	100	100	300	300	300	480	180

BREB = Bowen ratio energy balance.
IR = Infrared sensor.
Lysim = Lysimeter.
NP = Neutron probe.

Within each study area, a lysimeter facility was constructed in 1986. Each facility consists of two weighing lysimeters containing undisturbed monoliths of local soil and vegetation. Each lysimeter has dimensions of 153 by 153 by 153 cm and rests on a 9080 kg platform scale. One neutron probe access well is located in each lysimeter for soil water profile measurement. Micro-meteorological instruments and the platform scale under the lysimeter are read at 10-second intervals using data logging systems and hourly averages recorded and transmitted via radio to the laboratory. At each site, an IR temperature sensor (15° field of view) mounted on the top of a 1.4-m pipe was pointed down at the surface of one of the lysimeters. Bowen ratio data has been collected at this site during two growing seasons.

6.2.2 Grass 300 (G300) Site. The Grass 300 (G300) site is located in a slight depression with northeast-southwest orientation. The site is ~ 150 m wide by 300 m long. The vegetation is composed of cool season grasses: cheatgrass (*Bromus tectorum*) and Sandberg's bluegrass, with canopy-cover values of 35% and 27%, respectively. The growth of both grasses is confined to late fall and early spring. The soil, a Typic Torripsamment (Hajek 1966), is well drained and nearly uniform to a depth of 3.5 m. The top 0.6 m contains 79% sand, 17% silt, and 4% clay and is classed as a loamy sand. From 0.6 to 3.5 m, the soil contains 92% sand, 5% silt, and 3% clay and is classed as a sand. A rock/gravel layer lies below the 3.5-m depth. The rock/gravel layer is estimated to be several meters thick from observations of excavations at adjacent sites. The water table is near 10 m.

Water balance data at the site are collected by recording precipitation events; monitoring other meteorological variables, including air temperature, humidity, and wind speed; measuring the soil profile water content; and measuring ET losses from weighing lysimeters at the Buried Waste Test Facility site. The Buried Waste Test Facility site is ~5 km north of the G300 site. For two growing seasons, a Bowen ratio station has been operated at the G300 site.

6.2.3 Buried Waste Test Facility. The Buried Waste Test Facility was constructed in 1978 (Phillips et al. 1979). Of interest at this facility are two weighing lysimeters back filled with sandy soil. One has a bare surface (NWL); the other has a cheatgrass vegetation cover

(SWL). These weighing lysimeters are different from all other weighing lysimeters discussed in this document, because drainage occurs at the bottom. Drainage occurs because the coarse sandy soil was used to backfill the lysimeters. Data from this lysimeter complex has been used for model validation (bare soil) of UNSAT-H (Fayer and Gee 1985). A Bowen ratio station was operated at this site for a 1-month interval during 1987.

6.2.4 Field Lysimeter Test Facility. The Field Lysimeter Test Facility was built during 1987 near the HMS, to evaluate the effectiveness of barrier systems in limiting water infiltration (Kirkham et al. 1987). The facility contains 14 drainage lysimeters and 4 weighing lysimeters. An "as-built" document is available that provides detailed information on construction, instrumentation, and backfill soil properties (Gee et al. 1989). The texture of the lysimeter backfill soil is a silt-loam as compared to the natural fine sands found in the surrounding area; both soils have coarse gravels beginning at approximately 1 to 1.5 m. Two treatments are of particular interest to this work. Both receive natural rainfall; one has vegetation and the other has a bare soil surface. The treatments are located on weighing lysimeters, which will be described in detail in the next section. A Bowen ratio station was operated intermittently near this site during the growing season of 1989 and is referred to in plots with a site label of F_89.

6.3 Lysimeter Design

The lysimeters are a box-within-a-box. The outer box serves as a retaining wall for the surrounding soil and as a level base for a scale (Weigh-tronix, 9080-kg capacity). Four torsional "weighbars" (strain gauges) are used as the load-sensing element. These "weigh bars" are hermetically sealed and are wired in a bridge network with a sensitivity of 2-mV output signal per volt input at full load or 9090 kg. The scale is measured as a six-wire bridge with two wires for excitation, two for line resistance, and two for voltage output, with a sensitivity of 2-Mv output signal per volt input at full load. The resolution of the scales with signal averaging approaches 50 g or 14 W/m^2 under ideal calm wind conditions. All of the weighing lysimeters mentioned in the document follow the design of Kirkham et al. (1984).

The inner boxes have a top surface area of 1.5 by 1.5 m and range between 1.4 to 1.6 m in depth. Each inner box rests on a platform scale. The inner boxes of the last eight weighing lysimeters installed have sufficient structural integrity to be removed fully loaded if servicing of the platform scale is required. Spacing between the inner and outer boxes ranges between 5 and 15 cm, but in all cases is reduced to less than 1 cm by metal flanges at the surface. This spacing can be a source of error because too large an opening allows wind-blown material to be deposited adjacent to the scales. If the spacing is too narrow, the scale may "hang" because of differential thermal expansion of boxes, snow or ice bridging, or binding by sand and gravel particles. Elastic and packaging tapes were tested as coverings for the gap between inner and outer boxes, but these materials induce a variable loading force in response to surface temperature cycling, which is detected as a mass change. To date, only one lysimeter, located in a bare sandy soil area, has been removed because of excessive buildup of wind-blown soil in the bottom of the lysimeter next to the scales. The location of the lysimeters is shown in Figure 6.2.

6.4 Bowen Ratio

The BREB stations consist of two aspirated psychrometers mounted on an exchange mechanism. Both the exchanger and the aspiration fan use 12-volt motors. The switchable 5-volt logic produced by the data logger is used to actuate 12-volt relays and turn on the motors. Each psychrometer consists of a reservoir with the water level controlled by a float, two thermocouple temperature sensors, and two cylindrical radiation shields. The reservoir maintains a 1- to 2-cm head of water inside a ceramic wick surrounding one of the thermocouples. Water evaporates from the ceramic wick, cooling the wick to the wet bulb temperature. This temperature is measured by a thermocouple inside the wick. Air temperature is measured with a thermocouple, centered inside the inner radiation shield. Air is drawn continuously through the radiation shields to maintain the inner shield at air temperature, thus minimizing radiative energy flux to the thermocouple, and to the ceramic wick.

The Bowen ratio stations are similar in design to those described by Fritschen and Simpson (1982). Modifications include the use of thermocouples instead of platinum resistance elements for temperature measurement and the use of Campbell Scientific Inc. data

loggers (models CR-21X and CR-7). A CR-7 data logger operates at the G300 site year round, collecting hourly averages of soil and air temperatures and several other environmental variables. The program was modified during the spring to activate the Bowen ratio exchange mechanism and record data from additional sensors every 15 min.

The energy flux density (W/m^2) is measured with horizontal sensors as follows: R_N with net radiometers of the Fritschen design from Micromet Inc. and Radiation Energy Budget Systems (REBS) model (Q3); R_S with Eppley precision pyranometers; and soil heat flux (G) with soil heat flux plates (HFT-1 and -2) from REBS Inc. In 1987 and 1988, $R_L\uparrow$ was determined from an Everest IR sensor pointed approximately 15° off vertical in a southsouth west direction at the bunchgrass and sagebrush sites.

6.5 Satellite Data

Six Landsat scenes are available coinciding with ET measurements either from BREB stations or lysimeters. They were acquired 8-May-86, 11-May-87, 8-May-89, 1-Jun-89, 28-Feb-90, and 1-Apr-90 from path row 44/28. All scenes were collected with Landsat 5 except for 8-May-89 scene collected with Landsat 4. These images were obtained from the Earth Observation Satellite Company. The gains and offsets for the visible bands on each satellite are nearly identical and Table VI.2 contains the gains and offsets used with all scenes. The quadrant 1 centers vary slightly about values of 46.48 latitude and -119.75 longitude. The 8-May-89 image data is corrected for atmospheric conditions with the LOWTRAN 6 code (Kneizys et al. 1983), using local radiosonde data and ground-based thermal measurements (Gibbons et al. 1990). A subset of pixels with dimensions of 1361 by 600 (41 by 18 km) was selected from the 8-May-89 image. Identical coverage areas were selected from the remaining images by minimizing the differences apparent when subtracting the 8-May-89 image from each of the other images. A false color IR image is simulated using bands 4, 3, and 2 for each date, displayed as red, green, and blue, respectively in Figure 6.3. The image dates proceed left to right starting with 8-May-86 in the upper left and 1-Apr-90 in the lower right.

TABLE VI.2. Gains and Offsets for Landsat TM Bands 1 Through 7.

Landsat 4 and 5		mW/cm^2 sr. μm	
TM Band	Wavelength (μm)	Gain	Band
1	0.45 to 0.52	0.060235	-0.15
2	0.52 to 0.60	0.11749	-0.28024
3	0.63 to 0.69	0.08059	-0.120289
4	0.76 to 0.90	0.08145	-0.150397
5	1.55 to 1.75	0.01081	-0.037037
6	10.4 to 12.5	0.0056322[a]	+0.1238[a]
7	2.08 to 2.35	0.005697	-0.0148

(a) Proposed by Markham and Barker (1986).

This presents the information in chronological order. This same order continues in subsequent multi-image figures except where noted otherwise. Limited ground truth and atmospheric data are available to perform atmospheric corrections (Table VI.3).

The increased reflectance of the near IR (band 4) by vegetation appears as a more intense red color in both Figures 6.2 and 6.3. In general, the amount of vegetation increases with elevation as does precipitation. Elevation is shown in Figure 6.4 as both a colored relief and as an extract of U.S. Geological Survey 7.5 min., Snively Basin, Washington quadrangle near the 350-m contour of Rattlesnake Ridge encompassing the bunchgrass (b), sagebrush (c), and Lower Snively (d) field sites used in this project. Site slopes are less than 5% as determined from the U.S. Geological Survey map.

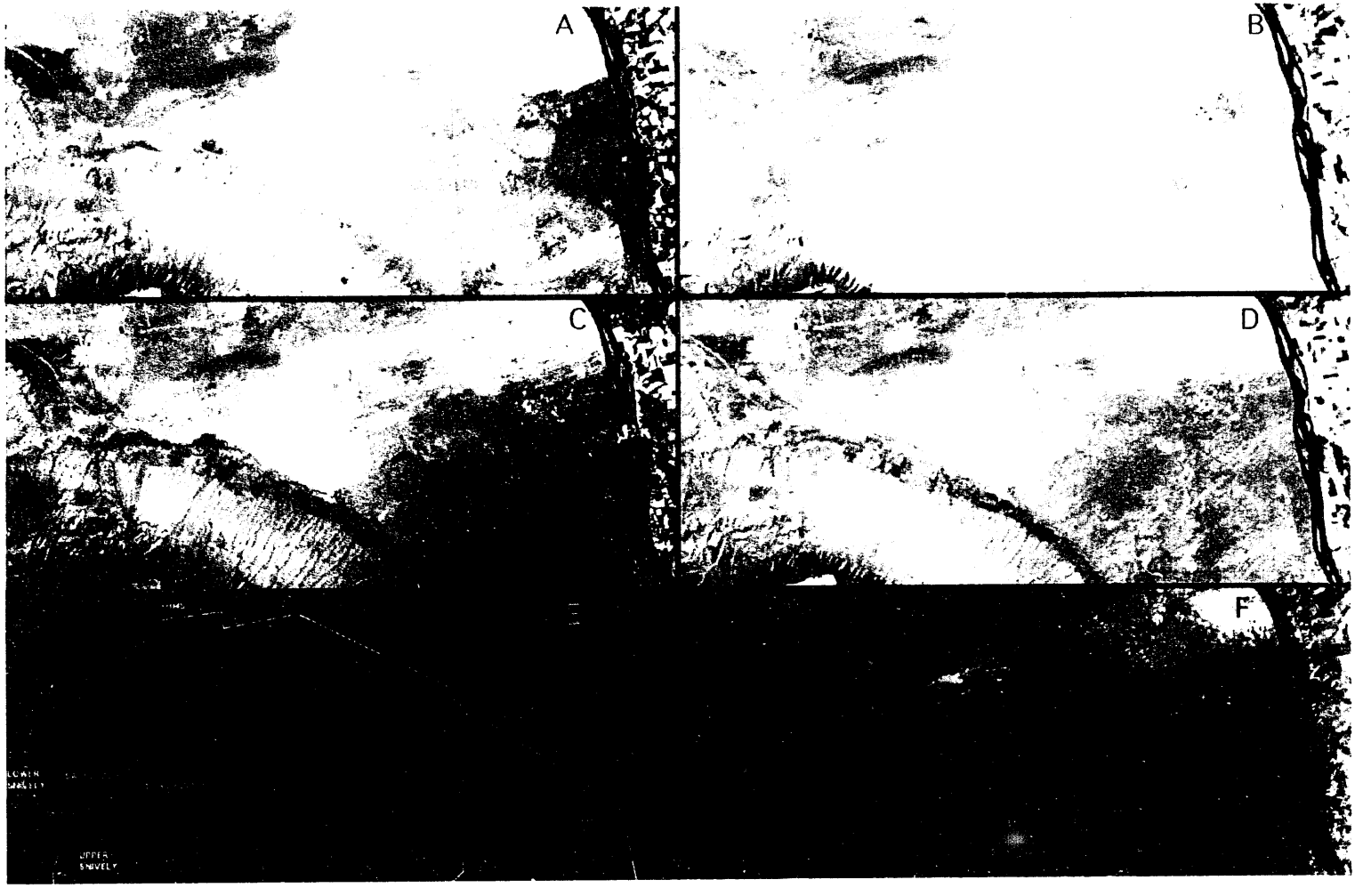

FIGURE 6.3. Simulated False Color IR for Landsat Subscenes of the Hanford Site, a) 8-May-86, b) 11-May-87, c) 8-May-89, d) 1-June-89, e) 28-Feb-90, f) 1-Apr-90.

TABLE VI.3. Atmospheric Corrections and Columbia River Temperatures for Six Landsat Overpasses.

Image Date	Image Source Path/Row 044/028	Atmospheric Corrections		Columbia River[c] Temperature
		Transmittance	Radiance	(°C)
8-May-86	TM5	0.855[a]	0.092[a]	9.5
11-May-87	TM5	0.87[b]	0.09[b]	11.4
8-May-89	TM4	0.832[a]	0.106[a]	11
1-Jun-89	TM5	0.89[b]	0.09[b]	13
28-Feb-89	TM5	0.86[b]	0.09[b]	4
1-Apr-90	TM5	0.89[b]	0.09[b]	6.5

(a) Lowtrans 6 results provided by with Guy McWethy, Technical Specialist, Pacific Northwest Laboratory.
(b) Values of transmittance and radiance were adjusted until temperature estimated from river pixels matched reported river temperatures.
(c) EarthInfo Inc. 1992.

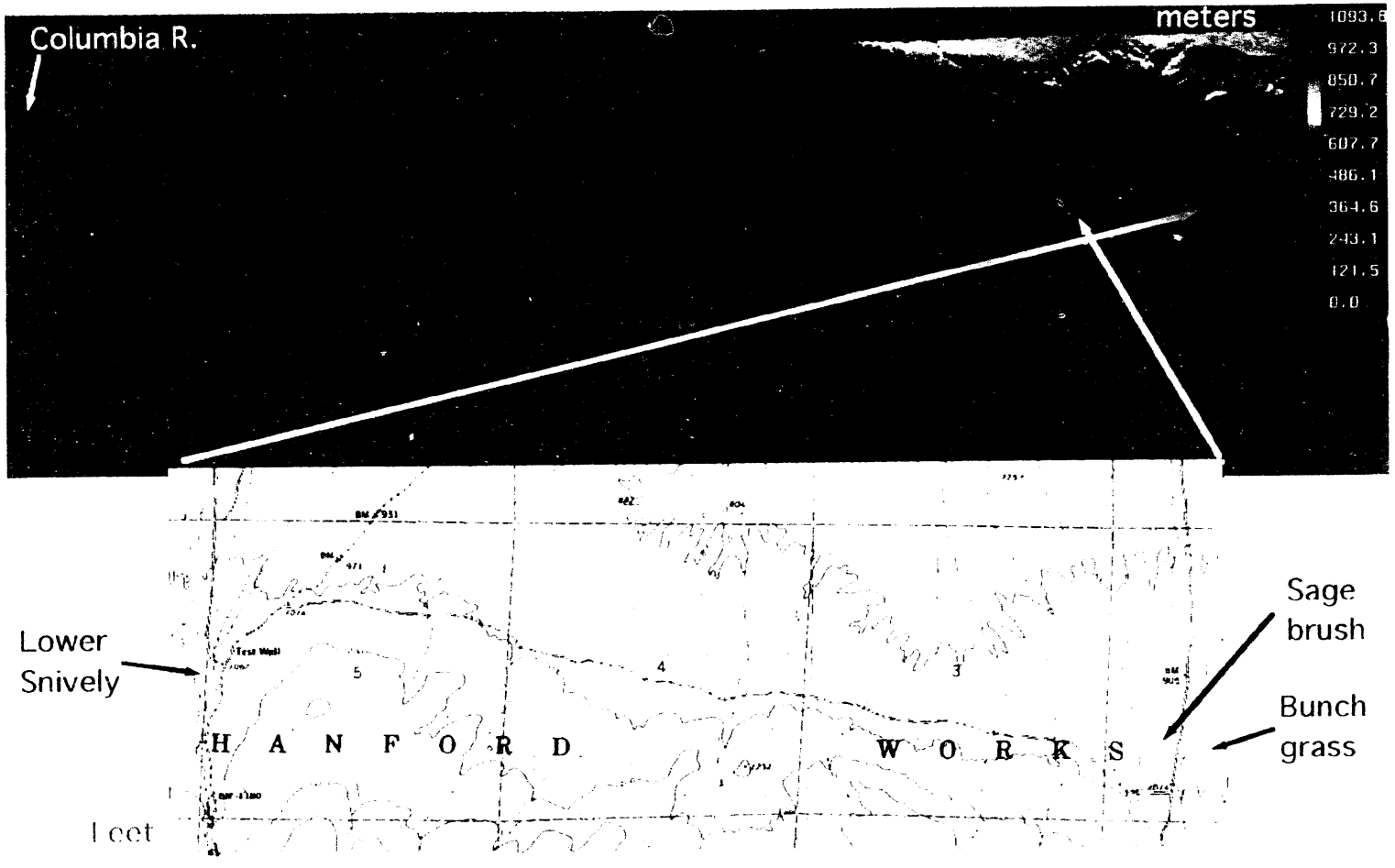

FIGURE 6.4. Digital Elevation Map and Portion of USGS Snively Basin, Washington, 7.5 Quadrangle of the Hanford Site.

7.0 Results

Before developing maps of the energy balance components for the Hanford Site, it is important to determine if the measurement methods, neutron probe, lysimetry, and BREB, that inherently make measurements at different scales provide similar results. Additionally, before using remotely sensed estimates of sensible heat flux, the mathematical relationships describing net radiation, soil heat flux, and sensible heat flux as functions of $R_S\downarrow$, $R_L\uparrow$, or NDVI must be validated for the semi-arid site. Data collected 1986 and 1990 have been used to check energy flux measurement methodology and to calibrate a sensible heat transport equation for use with satellite data from the same time period. The results are presented in order as follows, method comparison, equation calibration, and comparison of predicted and measured values of sensible heat flux density.

The following sections will show that the lysimeters are highly correlated with both neutron probe and BREB results. Then, the BREB energy flux measurements (R_N and $R_S\uparrow$) are shown to be in good agreement with Landsat-based estimates of the same quantities. The satellite estimates of energy balance require an estimate of soil heat flux density, and data collected during four Landsat overflights indicate that the use of a single equation (equation 16 or 18) does not effectively predict G_T as a function of NDVI. To continue the analysis, measured values of G_T at the time of satellite overflight are used. Calibration of the sensible heat flux equation requires surface temperature measurements that are only available in 1988. The BREB data is intermittent during 1988; hence, lysimeter data is used in place of BREB latent heat flux estimates.

The combined BREB and lysimeter data are used with the energy budget equation (equation 2), sensible heat flux equation (equation 9), and two forms of the aerodynamic resistance equation (equation 10) to determine suitable values of canopy height (h) and a value for the kB^{-1} term appropriate for grass- and sagebrush-covered areas of the Hanford Site. Finally, measured values of sensible heat flux at the time of Landsat overpasses are compared with Landsat-based estimates.

7.1 Direct Measurements of Energy Balance Components

Lysimeters generally provide continuous data, a significant attraction, but because the volume of the lysimeter is small, the data may not be representative of the surrounding environment. A detailed continuous record of lysimeter weight change or water balance has been obtained from the Hanford lysimeters. The semi-arid Hanford Site water balance is characterized by an annual cycle of winter precipitation accumulation and spring-summer ET loss. This annual cycle is apparent in all Hanford weighing lysimeters (Figure 7.1). The water loss curves for each lysimeter are set to 0 cm of water on 15-Aug-90 to facilitate comparison between lysimeters of different total weight. The SWL lysimeter shows the greatest change in storage because 1.0 cm of drainage was removed primarily during the spring of 1989. The Arid Lands Ecology Reserve lysimeters received supplemental moisture to maintain plant vitality during construction, resulting in increased water loss during the spring and summer of 1987. Thus, lysimeter data from 1987 is limited to providing an upper limit of latent energy loss or conversely a lower limit of sensible heat flux.

Determining whether lysimeter data can be used to estimate actual water loss from a soil-plant system is best answered by examining the performance of the lysimeters at two temporal scales against two independent estimates of latent heat flux. Estimates of daily latent heat flux density by (1) the sum of rainfall and monthly changes in soil moisture storage (monthly neutron probe data) or (2) the sum of rainfall and weight changes (midnight weighing lysimeter values) are in good agreement in 1989 (Table VII.1). A least-squares regression applied to these data sets yields regression coefficients of 0.96 and 0.88 with R^2 of 0.93 and 0.94 for the bunchgrass and sagebrush, respectively.

Also, hourly measurements of latent heat flux obtained from the BREB and lysimeters can be compared. Comparable data sets for three days in 1988 for bunchgrass and sagebrush are shown in Figures 7.2 and 7.3, respectively. The BREB 15-min values have been averaged and are reported as hourly values to coincide with hourly lysimeter values. The least-squares regression coefficient is 0.94 between the average of the two bunchgrass lysimeters and BREB data, with a correlation of $R^2 = 0.74$. The least-squares regression coefficient is 0.89 between the average of the two sagebrush lysimeters and the BREB, with a correlation of

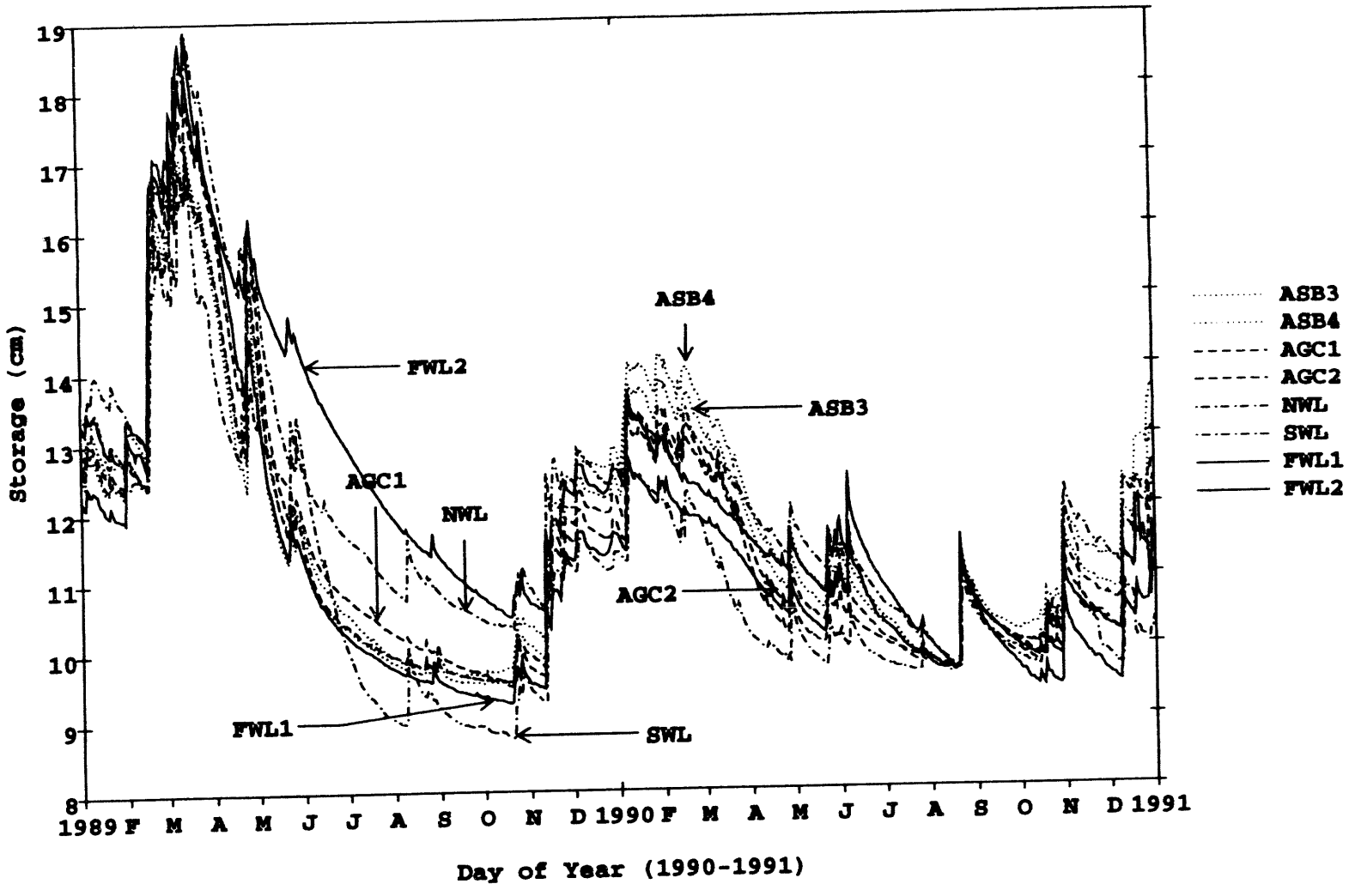

FIGURE 7.1. Lysimeter Total Storage Values for 1989 Through 1990.

TABLE VII.1. Average Daily Latent Heat Flux Determined from Weighing Lysimeters and Neutron Moisture Probes for the Bunchgrass and Sagebrush Sites.

	Date	Total Storage (cm)	Storage Change (cm)	Interval (Days)	Rain (cm)	Rain+ Storage (cm)	ET[a](cm) Neutron Probe	Lysimeter (cm)
Bunchgrass	23-Mar-89	28.46						
	25-Apr-89	26.33	2.13	33	0.89	3.02	0.10	0.13
	25-May-89	24.64	1.69	30	3.96	5.65	0.18	0.18
	29-Jun-89	23.40	1.25	35	0.42	1.67	0.05	0.05
	28-Jul-89	22.94	0.46	29	0.05	0.57	0.02	0.02
	28-Aug-89	22.60	0.34	31	0.48	0.82	0.03	0.03
	26-Sep-89	22.44	0.16	29	0.23	0.39	0.02	0.02
Totals							0.40	0.43
Sagebrush	23-Mar-89	28.55						
	25-Apr-89	25.60	2.95	33	0.89	3.84	0.12	0.14
	25-May-89	23.74	1.86	30	3.96	5.82	0.19	0.16
	29-Jun-89	22.55	1.19	35	0.42	1.61	0.05	0.04
	28-Jul-89	21.97	0.58	29	0.05	0.63	0.02	0.02
	28-Aug-89	21.59	0.37	31	0.48	0.85	0.03	0.03
	26-Sep-89	21.54	0.05	29	0.23	0.28	0.01	0.02
Totals							0.42	0.41

(a) ET = Evapotranspiration

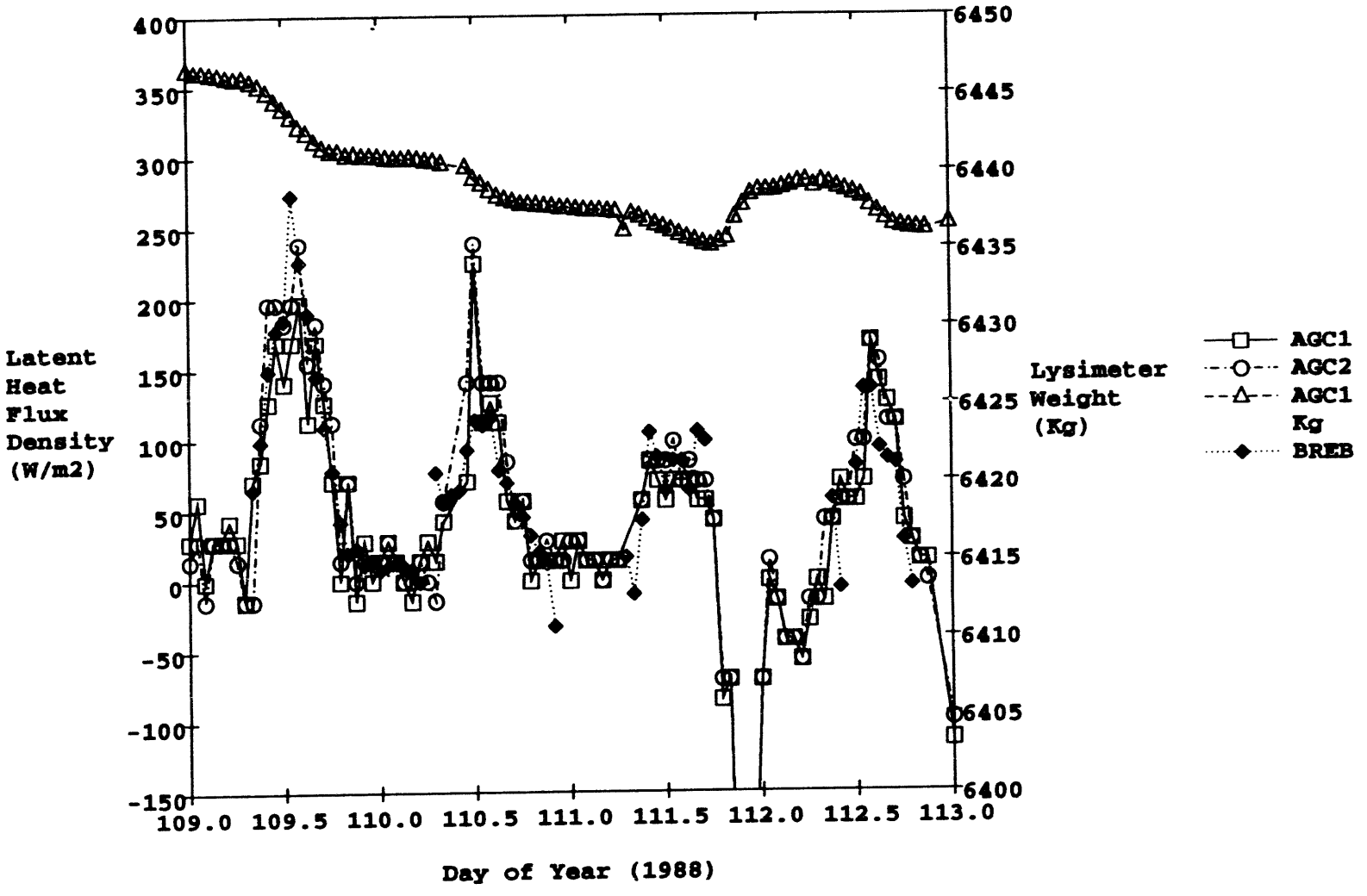

FIGURE 7.2. Lysimeter (AGC1 and AGC2) and BREB Latent Heat Flux Values, and Lysimeter (ASB3) Weight (Triangle) for the Bunchgrass Site for April 19-21, 1988 (days 109-112).

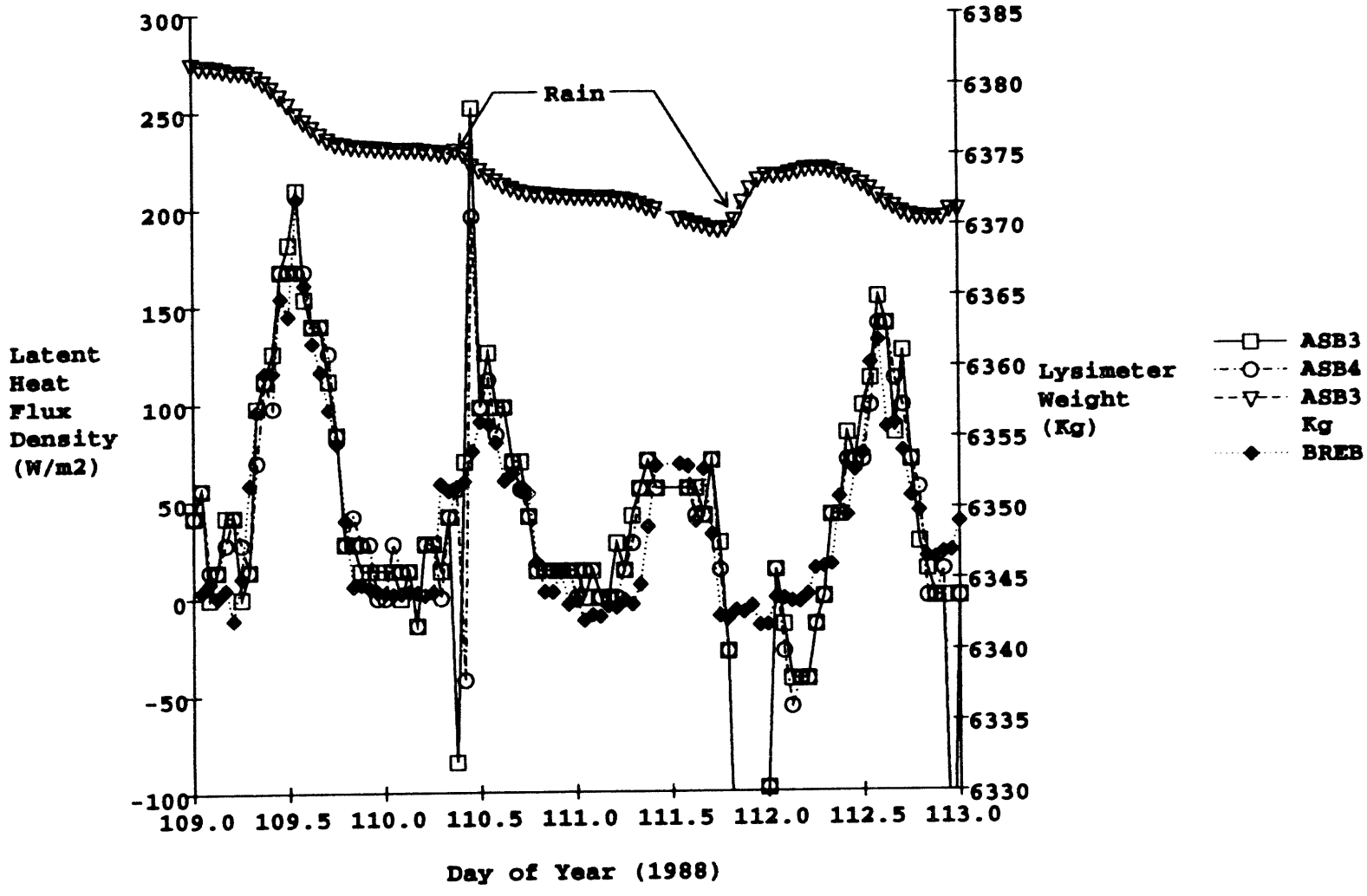

FIGURE 7.3. Lysimeter (ASB3 and ASB4) and BREB Latent Heat Flux Values, and Lysimeter (ASB3) Weight (Inverted Triangle) for the Sagebrush Site for April 19-21, 1988 (days 109-112).

$R^2 = 0.81$. At both sites, the BREB slightly underestimates the lysimeters (a net radiometer error explains part of this difference, see Section 7.2.4). Much of the measurement variability occurs during periods of lower energy flux. Hourly data sets from 1989 depicting the good correlation between lysimeters and BREB are also shown in Section 7.5.

These two measurement systems are in good agreement and either system can be used to estimate surface energy fluxes for comparison with satellite overflights.

7.2 Remote Estimates of Radiation Terms

The raw satellite DNs are converted to spectral radiance values then corrections are applied for sun angle, atmospheric transmission, and atmospheric irradiance. The complete set of equations used for these conversions are in Appendix B. Finally, the values are reported as irradiances with units of watts per square meter (W/m^2).

7.2.1 Remote Estimates of $R_S\uparrow$. The radiation measured by the six visible radiation bands is only a fraction of the total visible radiation reflected from the surface. Therefore, a multiplication factor of 2.54 was required to scale the summed Landsat visible bands to a value equivalent to the measured $R_{S\uparrow}$ from the inverted Eppley pyranometers. This multiplication factor is larger than the factor of 2 reported by Jackson (1984). This is because the eight-band Barnes multi-modular radiometer used by Jackson had one more band in the visible range than is available in the Landsat data. As suggested by Jackson (1984), band 1 (high background from atmospheric scatter) was removed from the summation.

The 8-May-89 and 1-Jun-89 estimates of short-wave radiation reflected from the surface correlate well ($R^2 = 0.77$) with reflected radiation estimated using inverted Eppley pyranometers (Figure 7.4). Values for $R_S\uparrow$ are calculated for the entire set of images using the 8-May-89 atmospheric correction (minor differences introduced by changes in atmospheric transmittance would not be visible in these color-scaled images) with the results shown in Figure 7.5. In all images, the bare soil associated with the sand dunes has the highest values of $R_S\uparrow$. Figure 7.5e is darker blue, as expected, because of low sun angle with most of the $R_S\uparrow$ values below 60 W/m^2 in late February. The 1-Jun-89 image also indicates more reflectance

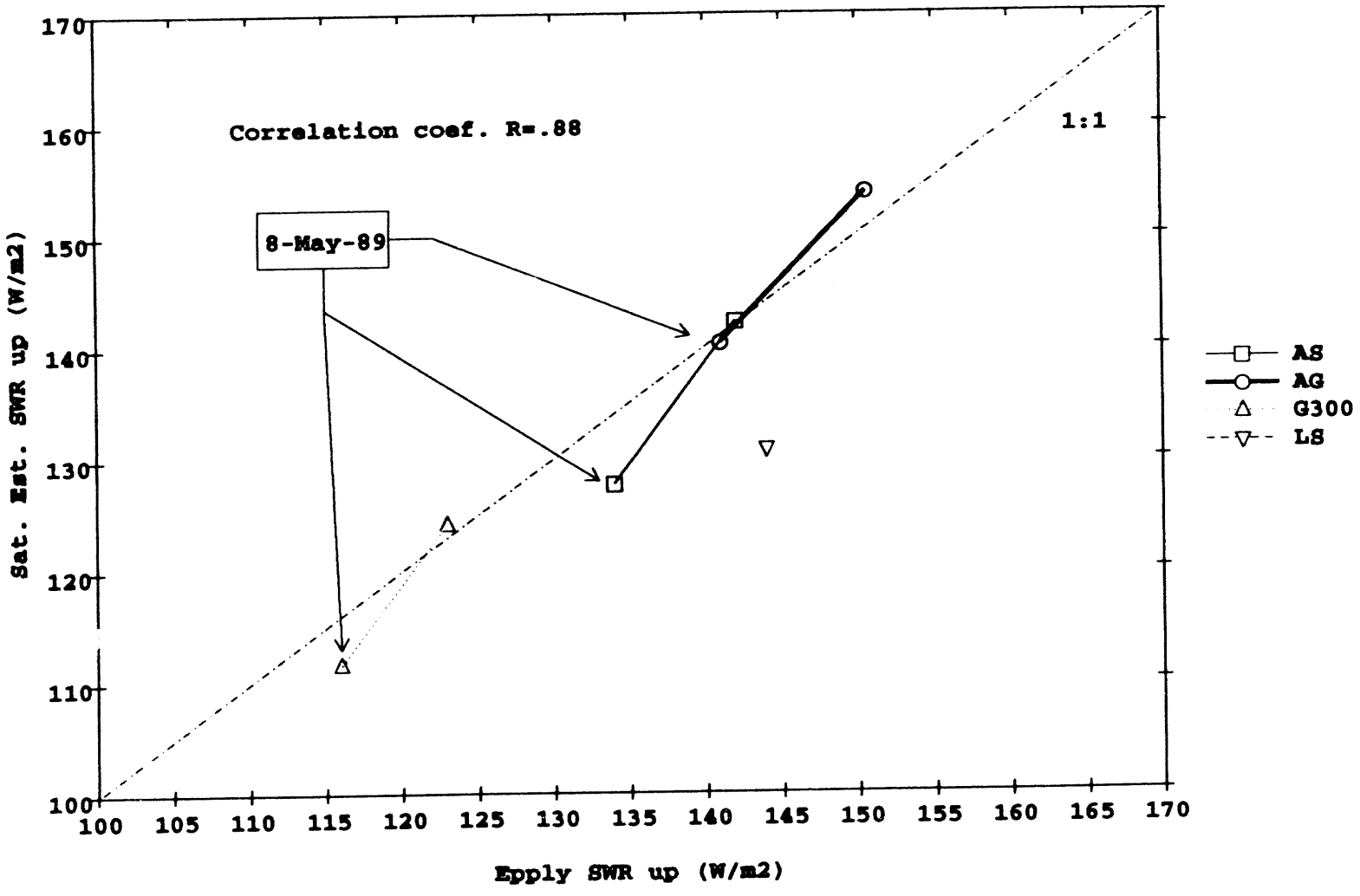

FIGURE 7.4. Landsat-Based Estimates and Measured Short-Wave Reflected Radiation for 8-May-89 and 1-Jun-89 Overflights.

FIGURE 7.5. Landsat Bands 2, 3, 4, 5, 7 Combined to Estimate Reflected Short-Wave Radiation for Six Dates.

than the 8-May-89 image, consistent with the vegetation senescence. The mean and variance for each image is contained in Table VII.2. The difference in mean reflectance between the three May images can be explained by climatic conditions: 8-May-86 (warm and wet) has low $R_S\uparrow$, 11-May-87 (hot and dry) has the highest $R_S\uparrow$, and 8-May-89 (warm and wet) has the lowest $R_S\uparrow$. The growing degree day value was higher for 11-May-87 (Figure 6.1) and the mean NDVI for the G300 site (Figure 7.17) was lower, both indicating early plant senescence.

TABLE VII.2. Image Means and Variances of Reflected Short-Wave, Long-Wave, and Net Radiation.

Date	$R_S\uparrow$		$R_L\uparrow$		R_N	
	Mean	s^2	Mean	s^2	Mean	s^2
8-May-86	139	26				
11-May-87	150	25				
8-May-89	129	22	592	44	423	54
1-Jun-89	139	23	597	40	460	52
28-Feb-90	71	14				
1-Apr-90	105	17				

7.2.2 Remote Estimates of $R_L\uparrow$. Long-wave radiation leaving the surface is estimated from the thermal (band 6) of Landsat. Band 6 measures radiation in the 10.4- to 12.5-μm wavelength interval. These values are reported either as $R_L\uparrow$ or as surface temperature using the Stefan-Boltzmann law. The calculation of $R_L\uparrow$ from band 6 DN values is in Appendix B. Direct measures of $R_L\uparrow$ are not available for this data set; therefore, the goodness of fit of this data set is evaluated indirectly by the goodness of fit of the R_N data.

Estimates of $R_L\uparrow$ for five Landsat images consistently show lower values at higher elevations and over water or irrigated surfaces (Figure 7.6). The mean and variance of $R_L\uparrow$ for each image is found in Table VII.2. The Landsat image uses a 120 by 120 m pixel size for the thermal band, which is about the same distance as that found between erosional features near the Arid Lands Ecology Reserve lysimeters. The limited thermal resolution of Landsat relative to the study sites is apparent in Figure 7.7 where a subset of both an 11-May-87 Landsat image (inset) and a subset of a high resolution aircraft thermal band image acquired 10-May-87 at 1330 hours of a small area left (east) of the highlighted roads are presented.[a] The ephemeral stream beds are rocky, with sparse vegetation, 2 m below grade, and as indicated by the Daedalus scanner have a surface temperature about 5°C higher than the surrounding bunchgrass areas. The pixel size in the aircraft data is approximately 1 m at the left edge with the x-axis increasing to the right. Near the center-bottom of the image, a faint oval is visible corresponding to the vehicle turnaround. Just below the turnaround, the cool spots represent the lysimeters and a large solar panel array. The 1000 and 1100 hours (24-hour clock) values for surface temperature (IR thermometer) of the lysimeter are 47.7 and 49.1°C. The 1000 and 1100 hours values from the 1-cm soil thermocouple located off the lysimeter are 52.6 and 52.7 °C, respectively. In general, the aircraft data values for surface temperature at this location are very similar to the 1-cm soil temperatures. The 1987 surface IR data are not used to develop aerodynamic transport equations because the supplemental moisture added during lysimeter construction supported a higher ET rate and a cooler surface through much of 1987. The 1988 lysimeter data are much more representative of the surrounding area. A composite of 1988 Everest IR and 1-cm soil temperatures (to approximate the radiometric temperature) are used to calibrate aerodynamic transport equations in a later section. Variations in emissivities between vegetation and soils are ignored for two reasons. First, the emissivity effects would be similar for the IR sensor and the satellite thermal band data. Second, the 1-cm soil temperature used as an analogue for soil surface temperature is potentially a greater source of error than the emissivity effects.

(a) Acquired with Daedalus AADS1268 scanner, data supplied by Dr. Lee Balick, EG&G, Las Vegas, Nevada.

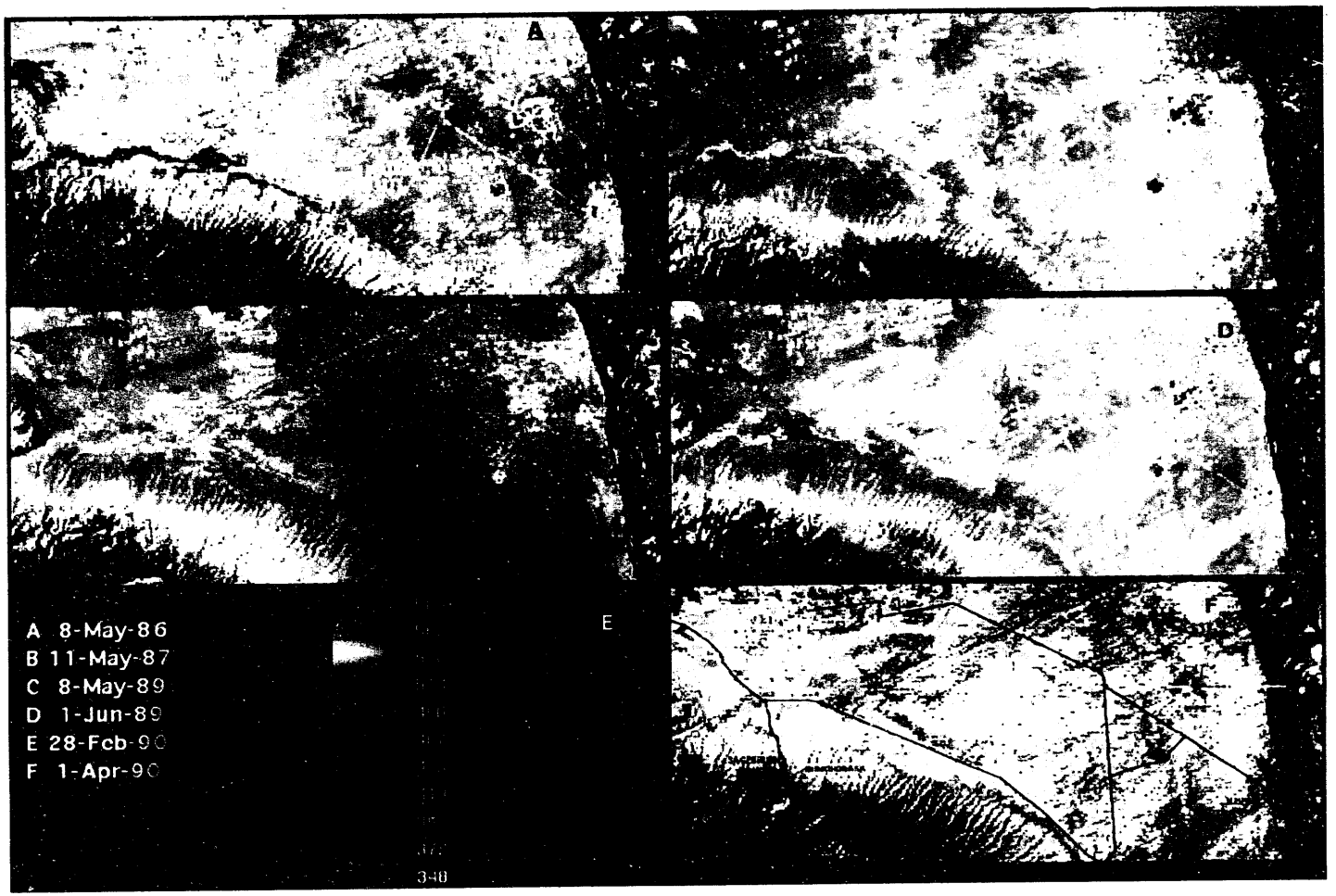

FIGURE 7.6. Estimated $R_L\uparrow$ (W/m^2) from Band 6 of Landsat Images for a) 8-May-86, b) 11-May-87, c) 8-May-89, d) 1-Jun-89, e) 28-Feb-90 not shown, f) 1-Apr-90.

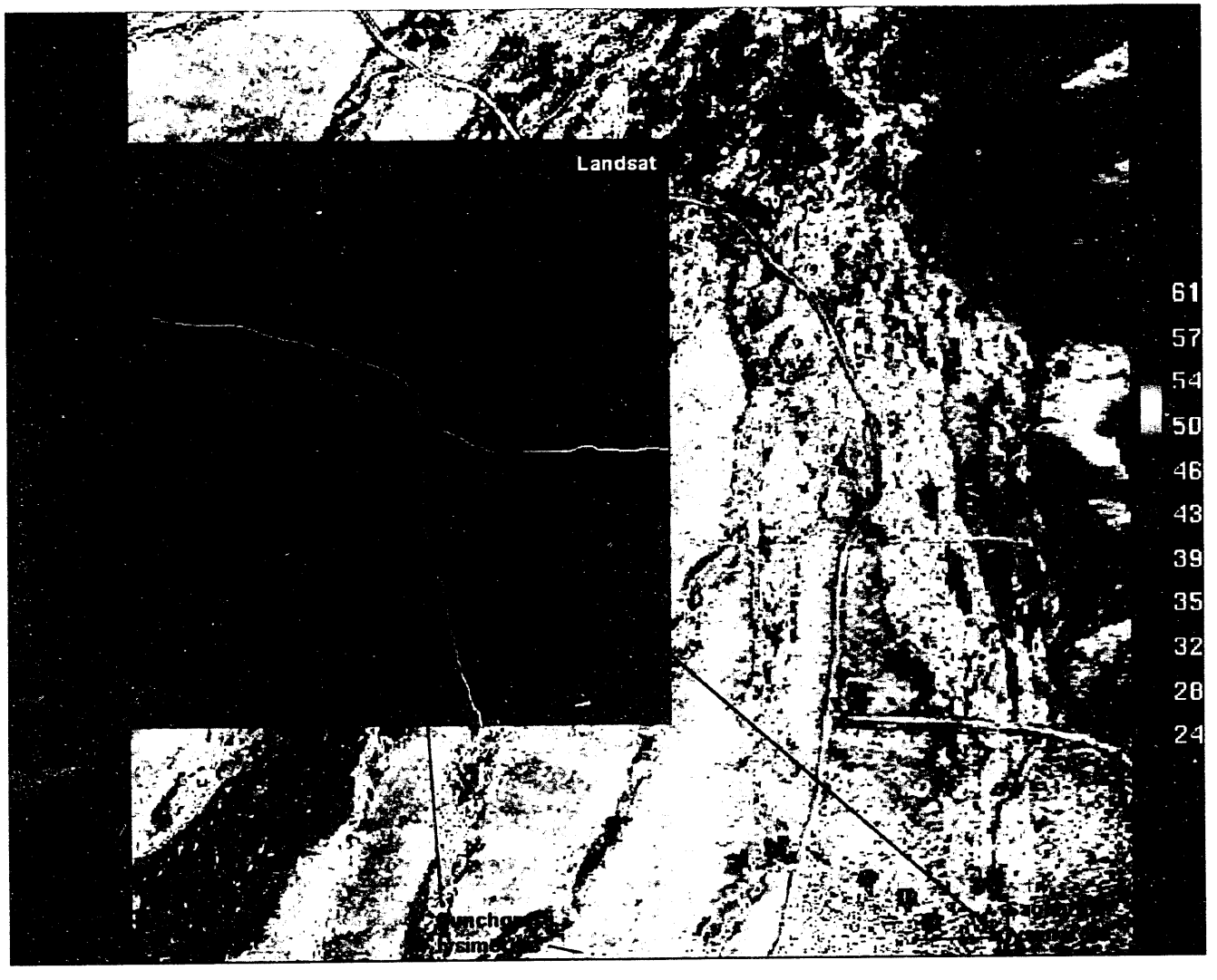

FIGURE 7.7. Bunchgrass and Sagebrush Site View by Landsat Thermal Band Subset 8-May-87 (1030 hours) and Aircraft Daedalus (1215 m) Thermal Band (1313 hours).

7.2.3 Remote Estimates of Incoming Long-Wave Radiation. Long-wave or sky radiation is emitted by the atmosphere and clouds both to space and downward toward the earth's surface. It is a significant component of the surface energy balance easily reaching values of 300 or 400 W/m^2. Using equations 17 and 18, we can estimate $R_L\downarrow$ and compare it against measured $R_L\downarrow$ for the G300 site on April 7, 10, 21, 1988 (Figure 7.8). There is good agreement between measured and estimated values in general with a correlation coefficient of $r^2 = 0.87$.

Values for 1030 hours (24-hour clock) appear to be near a crossover point between under and over estimating $R_L\downarrow$ by equation 17. Site T_{air} differences are minimal at 1030 hours (Figure 7.9). This is good for Landsat scenes but the estimation of $R_L\downarrow$ for satellites passing over at different times of the day would possibly need to include temperature variation across the scene. Also, the diurnal cycle is advanced at the bunchgrass and sagebrush sites. In addition, the slightly northwest aspect (or adjacent areas with pronounced aspect and slope differences) and higher elevation cause the Arid Lands Ecology Reserve sites to warm and cool earlier in the day compared with the lower elevation G300 site. Air temperatures from the Arid Lands Ecology Reserve and G300 sites between the hours of 1000 and 1100 hours indicate that the sagebrush site is several degrees warmer than the bunchgrass site, and that the T_{air} measurements for G300 are warmer than for bunchgrass (Figure 7.10). The difference between sagebrush and bunchgrass is caused by a greater heat exchange higher in the sagebrush canopy. The difference in T_{air} between bunchgrass and G300 sites, which have similar roughness, is close to the difference expected for the elevation difference times the adiabatic lapse rate.

7.2.4 Field and Remote Estimates of Net Radiation. As a check on the methodology for estimating R_N from individual radiation terms (used in remote sensing applications), measured and estimated R_N values were compared for data collected in 1987 and 1988 at the bunchgrass site. Linear equations were fit to $R_S\downarrow$ and R_N for radiation values obtained between 1000 and 1100 hours between day of year (DOY) 130 to 147 in 1987 and DOY 119 to 128 in 1988. The data points, the fitted equations, and R^2 values are shown in Figure 7.11. In examining the linear relationships between estimated $R_N\downarrow$ and measured R_N, it is apparent that a linear equation relating $R_S\downarrow$ to R_N (Figure 7.11) performs well ($R^2 = 0.98$ and $R^2 = 0.99$) but

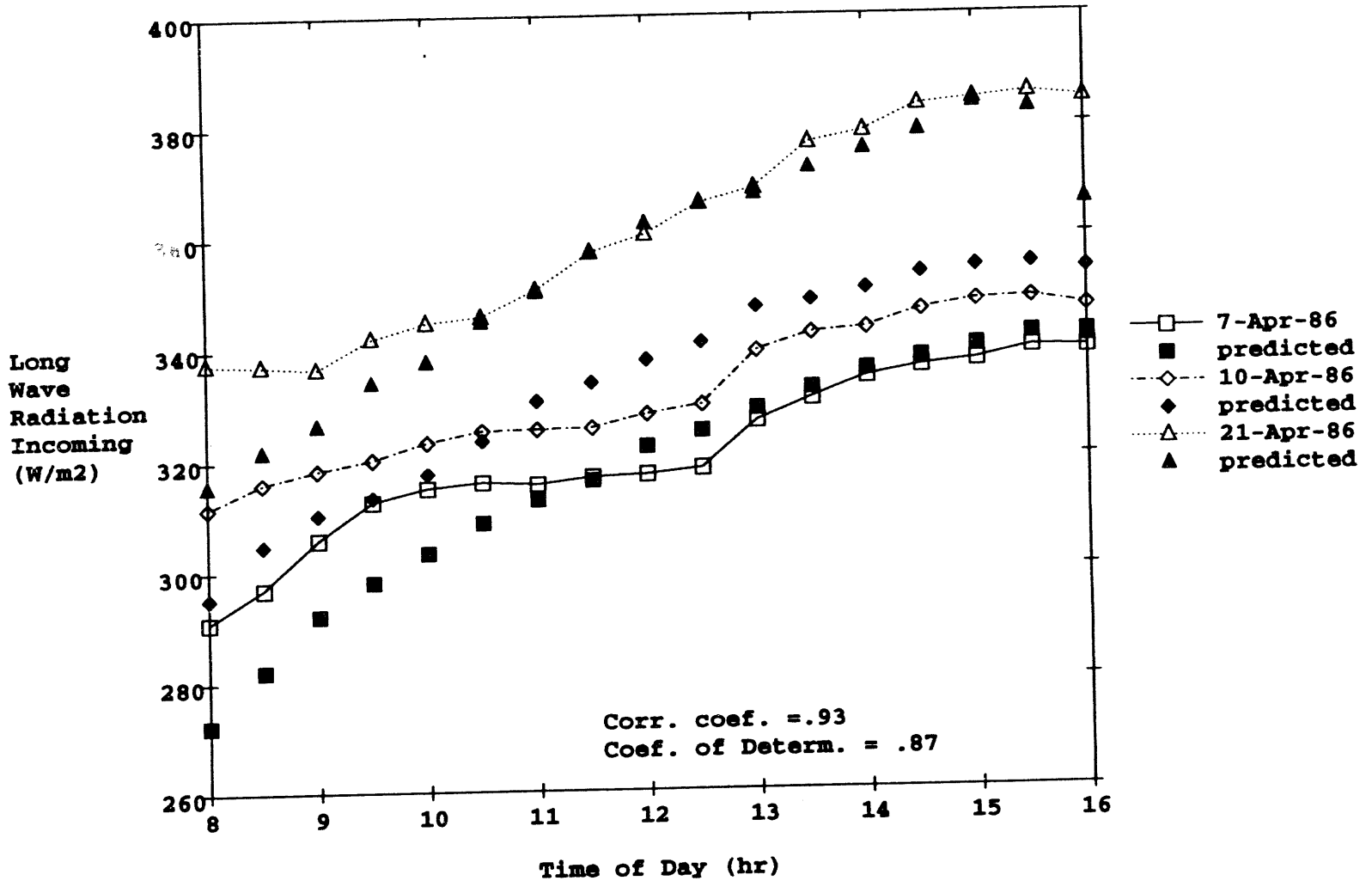

FIGURE 7.8. Measured and Estimated Incoming Long-Wave Radiation for the G300 Site on April 7, 10, and 21, 1988.

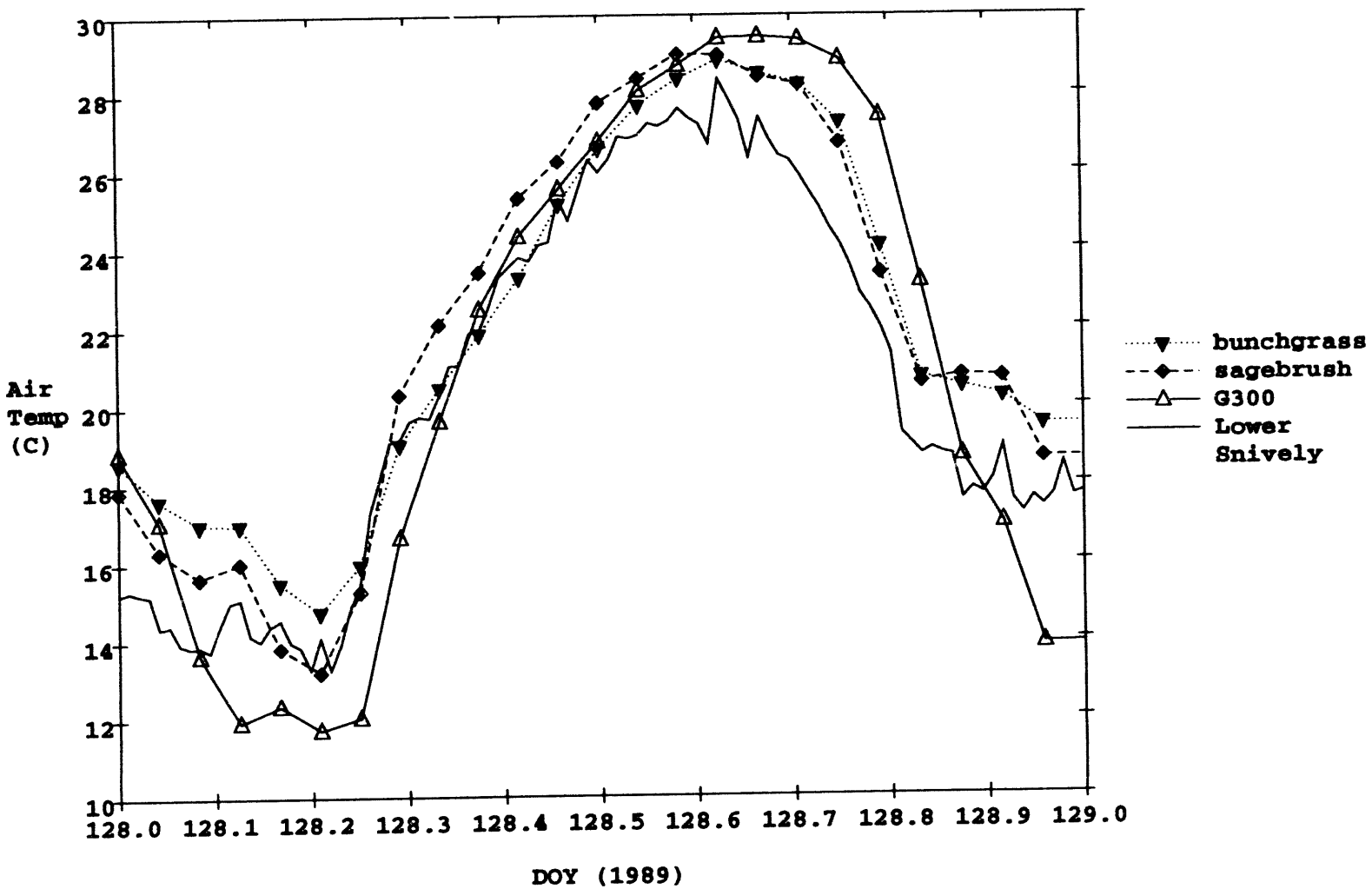

FIGURE 7.9. Diurnal Air Temperature Cycle for Four BREB Systems on 8-May-89.

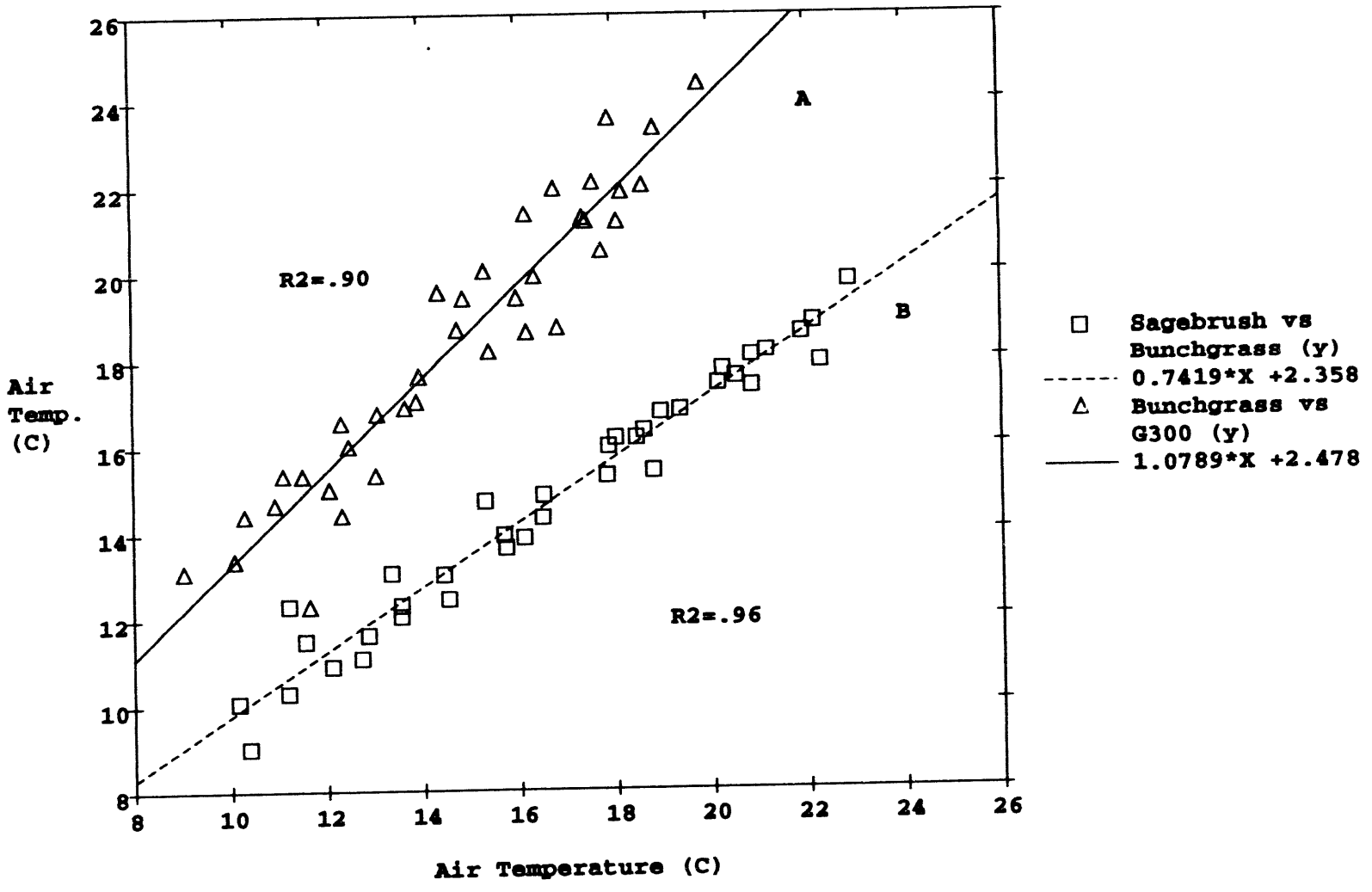

FIGURE 7.10. Comparison of Air Temperatures Between a) Sagebrush and Bunchgrass, b) Bunchgrass and G300 Sites, April 1988 (1000 to 1100 hours).

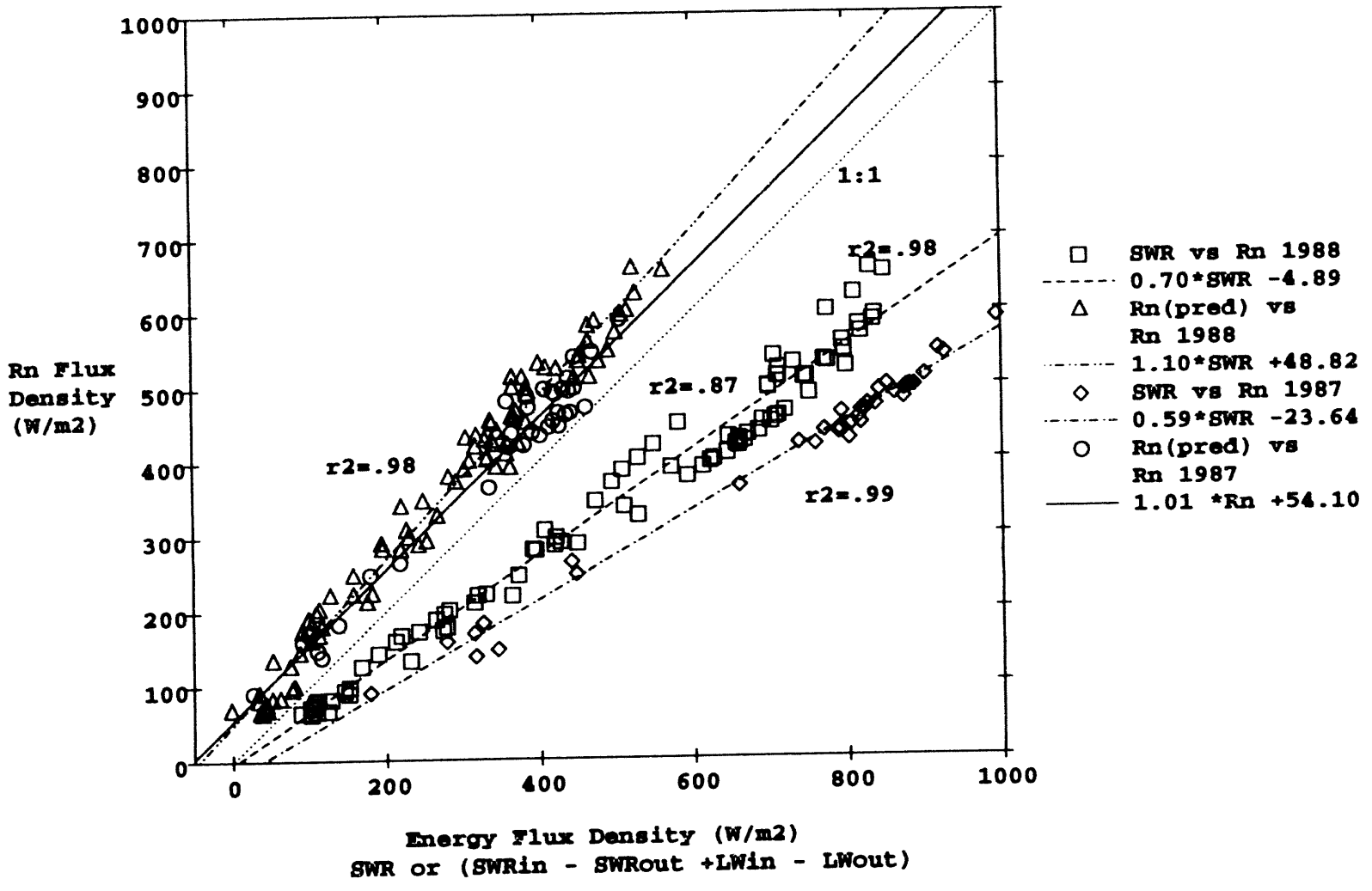

FIGURE 7.11. Incoming Short-Wave Radiation Compared to Net Radiation and the Estimate of Net Radiation Versus the Net Radiation for 1987 and 1988.

is specific to the site and the conditions at the site. The relationships are slightly different for each year, because of differences in the site albedo and mean temperature. The 1988 temperature values are consistently higher than the 1987 data by the following amounts: 1-cm soil, 8.1; air, 4.7; and surface IR, 8.2°C. The mean calculated $R_L\uparrow$ is also 50 W/m^2 higher in 1988. This difference is about the same as the average difference in offset between the two least-squares fitted equations for 1987 and 1988 values of R_S and R_N. The mean of $R_L\downarrow$ estimates differ by 4 W/m^2 and thus is not contributing to the offset in estimated R_N. To improve the estimate of R_N, estimates of $R_S\uparrow$ and $R_L\uparrow$ from either surface instruments or remotely sensed data is needed as input into equation 15. The revised estimates of R_N (Figure 7.11) are much better because both years data sets overlap and are near the 1:1 line. Variability has increased with the addition of two more measurements but the least squares regression coefficients are 1.0 and 1.1 and R^2 = 0.87 and 0.98.

Also Figure 7.11 and the offset of the equation relating R_N (predicted) to the measured R_N show that R_N is approximately 50 W/m^2 higher than the four-term estimate of R_N. Much of this difference is accounted for in recent cross-calibrations reported by Field et al. (1992). They find that long- and short-wave sensitivity as compared to a four-instrument radiation-balance measurement differ substantially for the REBS Q3 and Micromet Systems net radiometers used in this study.

The same analysis using air-temperature-based estimates of $R_L\downarrow$ and Landsat temperature measurements ($R_L\uparrow$) was used to calculate R_N values for five sites on May 8 and June 1 corresponding to Landsat overpasses (Figure 7.12). The correlation coefficient is R^2 = 0.97 between predicted and measured R_N for May data (site label at May value). The June data shows more scatter, and when combined with May data and forced through zero, the regression coefficient decreases to R^2 = 0.66. Similar to the previous ground-based estimates of net radiation, the satellite-based estimates are generally less than measured values by 40 to 50 W/m^2. As mentioned earlier, much of this offset can be accounted for by revised net radiometer calibrations.

The measured R_N values for the 1989 satellite overflight days are compared with satellite-based estimates of R_N in Figure 7.12. Note, 8-May-89 and 1-Jun-89 have air

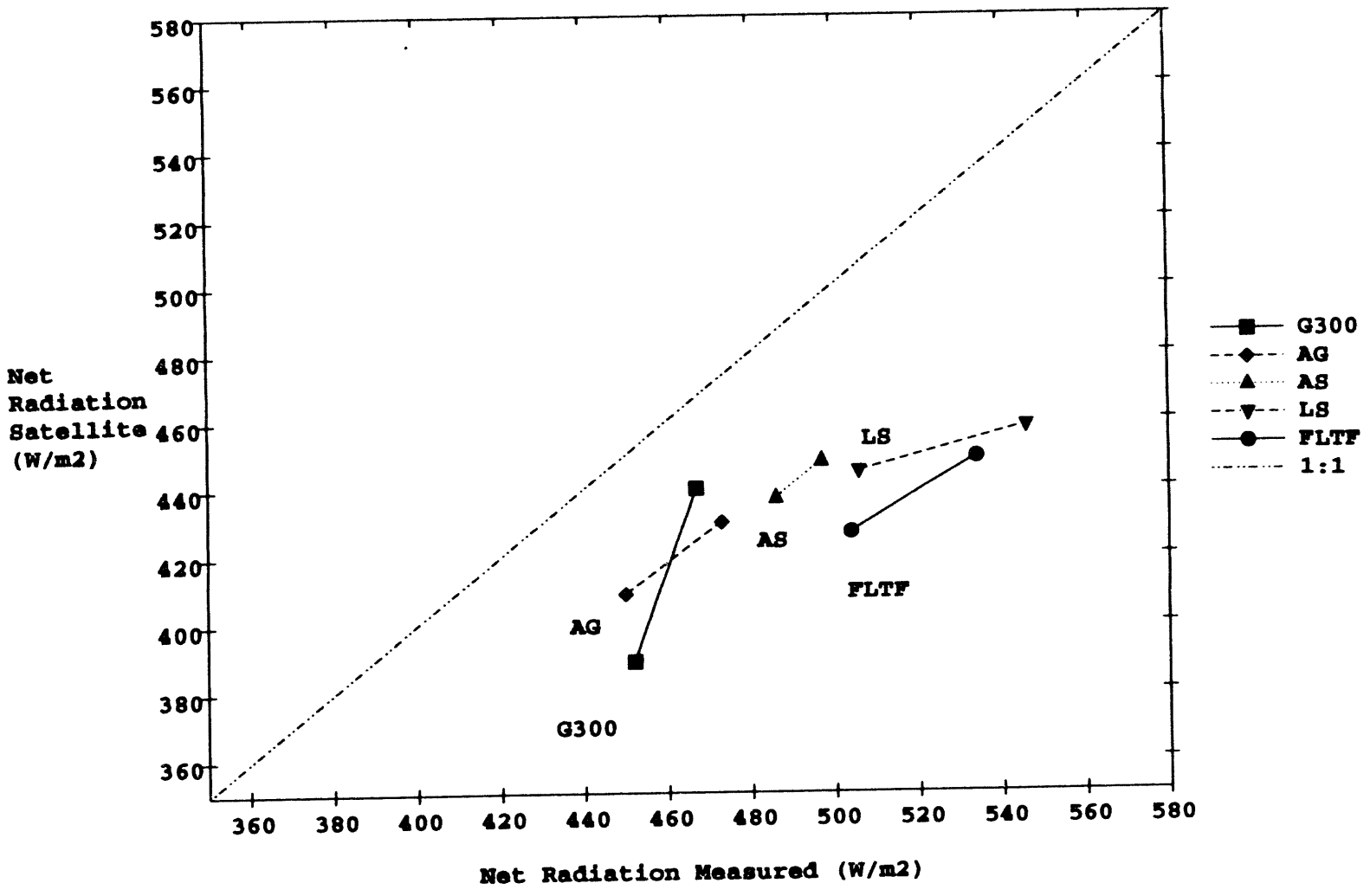

FIGURE 7.12. Net Radiometer Values from Five Sites on 8-May-89 and 1-Jun-89 Compared to the Sum of Short- and Long-Wave Radiation from Landsat.

temperatures much closer to mean air temperatures associated with the 1987 R_N predictive equation. If that equation $R_N = f(R_S\downarrow)$ is used, predicted R_N values are within 14 and 12 W/m^2 for the two dates at the time of overflight. Considering the above discussion and data sets, for a given $R_S\downarrow$ value, the surface reflectance and the surface radiative temperature are much more important than the incoming $R_L\downarrow$ term in predicting R_N and the use of an air temperature and $R_S\downarrow$ observations from a central location within the satellite scene are justified in cloud-free images. The bunchgrass, sagebrush, and Lower Snively sites are at the base of steeper portions of Rattlesnake Mountain with a northeast aspect. The elevation map in Figure 6.4 indicates that slopes are 3 to 5%. The comparison of R_N for 8-May-89 and 1-Jun-89, shown in Figure 7.13 does not show any temporal offset. For this study, slope and aspect adjustments to the incident radiation for the ground stations or the images are not performed. As expected, R_N is highest for the Lower Snively site because it has a complete cover of active cheatgrass and lowest for the G300 site having a low cover of senescent vegetation.

Net radiation flux density (W/m^2) was estimated using equation 15 with a three-point average of $R_S\downarrow$ and $R_L\downarrow$ determined from equation 20, for the 8-May-89 and 1-Jun-89 images (Figure 7.14). The sand dunes have low net radiation because $R_S\uparrow$ and $R_L\uparrow$ are high. Note, areas of steep slope are not correctly represented because $R_S\downarrow$ was not adjusted for slope or aspect.

7.3 Normalized Difference Vegetation Index as a Predictor of Soil Heat Flux

The importance of vegetation as a source term in the evaporation process is obvious, but the effect of vegetation upon soil heat flux is often ignored. When soil heat flux is included, it is generally modeled in a simple inverse of the amount of vegetation present. Vegetation amount might be measured on a weight, leaf area, or as change in reflected red light energy brought about by chlorophyll absorption. Either LAI (direct measure) or NDVI (remote sensing) can be used as an indicator of live vegetation amount, which is then used to estimate

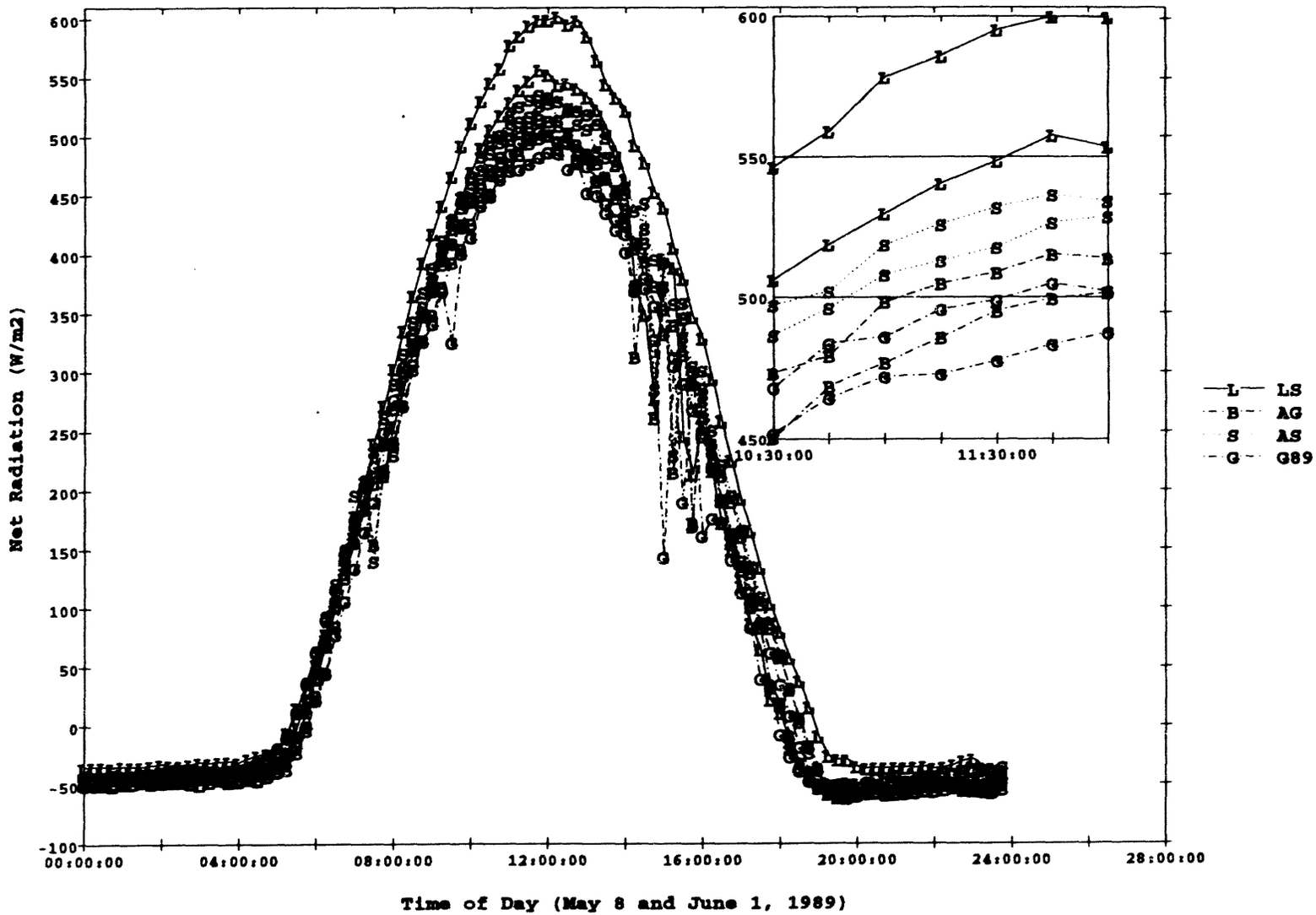

FIGURE 7.13. Net Radiation for Lower Snively (L), Bunchgrass (B), Sagebrush (S), and G300 (G) at 15-min Intervals During 8-May-89 and 1-Jun-89.

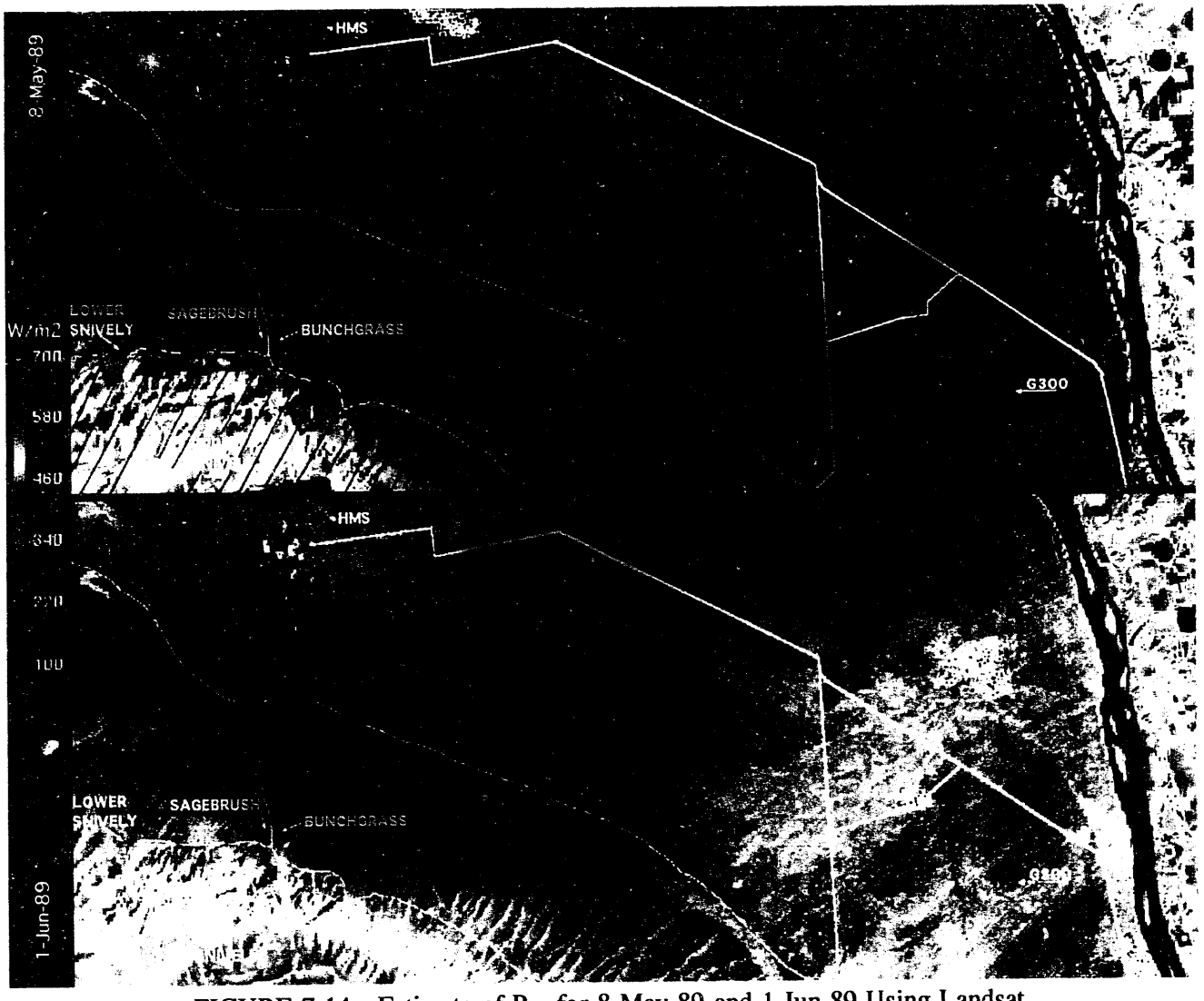

FIGURE 7.14. Estimate of R_N for 8-May-89 and 1-Jun-89 Using Landsat and Limited Ground-Station Measurements.

soil heat flux (Jackson et al. 1983). Most of these relationship are developed for agronomic crops, where litter is removed each year by tillage or in continuous crops where litter is relatively constant.

The effect of litter upon soil heat flux can be significant in semi-arid environments where the amount of litter is dependent on the previous year's climate. At this time, Landsat does not have the spectral bands available to discriminate dead grass and leaf material from the light-colored soils on the Hanford Site. Roberts et al. (1993) indicate that litter materials may be detectable based on the presence of lignin (2130 nm and 2270 nm) and cellulose (2090 nm and 2270 nm) absorbtions when high resolution extended range images are available. The G_T measurements are compared with NDVI values to see if a measure of live vegetation is sufficient to explain G_T measured on the Hanford Site. The definition of the NDVI ratio is clear, but considerable leeway exists in how the DN values are processed before ratioing (NDVI calculations are described in Appendix A).

The NDVI values (NDVI = (Near IR-Red)/(Near IR+Red)] were calculated with DNs processed four different ways for selected study sites on 8-May-1989 and 1-Jun-89 and are presented in Figure 7.15. The effort and complexity in processing the DNs increases with each of the following steps: 1) $NDVI_{DN}$ = raw DN values, 2) $NDVI_{BG}$ = DNs - background value (obtained over water), where the background is a surrogate for atmospheric radiance, 3) $NDVI_{REF}$ = $NDVI_{DN}$ values, which are atmospherically corrected for reflectance using Lowtrans 6 to determine transmittance and radiance values for the atmosphere, 4) $NDVI_{REF}$ = $NDVI_{RAD}$ values, where the reflectance values are converted to radiance. Temperature and humidity profiles obtained from a radiosonde flown on 8-May-89 were used with Lowtrans 6 for all images instead of the standard U.S. summer profile. The relative comparisons of NDVI calculated with data collected from the same instrument under identical environmental conditions can be made with any of the four estimates. The $NDVI_{REF}$ is the only method that should be comparable between different spectral instruments and should be used exclusively. The $NDVI_{REF}$ values for the Hanford field sites are within the range of values found in the literature (Moran et al. 1989; Kustas and Daughtry 1990).

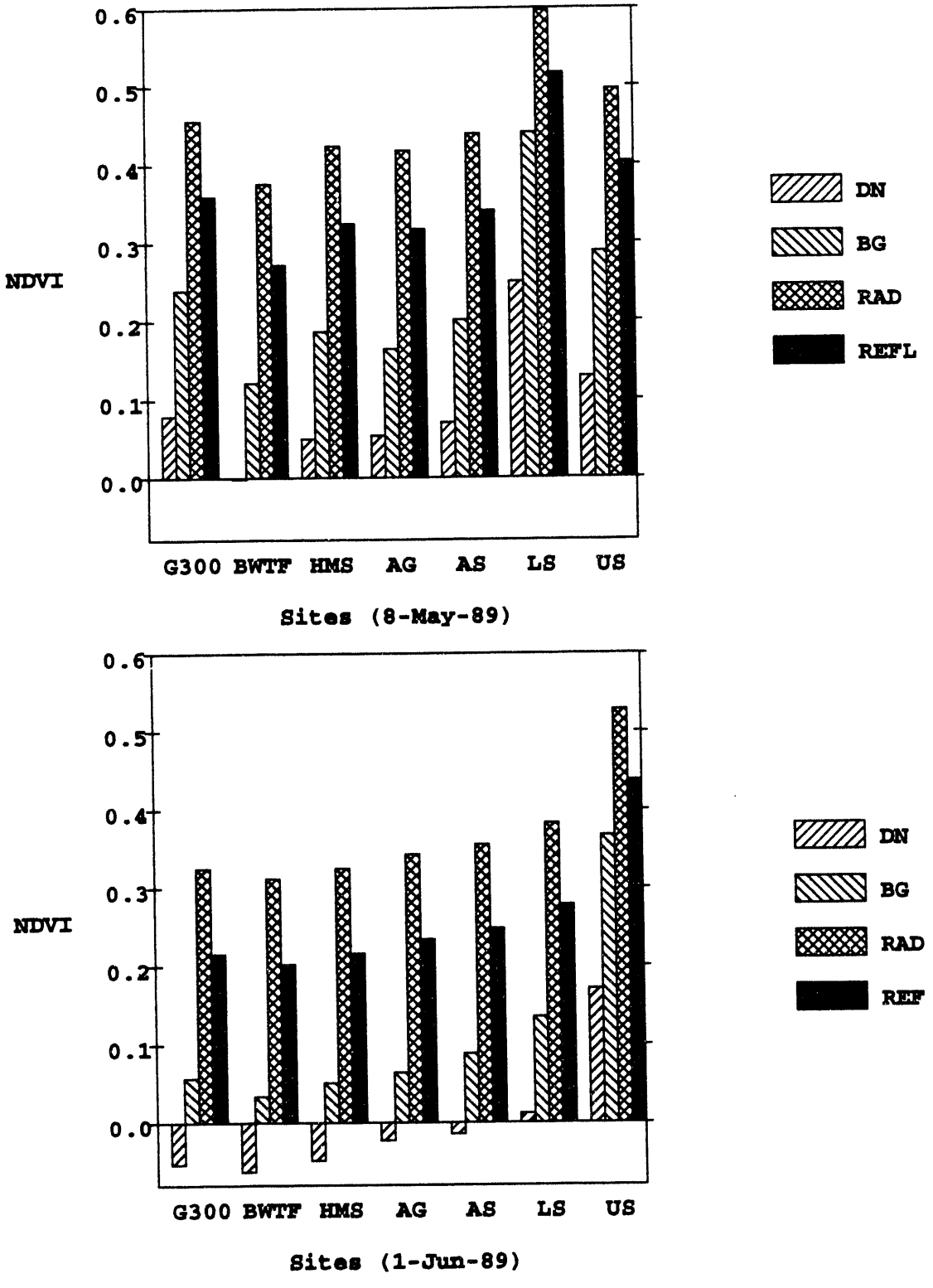

FIGURE 7.15. NDVI Calculated with Four Different DN Treatments for Seven Field Sites on 8-May-89 and 1-Jun-89.

Measured values of soil heat flux density (G) and 0-5 cm soil heat storage (G_s), and the summation of those two terms (G_T) are presented for four sites in Figure 7.16. Differences occur in the diurnal exchange of energy in the soil at these four sites. Lower Snively has the lowest flux amounts because of a greater litter layer and uniform cheatgrass cover. The G300 values are larger because of minimal litter, and the soil has a sand texture with higher thermal conductivity than the silt-loam soils found at the other sites (Rosenberg et al. 1983, p. 96). Also, the G300 site is located at low elevation and in an area of flat topography, thus experiencing the largest diurnal cycle in air temperature as shown previously (Figure 7.9). The sagebrush site has a much larger diurnal amplitude than the bunchgrass site. This larger amplitude most likely occurs because canopy resistance is higher as a result of the rougher surface and soil shading during early and late daylight hours. The sagebrush reduces air flow near the surface, which reduces heat loss during the day and probably reduces the mixing effect of nocturnal cold air drainage typical of the mountainous slope. See Table VII.3. Note, daily G_T while low can be one third of the daily ET. This can result in a measurable energy balance error when accumulated over several days. Unfortunately, in the remote sensing application, we are trying to balance the energy budget during a time interval almost coinciding with the maximum soil heat flux density.

Simple linear (equation 18) and exponential functions (equation 16) are proposed to predict soil heat flux as a function of NDVI. Pairs of data points obtained from five sites at Hanford at the Landsat overflight times of 8-May-89 and 1-Jun-89 are connected by straight lines (Figure 7.17). The proposed NDVI-G_T relationships are plotted; the equations do not describe G_T for all sites. The K symbol represents the high and low values of NDVIs reported by Kustas and Daughtry (1990). The Hanford Site May NDVI values are consistently higher than the June values, as expected, and G_T increases with decreasing NDVI. It appears that there may be a threshold NDVI value (with only the Lower Snively site having NDVI greater than this value) where G_T is relatively constant because of litter accumulation. The amount of litter at the end of the growing season would be plant community specific. More research would be needed to determine whether single NDVI values used with growing-degree-day-based phenology tables could project litter amounts or if multiple measurements during the growing season are required to predict litter amounts.

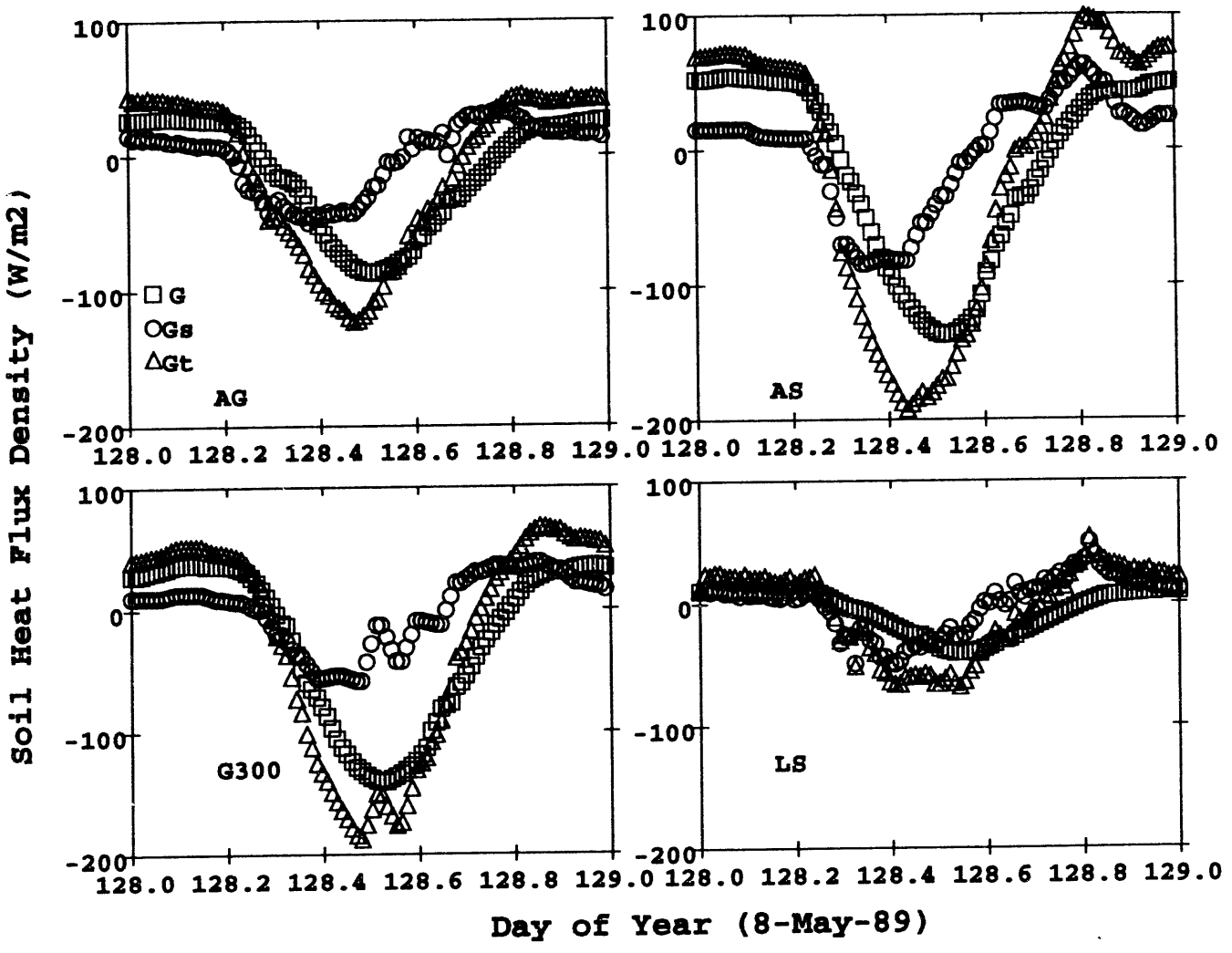

FIGURE 7.16. Soil Heat Flux Density (G), 0-5 cm Storage (G_S), and Their Sum (G_T) for Four Sites (AG = bunchgrass, AS = sagebrush, G300 = Grass 300, LS = Lower Snively) on 8-May-89 (dependent axis = W/m^2).

TABLE VII.3. Daily Average G_T Density (W/m^2).

Site	8-May-89	1-Jun-89
Bunchgrass	-12.6	-19.8
Sagebrush	-12.2	-28.9
G300	-24.8	-33.5 (0.11)[a]
Lower Snively	-6.6 (0.02)[a]	-10.5

(a) Values in parenthesis are equivalent evaporation in centimeters of H_2O.

Most of the differences in G_T between sites for different years can be explained by the differences in the amount of potential litter on the soil surface each year. The year 1986 was wetter and warmer than normal, 1987 and 1988 were very dry, and 1987, 1988, and 1989 were all warmer than normal. Litter production would have been high in 1986 and low in 1988. The low ratio of G_T/R_N in 1986 and 1987 might be explained by increased litter accumulation. The 1987 NDVI values are probably lower than 1986 because of the much larger growing degree days that accrued in 1986 as compared to 1987 (Figure 6.1). The G_T/R_N values for 1989 data at the G300 and sagebrush sites are higher and may be a result of lower litter accumulation; this lower accumulation is because 1988 was the second driest year on record.

Both equations 16 and 18 predicting G_T as a function of NDVI (dot and dot-dash lines, respectively, on Figure 7.17) pass through the Hanford data set but neither function adequately predicts G_T at all sites. These equations relating NDVI to G_T were developed in agricultural conditions where the litter is generally removed (tillage) or relatively constant (irrigation) from year to year. These conditions are less likely to occur in the natural arid communities where the diversity of species allows different vegetative responses within the plant community. Possible responses range from increases in biomass, longer active transpiration periods, or a combination of growth and longer lived vegetation. The amount of litter remaining after winter depends on physical factors such as snowpack, soil moisture, and temperature, and on biotic consumption by insects and herbivores.

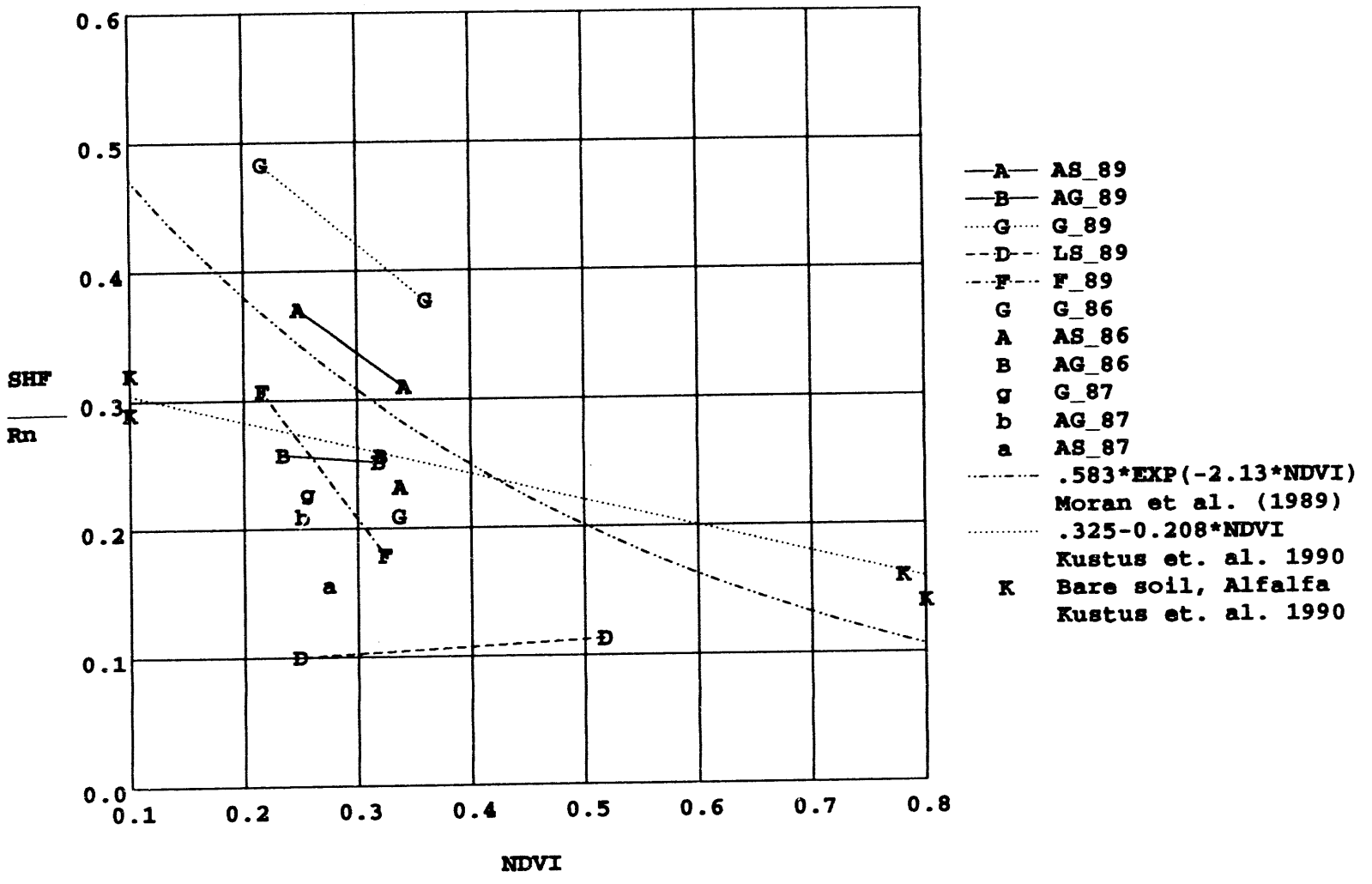

FIGURE 7.17. NDVI from Landsat Data Versus the Ratio of Soil Heat Flux to Net Radiation (G_T/R_N) for 1986, 1987, and 1989 Data.

Six subscene Landsat images have been converted to NDVI values in the same order as previously described (Figure 7.18) with red representing increased levels of green vegetation. Agricultural areas east of the Columbia River and ephemeral streams have the highest amounts of vegetation. The differences in NDVI that are apparent in Figure 7.17 (G_T/R_N versus NDVI) are also apparent in Figure 7.18. The NDVI on 8-May-89 (c) is higher than that on the 1-Jun-89 image (d). Both of the 1989 images have higher NDVI values than the 8-May-86 (a) and 11-May-87 (b) images. The 28-Feb-89 image (e) shows the least red area (agricultural and stream bed vegetation) but indicates moderate increases in the general Hanford Site. This could be in response to the greening of the cryptogram cover found on much of the undisturbed soil surfaces or an effect of low sun angle. In some flat upper elevation areas of historically high vegetation cover and litter amounts, the 28-Feb-89 image indicates low NDVI amounts. In these areas, bare soil or cryptogram cover, if it exists, is hidden by the litter. If sun angle is responsible for the increase in NDVI, it only affects areas where soil is exposed.

7.4 Development of Resistance Term for Sensible Heat Transport

The resistance term in the sensible heat flux equation (see equation 9) is a function of several atmospheric and vegetation variables and can be different for different vegetation communities. To estimate resistance, 38 bunchgrass (Table VII.4) and 60 sagebrush (Appendix C) hourly measurements of energy balance and lysimeter data collected between 1000 and 1200 hours between April 11 and May 9, 1988, were used to determine H. Sensible heat flux density was derived as the available energy (R_N-G_S-G) minus the latent heat flux measured with the lysimeters. Data sets collected during this time were used to determine values of the bulk Richardson number (Ri), stability functions (kB^{-1}), and resistance to heat transfer (r_h). Details of these calculations are in Appendix B. During this time period, four rainfall events were recorded by the weighing lysimeters as indicated by the increase in weight on days 108, 111, 113, and 119 in all four curves shown in Figure 7.19. The sensible heat flux is also lower immediately after these rainfall events.

Two equations similar to equation 10 for are used to estimate r_h. These resistance equations have been fit to the bunchgrass and sagebrush hourly data set using an iterative

FIGURE 7.18. NDVI Calculated from Reflectance Values for Six Subscenes of the Hanford Site.

TABLE VII.4. Statistic for Resistance Equation Development.

Site	Solved for	γ	Γ	s^2	r
Sagebrush	h = 0.18			3080	0.77
	γ	0.080		2448	0.77
	γ and Γ	0.192	0.038	2152	0.80
Bunchgrass	h = 0.08			10,280	0.53
	γ	0.013		10,240	0.53
	γ and Γ	0.516	0.198	2801	0.89

solution to minimize the sum of squares (s^2) of the difference between the measured H and the value of $\rho Cp*dT$ divided by r_h. The first equation (see calculations in Appendix C) was used by Moran et al. (1989) in alfalfa, wheat, and cotton at the Maricopa Agricultural Center in Phoenix, Arizona (Figure 7.20). They measured plant height and estimated z_o and d as 0.13h and 0.63h, respectively. In this application, the best fit value of h was determined with 1988 data. The fitting variable for this equation was plant height (h). In Figure 7.20, the graph represents the resistance that would be calculated for a range of wind speeds (u) and surface to air temperature differences (ΔT). Note, this equation predicts resistances that approach a low value with increases in either u or dt. The second equation (Figure 7.21) uses the plant height (h) solved for in the first equation and adds the kB^{-1} term (Kustas 1990) and an additional fitted term (Γ), a fraction of the amount of available energy at the surface. This last term was added because Kustas (1989) indicated kB^{-1} was sensitive to surface temperature. If the equations are first fit for h (rather than h measured, to estimates z_o and d), the addition of kB^{-1} alone decreases s^2 only marginally, while the addition of Γ alone increases s^2. The addition of both kB^{-1} and Γ reduce s^2 as shown in Table VII.4. The sagebrush value of h is only twice that of the bunchgrass and much lower than the top of canopy heights of 0.3 and 1.5 m, respectively, for the bunchgrass and sagebrush sites (Table VII.4).

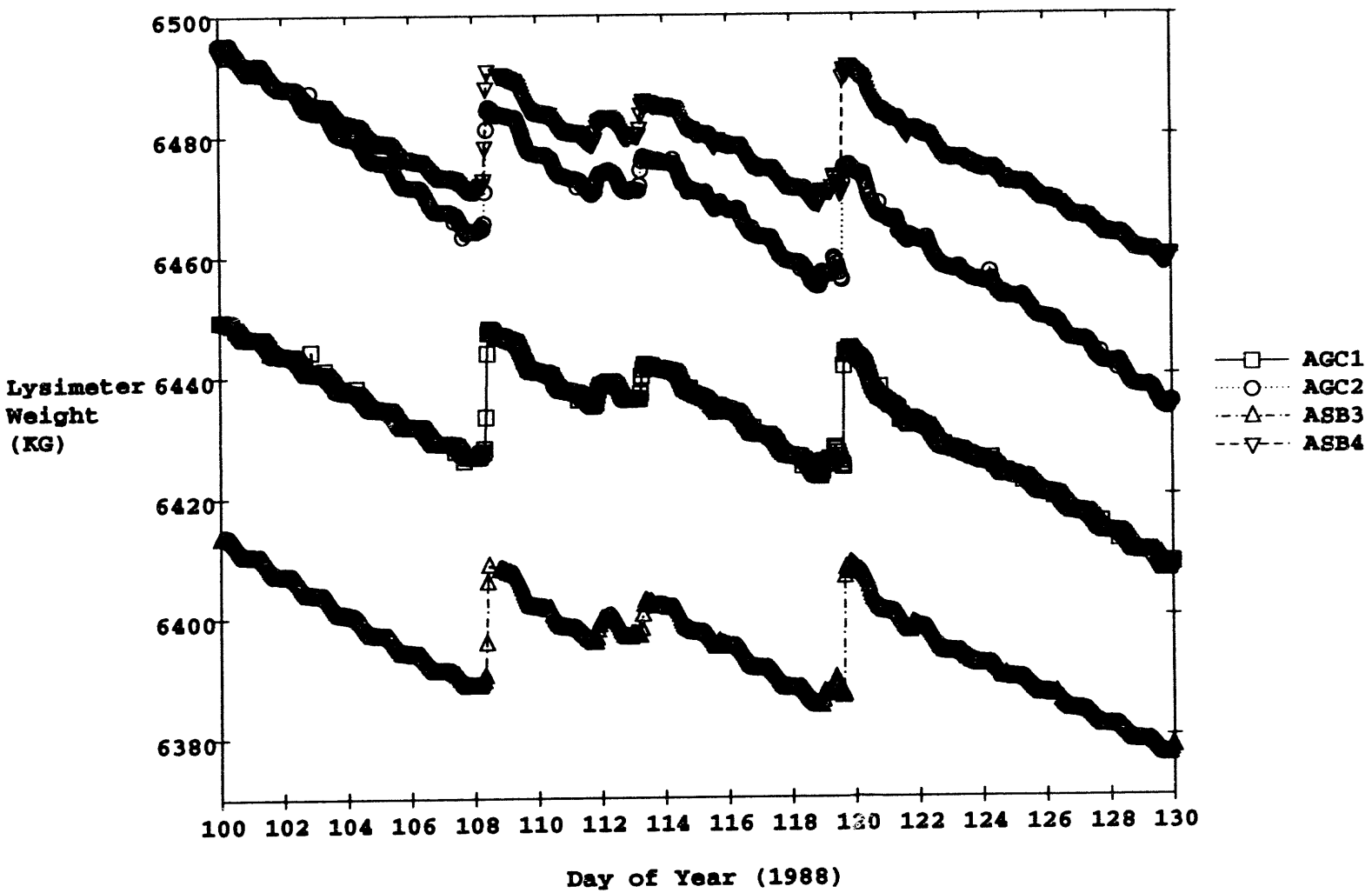

FIGURE 7.19. Weight Changes in Bunchgrass and Sagebrush Lysimeters Caused by Evapotranspiration and Precipitation During the Calibration Period in April 1988.

$j := 0..7$ **wind speed** $\quad$ $tempdif := 0..30$ **Surface-Air**

$$ri_{tempdif,j} := \frac{9.8}{40 + 273} \cdot -(tempdif + 1) \cdot \frac{z - d_o}{((j + 1) \cdot .44)^2}$$

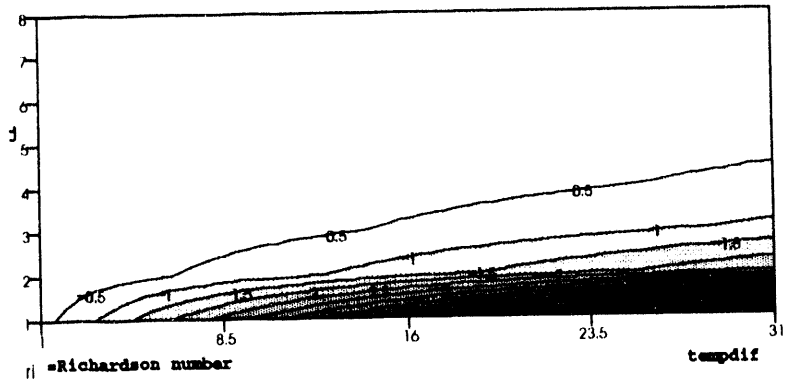

Equations used to developed best least squares fit of η (height) for Alegrass 1988 data

AG6=wind speed
AG5=air temp

See Appendix C for more detail

$$C := 75 \cdot k^2 \cdot \frac{\left(\frac{z - d_o + z_{om}}{z_{om}}\right)^{.5}}{\ln\left(\frac{z - d_o + z_{om}}{z_{om}}\right)^2}$$

$$G(AG6, AG5, dt, \eta) := \left[\left[\frac{\ln\left[\frac{\left(z - \eta \cdot \frac{2}{3}\right)}{\left(\frac{\eta}{8}\right)}\right]}{k}\right]^2 \cdot \frac{\left[1 - 15 \cdot \left[\left(\frac{9.8}{AG5 + 273}\right) \cdot ((-dt)) \cdot \frac{z - \eta \cdot \frac{2}{3}}{(AG6 \cdot .44)^2}\right]\right]^{-1}}{\left[1 + C \cdot \left[\left[-\left[\left(\frac{9.8}{AG5 + 273}\right) \cdot ((-dt)) \cdot \frac{z - \eta \cdot \frac{2}{3}}{(AG6 \cdot .44)^2}\right]\right]\right]^{.5}\right]}{AG6 \cdot .44}\right]$$

$$Sensible_Heat_Flux_c := \left(\frac{\rho \cdot C_p \cdot dt_c}{G(AG6_c, AG5_c, dt_c, \eta)}\right)$$

$$M_{tempdif,j} := G(j + 1, ri_{tempdif,j}, tempdif + 1, \eta)$$

with values of j=u, ri=f(j,tempdif),k=dt, η=height

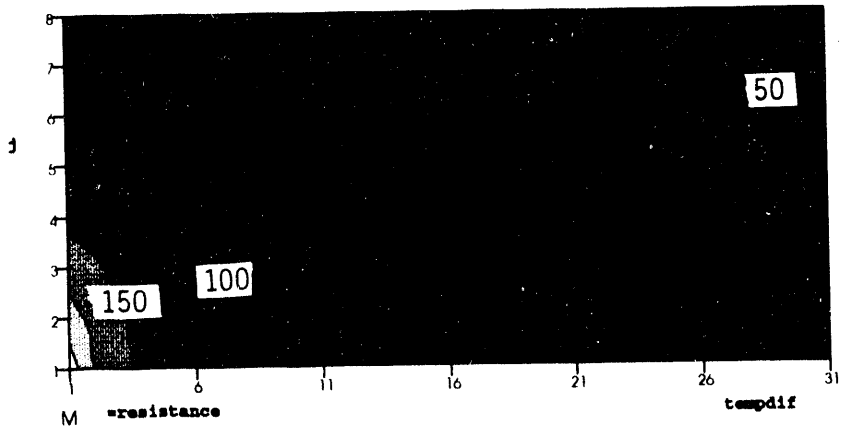

FIGURE 7.20. Resistance Equation Used to Solve Plant Height (h) and Example Plot with Varying Wind Speed (u) and Temperature Difference (dt).

Equations used to develop best least squares fit of (γ *wind speed * dt) a substitute for KB and a further adjustment base on the available energy

$$F(AS6, AS8, RI, dt, \beta, \gamma) := \left[\left[\frac{\ln\left[\frac{(z - d_o)}{z_{om}}\right]}{k} \right] \cdot \left[\frac{\ln\left[\frac{(z - d_o)}{z_{om}}\right]}{k} + (\gamma \cdot (AS6 \cdot .44) \cdot (dt)) \right] \cdot \left[\frac{\left[\frac{1 - 15 \cdot RI}{1 + 75 \cdot k^2 \cdot \frac{\left[\frac{z - \eta \cdot \frac{2}{3} + \frac{\eta}{8}}{\left(\frac{\eta}{8}\right)} \right]^{.5}}{\ln\left[\frac{z - \eta \cdot \frac{2}{3} + \frac{\eta}{8}}{\left(\frac{\eta}{8}\right)} \right]^2} \cdot ((-RI))^{.5}} \right]^{-1}}{AS6 \cdot .44} \right] - \beta \cdot AS8 \right]$$

$$RI2(w1, tf) := \left[\frac{9.8}{(40) + 273} \right] \cdot ((-tf + 1)) \cdot \frac{z - d_o}{((w1 + 1 \cdot .44))^2}$$ **Richardson value**

See Appendix D for complete equations

$w := 0..7$ **Wind speed** $\quad$ $tempdif := 0..30$ **Surface - Air**

$M_{w,tempdif} := F(w + 1, 400, RI2(w, tempdif), tempdif, \beta, \gamma)$ **w=windspeed tempdif = surface - air temperature**

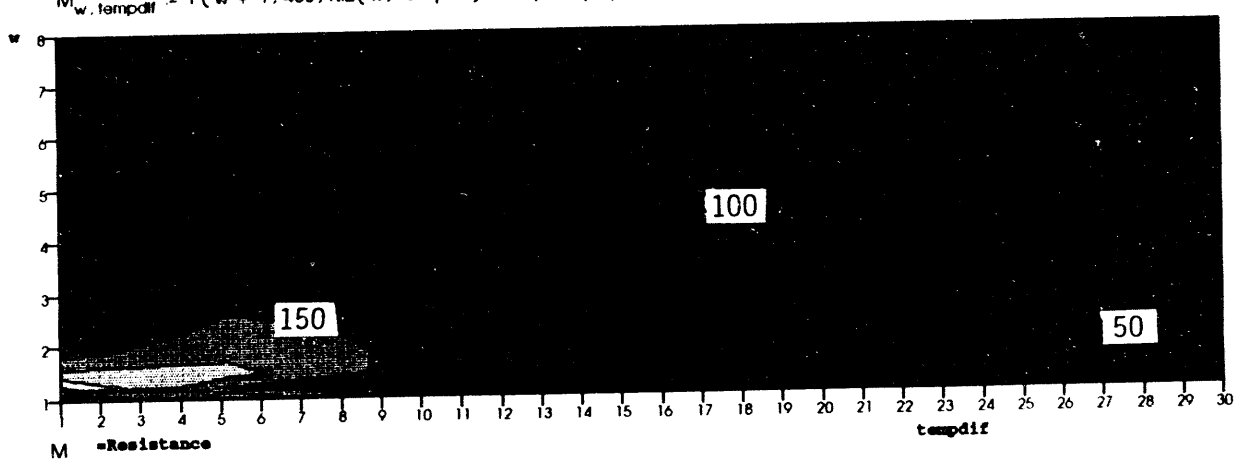

FIGURE 7.21. Resistance Equation Used to Solve for λ and Additional Fitted Term (Γ), and Surface Plot with Varying Wind Speed (u) and Temperature Difference (dt).

Unfortunately, for kB^{-1} to be useful, it must be estimated from readily available information. Kustas (1990) proposed that

$$kB^{-1} = 0.17 * U * \Delta T_s \tag{23}$$

and his mean kB^{-1} was 5.6 in a sparse canopy. Values of kB^{-1} calculated for this analysis are about the same. However, when examined in the context of equation 10, the choice of h determines the value of kB^{-1}, because the following equations are assumed: $d_o = (2/3)h$ and $z_{om} = h/8$. Examining the estimates of sensible heat flux generated by the two equations in Figures 7.22 (bunchgrass) and 7.23 (sagebrush) indicates that the estimates of sensible heat flux for the bunchgrass site would benefit the most from the inclusion of r and Γ.

Applying this equation (using fitted values for r and Γ) to satellite data as described in Section 7.5 gave unrealistic predictions of sensible heat. The calculated resistance plotted in Figure 7.21 shows that at large temperature difference between the surface and T_{air} increasing wind speed causes the resistance begins to increase instead of continuing to decrease. Because we are applying these techniques to a semi-arid system, this region of high dt coincides with most of the satellite data used in this study. Even though this equation performed better on the 1988 calibration dataset, it should not be used at the Hanford Site until a wider range of calibration data is obtained during hot temperatures.

7.5 Comparison of Remote Energy Balance Results with Measured Values

Energy balance results for the bunchgrass site obtained from BREB and lysimeters on 8-May-89 and 1-Jun-89, respectively, were examined because these dates correspond to Landsat overflights. As was shown previously for the 1988 data, the lysimeter and BREB latent heat fluxes (Figure 7.24) compare quite well on 1-Jun-89. The latent heat flux density measured at the bunchgrass site by the BREB method is less than that indicated by the lysimeters after 1000 hours (24-hour clock) on 8-May-89. One wet bulb of the BREB station was underestimating the wet bulb temperature gradient, necessitating a correction to that portion of the BREB data. The inadequately cooled wet bulb was scaled to match the other (cooler)

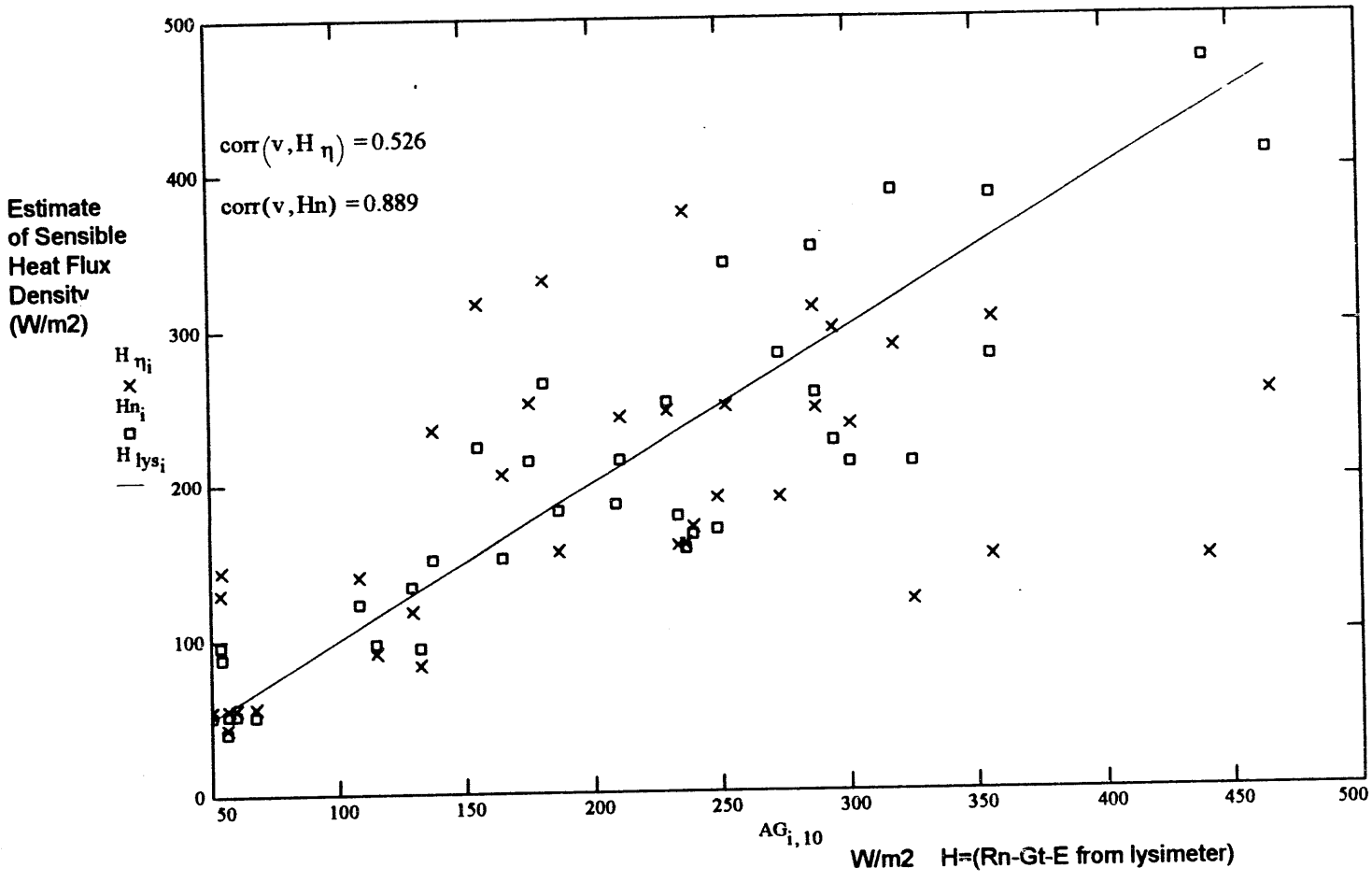

FIGURE 7.22. Estimated Sensible Heat Flux for Bunchgrass (BREB and Lysimeters), 1988.

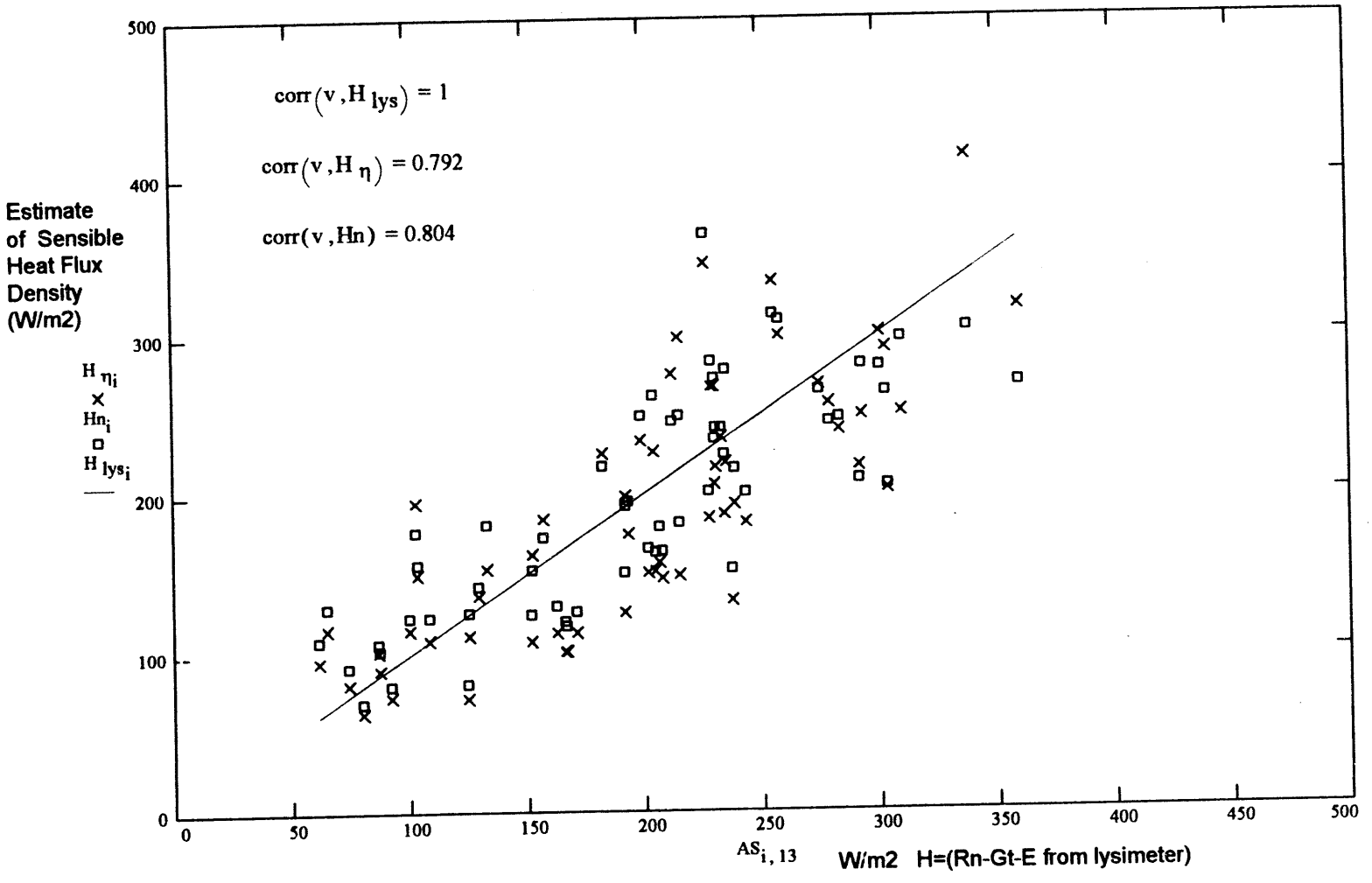

FIGURE 7.23. Estimated Sensible Heat Transport for Sagebrush (BREB and Lysimeters), 1988.

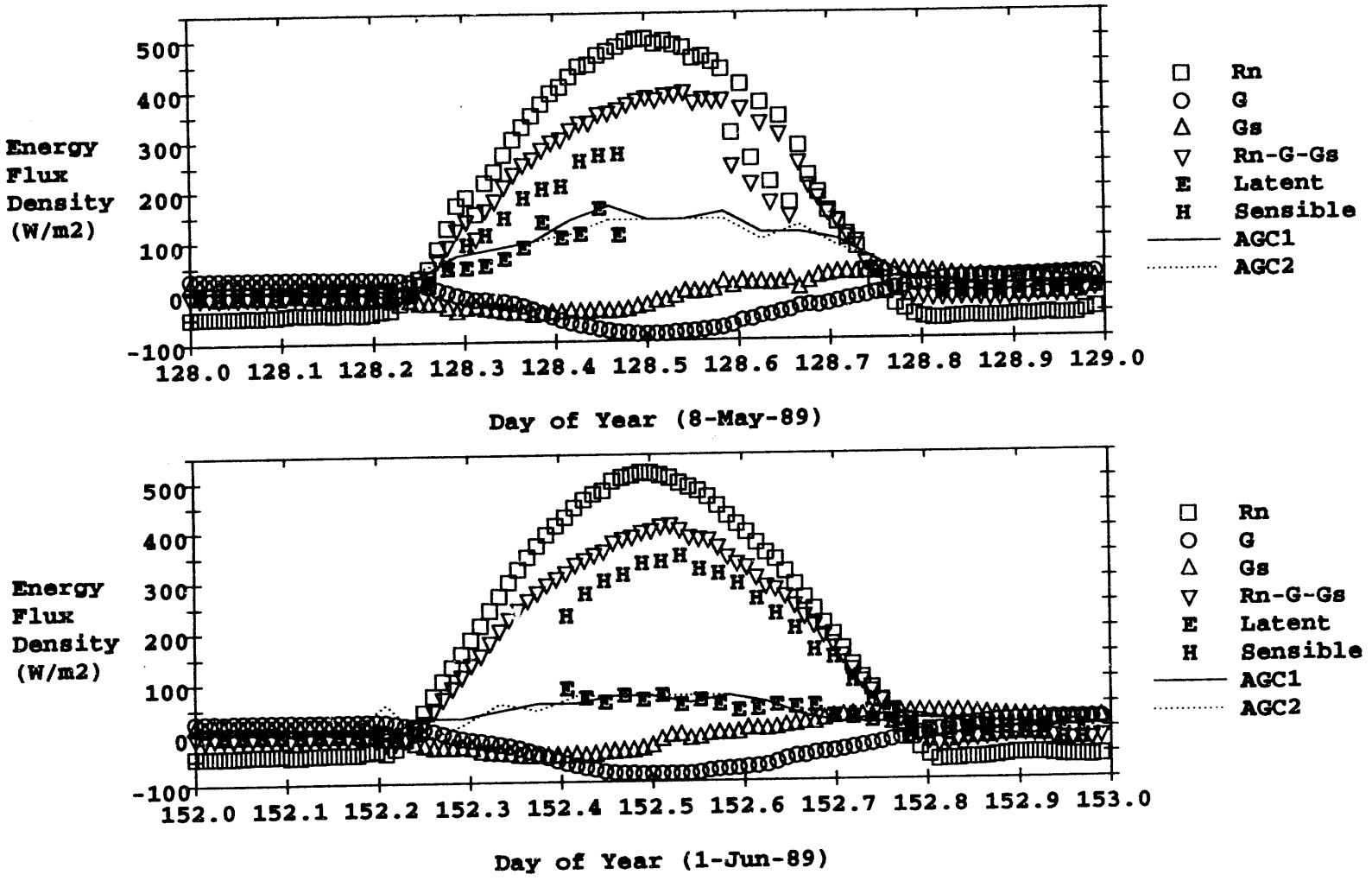

FIGURE 7.24. Energy Balance for Bunchgrass Site (BREB and Lysimeters) on 8-May-89 and 1-Jun-89.

wet bulb sensor; such corrections can easily increase the error to the same magnitude as the 50 W/m^2 difference observed between BREB and lysimeter in Figure 7.24.

Similar data for the sagebrush site, for the same time period, show excellent agreement between the methods on 8-May-89, but the BREB data indicates a slightly higher latent heat flux during the middle of the day of 1-Jun-89 (Figure 7.25). Latent heat fluxes are greater at the Lower Snively site compared to the other three sites, and increase still more on 1-Jun-89 (Figure 7.26). The Lower Snively site is the only site to show an increase in latent heat flux on 1-Jun-89 as compared to the 8-May-89 value. The G300 BREB estimate of latent heat flux is higher than either the bare- or grass-covered lysimeter located at Buried Waste Test Facility (5 km north). The vegetation cover is more uniform at the G300 site compared to the vegetative-cover lysimeter (see Figure 7.27).

The Landsat overpass varies slightly around 1020 hours. Ground observations of energy flux density between 1000 and 1100 hours obtained from the BREB stations for the four sites appear in Tables VII.5, VII.6, VII.7, and VII.8. The average of sensible heat flux density at 1000 and 1100 hours is poorly correlated with the Landsat estimate of sensible heat flux (8-May-86, 8-May-89, and 1-Jun-89) for the bunchgrass, sagebrush, and G300 sites (Table VII.9). These results are not encouraging because this is the most conservative case where T_{air}, G_T, and u are measured values rather than T_{air} being a function of elevation, G_T being a function of NDVI, and u being some function of wind speed at the nearest wind speed site. This final image is not produced because without the correction for soil heat flux, which differs between sites as much as the measured sensible heat flux differs between sites, closure is not achieved on the energy balance equation.

In Table VII.9 shows that the simple equation (calibrated in Section 7.4) shown in Appendix C greatly overestimates the sensible heat flux. By solving the transport equations for kB^{-1} only [($kB^{-1} = \lambda * U * \Delta T$) Kustas et al. (1989) used $\lambda = 0.17$] (see Appendix C) with $\beta = 0$, the data can be adjusted on to the 1:1 line with a $\gamma = 0.21$, which is not significantly different. The scatter of this Landsat/Bowen ratio data set is apparent in Figure 7.28 only slightly more than that reported by Kustas et al. (1989) or Brunel (1989) where the data range is approximately ± 80 W/m^2 from the best fit lines.

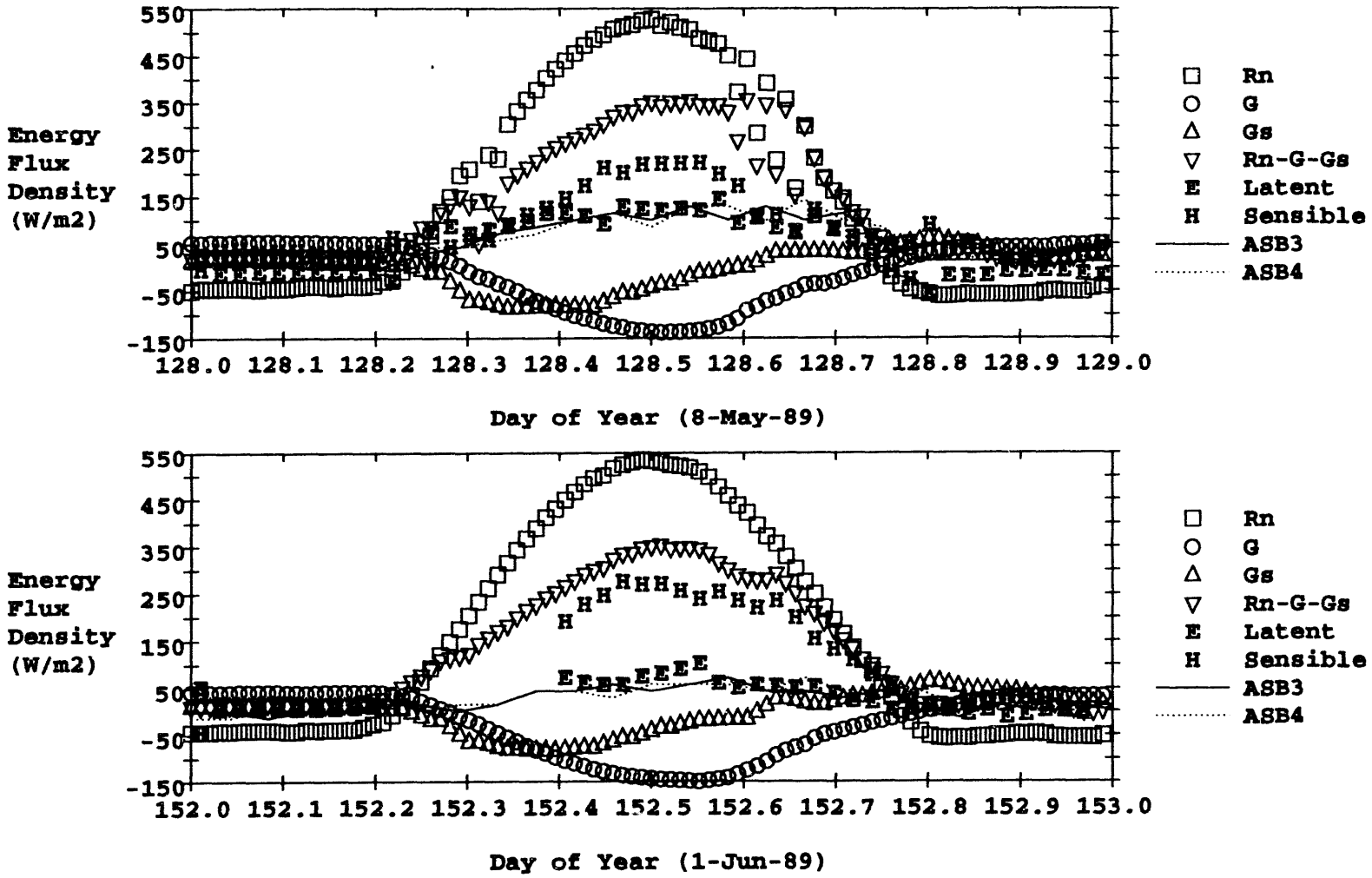

FIGURE 7.25. Energy Balance for Sagebrush (BREB and Lysimeters) on 8-May-89 and 1-Jun-89.

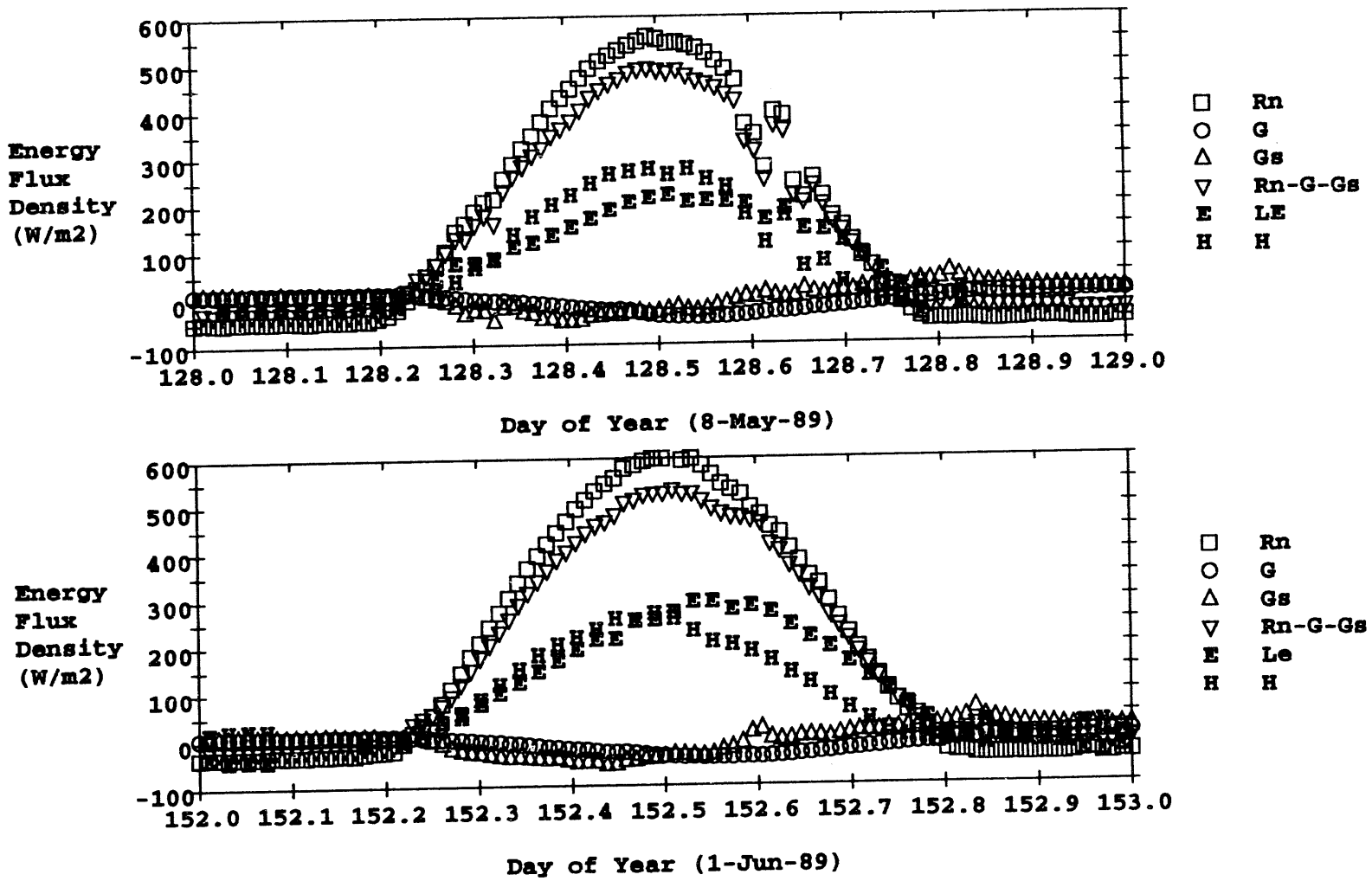

FIGURE 7.26. Energy Balance at Lower Snively (BREB) on 8-May-89 and 1-Jun-89.

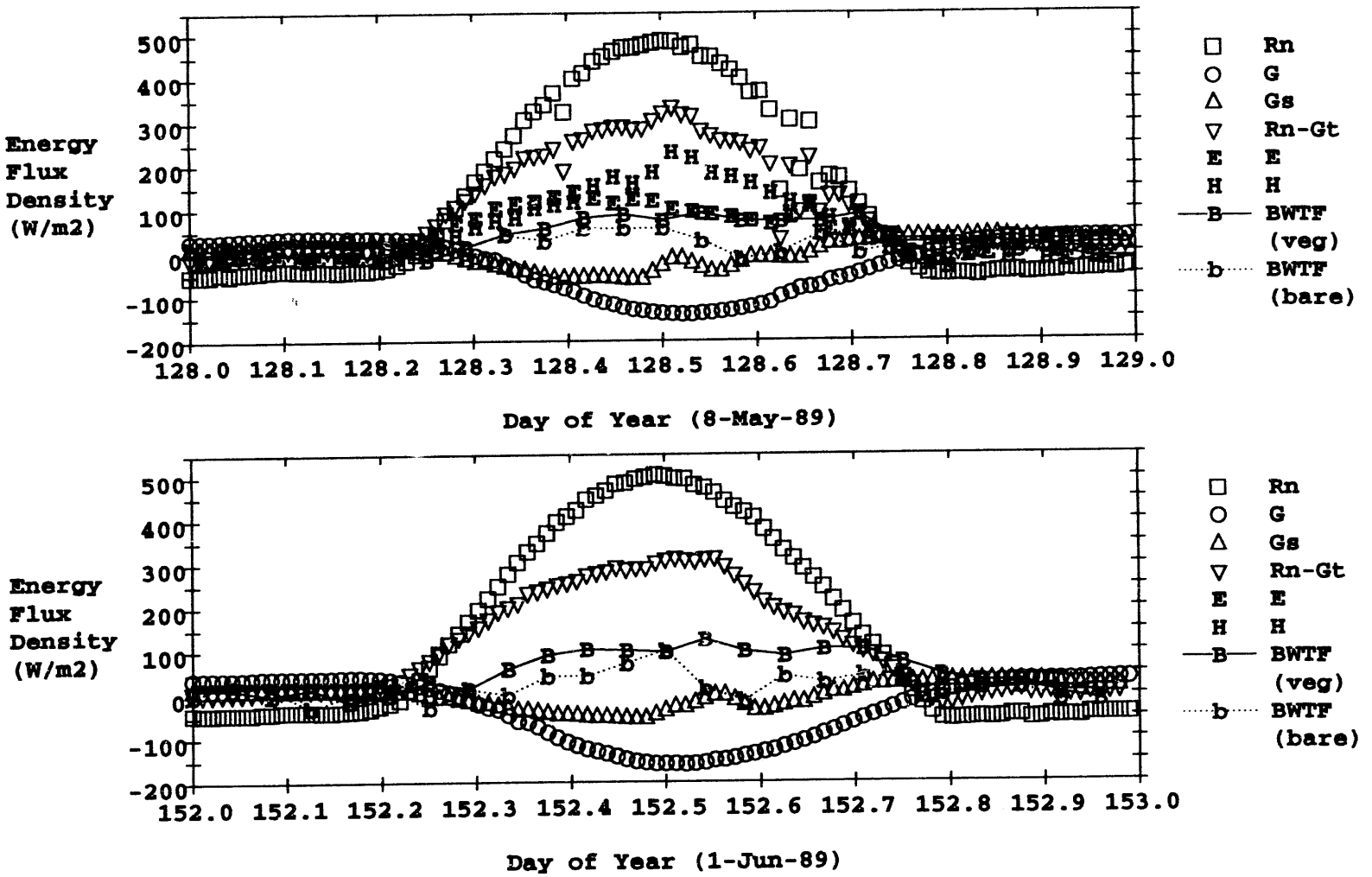

FIGURE 7.27. Energy Balance at the G300 Site and Buried Waste Test Facility (Vegetation and Bare Lysimeters) on 8-May-89 and 1-Jun-89.

TABLE VII.5. Surface Observations at Sagebrush Site on 8-May-89 and 1-Jun-89.

Day	Hr	Wet L (°C)	Dry L (°C)	R_N (W/m^2)	$R_S\downarrow$ (W/m^2)	$R_S\uparrow$ (W/m^2)	β	G_S (W/m^2)	G_T (W/m^2)	Avail (W/m^2)	E (W/m^2)	H (W/m^2)
128	1000	14.41	22.33	457	760	125		81	182	275		
128	1015	13.91	23.38	473	787	129	1.57	82	189	284	111	174
128	1030	14.54	23.02	487	809	134		82	194	293		
128	1045	14.19	24.17	496	829	137	2.28	72	190	306	94	213
128	1100	14.20	23.07	508	843	138		63	186	323		
152	1000	16.20	25.86	467	861	136		77	188	279		
152	1015	15.93	26.77	484	867	139	3.59	76	192	292	64	228
152	1030	16.56	26.62	497	846	142		76	197	300		
152	1045	16.45	27.69	502	837	144	4.22	69	196	306	59	248
152	1100	17.18	27.85	519	843	148		62	194	325		

TABLE VII.6. Surface Observations at Bunchgrass Site on 8-May-89 and 1-Jun-89.

Day	Hr	Wet R (°C)	Dry R (°C)	R_N (W/m^2)	$R_S\downarrow$ (W/m^2)	$R_S\uparrow$ (W/m^2)	β	G_S (W/m^2)	G_T (W/m^2)	Avail (W/m^2)	E (W/m^2)	H (W/m^2)
128	1000	13.62	22.18	427	774	134		-41	-105	322		
128	1015	14.47	23.83	446	801	139	1.97	-43	-111	335	113	223
128	1030	13.75	22.82	450	819	141		-42	-114	336		
128	1045	14.69	24.57	469	837	145	1.15	-40	-116	353	164	188
128	1100	14.09	23.50	477	851	147		-42	-121	356		
152	1000	15.67	26.35	446	803	144		-46	-112	334		
152	1015	16.37	27.70	461	828	148	4.02	-49	-119	342	68	274
152	1030	15.95	26.89	473	849	151		-46	-121	353		
152	1045	16.74	28.55	480	858	151	5.06	-42	-120	359	59	300
152	1100	16.48	27.76	498	878	155		-41	-121	377		

TABLE VII.7. Surface Energy Budget Values at G300 During 8-May-89 and 1-Jun-89 Landsat Overflights.

Daytime	Day	Time	Wet R (°C)	Dry R (°C)	R_N (W/m^2)	$R_S\downarrow$ (W/m^2)	$R_S\uparrow$ (W/m^2)	β	G_S (W/m^2)	G_T (W/m^2)	Avail (W/m^2)	E (W/m^2)	H (W/m^2)
128.42	128	1000	21.78	13.32	471	422	144		-46	-67	404		
128.43	128	1015	23.72	14.56	491	423	145	1.44	-39	-61	430	171	246
128.42	128	1000	16.26	25.59	415	763	112		-54	-150	265		
128.43	128	1015	13.91	23.82	442	793	114	1.21	-53	-158	284	129	156
128.44	128	1030	15.49	26.01	452	814	116		-53	-165	287		
128.45	128	1045	14.04	24.63	464	837	116	1.50	-55	-172	292	117	175
128.46	128	1100	15.79	27.07	472	853	118		-56	-179	292		
152.42	152	1000	16.15	26.54	447	801	120		-48	-171	276		
152.43	152	1015	16.09	26.42	457	823	121		-50	-177	281		
152.44	152	1030	16.31	27.25	468	845	123		-50	-182	286		
152.45	152	1045	16.27	27.36	484	867	125		-51	-190	294		
152.46	152	1100	16.88	28.49	486	881	127		-52	-198	288		

TABLE VII.8. Surface Energy Budget Values at Lower Snively During 8-May-89 and 1-Jun-89 Landsat Overflights.

Daytime	Day	Time (°C)	Wet R (°C)	Dry R (°C)	R_N (W/m^2)	$R_S\downarrow$ (W/m^2)	$R_S\uparrow$ (W/m^2)	β	G_S (W/m^2)	G_T (W/m^2)	Avail (W/m^2)	E (W/m^2)	H (W/m^2)
128.42	128	1000	21.78	13.32	471	422	144		-46	-67	404		
128.43	128	1015	23.72	14.56	491	423	145	1.44	-39	-61	430	171	246
128.44	128	1030	22.32	13.56	506	423	147		-37	-61	445		
128.45	128	1045	24.20	14.69	519	419	147	1.41	-34	-60	459	188	265
128.46	128	1100	23.18	13.94	530	421	147		-36	-61	469		
152.42	152	1000	25.95	15.61	513	835	141		-48	-70	442		
152.43	152	1015	28.79	16.91	531	859	143	1.10	-49	-73	458	214	236
152.44	152	1030	26.63	16.04	547	883	144		-55	-81	466		
152.45	152	1045	29.84	17.34	559	899	145	1.20	-53	-80	480	215	258
152.46	152	1100	27.51	16.39	579	916	146		-46	-72	506		

TABLE VII.9. Surface Observations, Predicted Aerodynamic Resistance and Sensible Heat Flux, and Measure Sensible Heat Flux for Landsat Overflights

1000 Hours	Surface Observations					$f(\eta)$		$f(\beta=0,\gamma)$		Bowen Ratio
Site	T_{Air} (°C)	U (m/s)	T_S (°C)	R_N (W/m^2)	G_T (W/m^2)	ra (s/m)	H (W/m^2)	ra (s/m)	H (W/m^2)	H (W/m^2)
AG 5/8/86	16.33	2.3	38.42	517	136	60	428	114	226	263
AG 5/8/89	22.82	3.5	48.25	450	113	57	519	148	201	205
AG 6/1/89	26.89	4.5	46.29	473	120	64	351	164	139	287
G300 5/8/89	26.01	2.5	51.47	452	165	57	519	157	189	166
G300 6/1/89	27.25	2.7	49.00	468	182	58	434	193	132	n.d.
LS 5/8/89	22.32	2.2	44.14	506	61	60	425	175	145	255
LS 5/8/89	26.63	0.3	45.50	547	81	63	349	76	290	247
AS 5/8/86	16.91	2.5	36.90	556	135	52	659	133	175	372
AS 5/8/89	23.02	2.6	45.80	486	190	49	774	128	208	193
AS 6/1/89	26.60	3.8	45.17	497	197	56	472	145	150	238

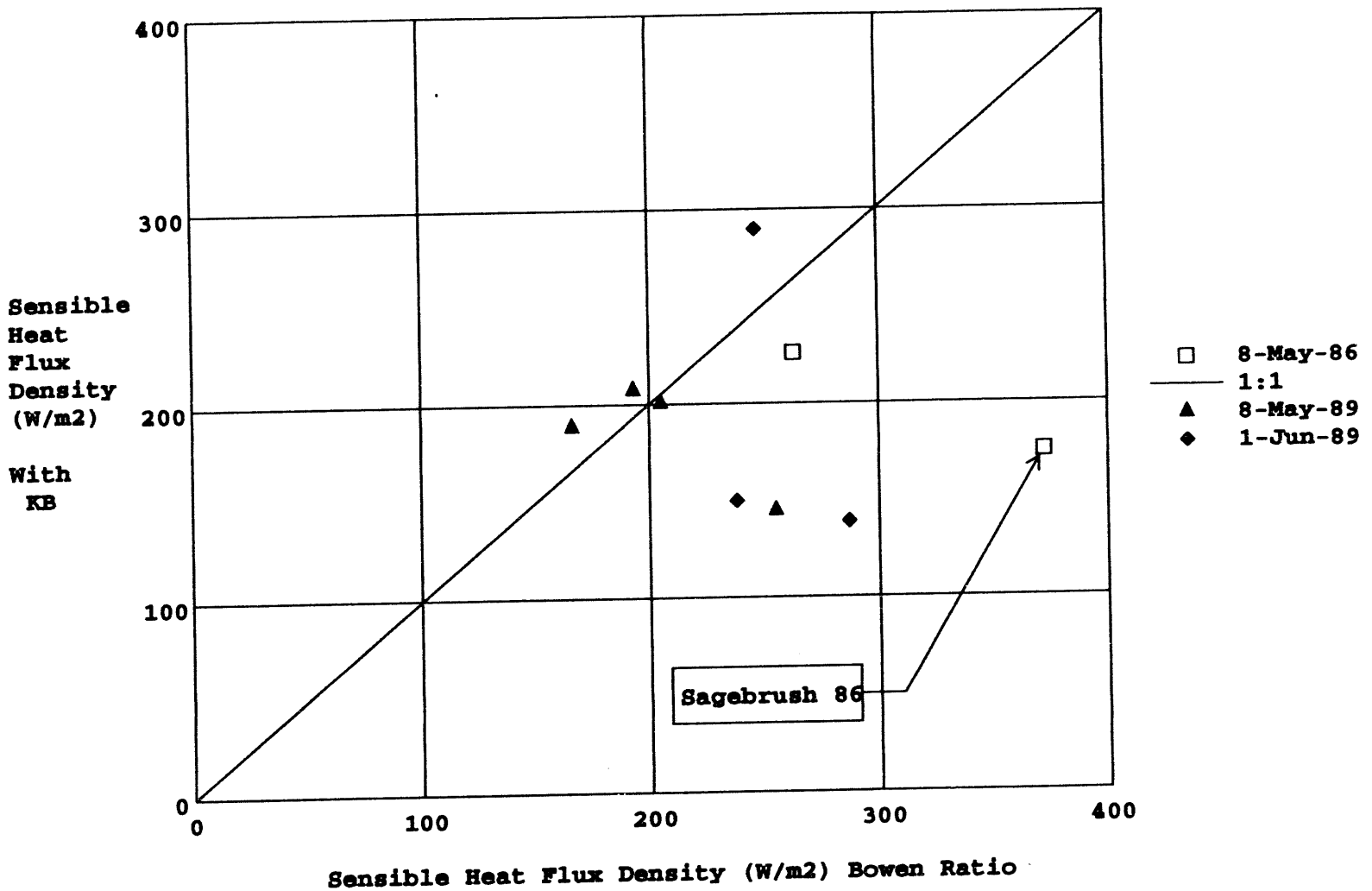

FIGURE 7.28. Sensible Heat Flux Density Determined with Landsat and Average Values of Incoming Short- and Long-Wave Radiation Compared to Sensible Heat Estimates Obtained with BREB Stations for Selected Sites in 1986 and 1989.

8.0 Conclusions and Recommendations

Application of remote sensing to environmental assessment has been an active research area at the Hanford Site for many years. Much of the field research has focused on calibrating the Landsat thermal band and more recently on predicting ET (Wukelic et al. 1989; Gibbons et al. 1990; Link et al. 1991). This early effort has produced net radiation maps of portions of the Hanford Site and simple relationships predicting latent heat flux as a function of surface temperature and NDVI. A simple set of Mathcad programs has been developed (Appendix B) to facilitate evaluation of algorithms used for atmospheric corrections, sun angle adjustments, as well as calculations of net radiation and NDVI values from DN values obtained from Landsat.

This dissertation reports field measurements used to calibrate net radiation, soil heat flux, and sensible heat transport equations necessary for a mechanistically based approach to estimating water balance with remotely sensed data. The outcome has only been partially successful. The results of the research have characterized the energy balance at four sites with different semi-arid communities on two Landsat overflight days in 1989. Also, this thesis has shown latent heat flux density to be nearly equal to or less than soil heat flux density (within data noise level) at three sites. The fourth site with uniform dense grass cover has a latent heat flux density nearly three times the soil heat flux density value, and slightly higher than the other site's latent heat flux density values.

Four days of energy balance data collected in 1988 at the bunchgrass and sagebrush sites are also reported and agreement between Bowen ratio method and lysimeters is very good. The data from the lysimeters (2.25 m^2 in area) match quite well with the Bowen ratio measurements, which have a mixed sampling footprint of hundreds of square meters for the air temperature and vapor pressure measurements, less than 5 m^2 for net and reflected radiation, and less than 0.1 m^2 for soil heat flux.

Successful application of remote sensing for estimating latent and sensible heat flux in arid systems must address two major limitations that have been revealed in this dissertation. First, soil heat flux is significantly different across the Hanford Site ranging from 10 to

almost 50% of the R_N value. Several researchers have advocated the use of NDVI as an indicator of G_T, and data collected at the Hanford Site indicates that decreases in NDVI are associated with increases in G_T except under dense grass canopies. But, there are significant differences in the G_T/R_N ratios between years and measurement sites. The differences are in part a function of soil type and soil moisture; but after reviewing the G_T, rainfall, and temperature data, yearly precipitation and temperature differences may control accumulated litter that in turn affects soil heat flux and reflected radiant energy.

A few Hanford Site studies have measured standing biomass, but the litter is generally ignored (Bolton et al. 1991). The wide range in soil heat flux density was not expected when the monitor program started, so a properly designed experiment collecting G_T, litter, and NDVI was not setup. In the future, a simple measurement program using diurnal soil temperature profile changes, vegetation and litter sampling, and spectral reflectance measurements would be an inexpensive and enlightening study.

The most severe limitation is the lack of a simple equation to predict sensible heat flux accurately at a specific time of day. Only recently have a few studies (Hall et al. 1992, Kohsiek et al. 1993) shown the poor predictive capabilities of simple aerodynamic transport equations. Many earlier papers have reported on applying transport equations to diurnal cycles where fluxes range from 0 to several hundred watts per square meter achieving good correlations between measurements and predictive equations.

This research has calibrated a sensible heat transport equation to a bunchgrass and sagebrush environment, using 1988 data acquired within an hour of the typical Landsat (daylight) overpass time. The equation is used with Landsat overpasses acquired in 1986 and 1989. Using the equations developed from data sets limited to near-overpass time periods considerable variability remains between predicted and measured values of sensible heat flux at the time of overflight.

In light of these results, a set of equations that partition available energy between soil and vegetation may be necessary. Recently, additional data sets have been acquired by the author to examine partitioned canopy representations of energy balance at a sagebrush site. If these

more complex algorithms prove successful at an intensely instrumented site, it may be possible to re-examine the data sets collected since 1986 and partition available energy before applying the flux equations.

Bibliography

Aboukhaled, A., A. Alfaro, and M. Smith, 1982. *Lysimeters*. FAO Irrigation and Drainage Paper #39, FAO of the United Nations (Rome).

Allen, R. G., T. A. Howell, W. O. Pruitt, I. A. Walter, and M. E. Jensen, eds., 1991. *Lysimeters for Evapotranspiration and Environmental Measurements*. American Soc. of Ag. Eng., St. Joseph, Michigan, 444 pp.

Andre, J. C., J. P. Goutorbe, and A. Perrier, 1986. "HAPEX-MOBILHY: A Hydrologic Atmospheric Experiment for the Study of Water Budget and Evaporation Flux at the Climatic Scale." *Bull. Am. Meteorol. Soc.* 67:138-144.

Angus, D. E. and P. J. Watts, 1984. "Evapotranspiration - How Good is the Bowen Ratio Method?" *Agric. Water Management* 8:133-150.

Arya, S.P.S., 1988. *Introduction to Micrometerology*, Academis Press, Inc., San Diego, California.

Bolton, H. Jr., S. O. Link, J. L. Smith, J. L. Downs, and M. E. Thiede, 1991. "Dynamics of Soil Inorganic Nitrogen Beneath Bromus Tectorum." In *Part 2: Environmental Sciences*, PNL-8000, Part 2 of *Pacific Northwest Laboratory Annual Report for 1991 to the DOE Office of Energy Research*, pp. 74-77. Pacific Northwest Laboratory, Richland, Washington.

Bowen, I. S., 1926. "The Ratio of Heat Losses by Conduction and by Evaporation from Any Water Surface." *Phys. Rev.* 27:779-787.

Brownell, L. E., J. G. Backer, R. E. Isaacson, and D. J. Brown, 1975. *Soil Moisture Transport in Arid Site Vadose Zones*. ARH-ST-123, National Technical Information Service, Springfield, Virginia.

Brunel, J. P., 1989. "Estimation of Sensible Heat Flux from Measurements of Surface Radiative Temperature and Air Temperature at Two Meters: Application to Determine Actual Evaporation Rate." *Agric. For. Meteor.* 46:179-191.

Brutsaert, W. H., 1975. "On a Derivable Formula for Long-Wave Radiation from Clear Skies." *Water Resour. Res.* 11:742-744.

Brutsaert, W. H., 1982. *Evaporation into the Atmosphere*. Reidel, Dordrecht, The Netherlands, 299 pp.

Buttler, I. W., and S. J. Riha, 1989. A General Purpose Simulation Model of the Soil-Plant-Atmosphere System (Software version 1.1). Cornell Research Foundation.

Campbell, G. S., 1977. *An Introduction to Environmental Biophysics*. Springer-Verlag, New York, Inc., New York.

Camuffo, D., and A. Bernardi, 1982. "An Observational Study of Heat Fluxes and Their Relationship with Net Radiation." *Boundary Layer Meteor.* 23:359-368.

Chatters, J. C., ed., 1989. *Hanford Cultural Resources Management Plan.* PNL-6942, Pacific Northwest Laboratory, Richland, Washington.

Choudhury, B. J., 1991. "Multispectral Satellite Data in the Context of Land Surface Heat Balance." *Reviews of Geophysics* 29:217-236.

Choudhury, B. J., S. B. Idso, and R. J. Reginato, 1987. "Analysis of an Empirical Model for Soil Heat Flux under a Growing Wheat Crop for Estimating Evaporation by an Infrared-Temperature Based Energy Balance Equation." *Agric. For. Meteor.* 39:283-297.

DOE. See U.S. Department of Energy.

Doran, J. C., F. J. Barnes, R. L. Coulter, T. L. Crawford, D. D. Baldocchi, L. Balick, D. R. Cook, D. Cooper, R. J. Dobosy, W. A. Dugas, L. Fritschen, R. L. Hart, L. Hipps, J. M. Hubbe, W. Gao, R. Hicks, R. R. Kirkham, K. E. Kunkel, T. J. Martin, T. P. Meyers, W. Proch, J. D. Shannon, W. J. Shaw, E. Swiatek, and D. D. Whiteman. 1992. "The Boardman Regional Flux Experiment." *Bulletin of American Meteor. Society* 73(11):785-795.

EarthInfo, Inc., 1992. *EarthInfo's USGS Daily Values: User's Manual.* EarthInfo, Inc., Boulder, Colorado.

Fayer, M. J., and G. W. Gee, 1985. *UNSAT-H, An Unsaturated Soil Water Flow Code for Use at the Hanford Site: Code Documentation.* PNL-5585, Pacific Northwest Laboratory, Richland, Washington.

Field, R. T., L. J. Fritschen, E. T. Kanemasu, E. A. Smith, J. B. Stewart, S. B. Verma, and W. P. Kustas, 1992. "Calibration, Comparison, and Correction of Net Radiation Instruments Used During FIFE." *J. Geophs. Res.* 97:18681-18695.

FIFE Special Issue, 1992. *First ISLSCP Field Experiment.* American Geophysical Union, Washington, D.C.

Fritschen, L. J., and J. R. Simpson, 1982. "An Automatic System for Measuring Bowen Ratio Gradients Using Platinum Resistance Elements." In *Temperature Its Measurement and Control in Science and Industry*, Vol. 5, pt. 2, pp. 739-742, American Institute of Physics, New York.

Fritschen, L. J., and J. R. Simpson, 1989. "Surface Energy and Radiation Balance Systems: General Description and Improvements." *J. Appl. Meteor.* 28:680-689.

Fritschen, L. J., J. Hsia, and P. Doraiswamy, 1977. "Evapotranspiration of a Douglas Fir Determined with a Weighing Lysimeter." *Water Resour. Res.* 13:145-148.

Fuchs, M. and A. Hadas, 1972. "The Heat Flux Density in a Non-Homogeneous Bare Loessial Soil." *Boundary Layer Meteor.* 3:191-200.

Gee, G. W., 1987. *Recharge at the Hanford Site: Status Report.* PNL-6403, Pacific Northwest Laboratory, Richland, Washington.

Gee, G. W. and D. Hillel, 1988. "Groundwater Recharge in Arid Regions: Review and Critique of Estimation Methods." *J. Hydrological Processes* 2:255-266.

Gee, G. W. and R. R. Kirkham, 1984. *Arid Site Water Balance: Evapotranspiration Modeling and Measurements.* PNL-5177, Pacific Northwest Laboratory, Richland, Washington.

Gee, G. W., M. D. Campbell, and S. O. Link, 1991. "Arid Site Water Balance Using Monolith Lysimeters." In *Lysimeters for Evapotranspiration and Environmental Measurements.* American Society of Civil Engineers, New York.

Gee, G. W., M. J. Fayer, M. L. Rockhold, and M. D. Campbell, 1992. "Variations in Recharge at the Hanford Site." *Northwest Science* 66:237-250.

Gee, G. W., R. R. Kirkham, J. L. Downs, and M. D. Campbell, 1989. *The Field Lysimeter Test Facility (FLTF) at the Hanford Site: Installation and Initial Tests.* PNL-6810, Pacific Northwest Laboratory, Richland, Washington.

Gee, G. W., M. L. Rockhold, and J. L. Downs, 1989. *Status of FY 1988 Soil-Water Balance Studies on the Hanford Site.* PNL-6750, Pacific Northwest Laboratory, Richland, Washington.

Gibbons, D. E., S. O. Link, B. A. LeBaron, R. R. Kirkham, and G. W. McWethy, 1991. "Landscape Ecological Studies: Quantitative Remote Sensing of Evapotranspiration." In *Part 2: Environmental Sciences*, PNL-7600, Part 2 of *Pacific Northwest Laboratory Annual Report for 1990 to the DOE Office of Energy Research*, pp. 64-70. Pacific Northwest Laboratory, Richland, Washington.

Greacen, E. L. ed., 1981. *Soil Water Assessment by the Neutron Method.* CSIRO, Adelaide, Australia.

Hajek, B. F., 1966. *Soil Survey-Hanford Project in Benton County, Washington.* BNWL-243, Pacific Northwest Laboratory, Richland, Washington.

Hall, F. G., K. F. Huemmrich, S. J. Goetz, P. J. Sellers, and J. E. Nickeson, 1992. "Satellite Remote Sensing of Surface Energy Balance: Success, Failures, and Unresolved Issues in FIFE." *J. Geophys. Res.* 97:19061-19089.

Ham, J. M., and J. L. Heilman, 1991. "Aerodynamic and Surface Resistance Affecting Energy-Transport in Sparse Crop." *J. Agri. and Forest Meteorology* 53:267-284.

Hanks, R. J., and G. Ashcroft, 1980. *Applied Soil Physics*. Springer-Varlag, New York, Inc, New York.

Harrold, L. L., and F. R. Dreibelbis, 1967. *Evaluation of Agricultural Hydrology by Monolith Lysimeters*. Tech. Bull. No. 1367, U.S. Department of Agriculture, Washington, D.C., 123 pp.

Hatfield, J. L., D. F. Wanjura, and G. L. Barker, 1985. "Canopy Temperature Response to Water Stress Under Partial Canopy." *Transactions of the ASHE* 28(5):1607-1611.

Hillel, D., 1982. *Introduction to Soil Physics*. Academic Press, New York.

Holwill, C. J., and J. B. Stewart, 1992. "Spatial Variability of Evaporation Derived from Aircraft and Ground-Based Data." *J. Geophys. Res.* 97:18673-18680.

Howell, J. V., 1957. *Glossary of Geology and Related Sciences. American Geologic Institute*. National Academy of Sciences - National Research Council, Washington, D.C., p. 174.

Howell, T. A., A. D. Schneider, and M. E. Jensen, 1991. "History of Lysimeter Design and Use for Evapotranspiration Measurements." In *Lysimeters for Evapotranspiration and Environmental Measurements*. American Soc. of Ag. Eng, St. Joseph, Michigan, 444 pp.

Jackson, R. D., 1984. "Total Reflected Solar Radiation Calculated from Multi-Band Sensor Data." *Agric. For. Meteor.* 33:163-175.

Jackson, R. D., P. J. Pinter, Jr., and R. J. Reginato, 1985. "Net Radiation Calculated from Remote Multispectral and Ground Station Meteorological Data." *Agric. For. Meteor.* 35:153-164.

Jackson, R. D., R. J. Reginato, and S. B. Idso, 1977. "Wheat Canopy Temperature: A Practical Tool for Evaluating Water Requirements." *Water Resour. Res.* 13:651-656.

Jackson, R. D., P. N. Slater, and P. J. Pinter, Jr., 1983. "Discrimination of Growth and Water Stress in Wheat by Various Vegetation Indices through Clear and Turbid Atmospheres." *Remote Sens. Env.* 13:187-208.

Jones, T. L., 1989. *Simulating the Water Balance of an Arid Site*. Ph.D. Thesis, Washington State University, Pullman, Washington.

Kirkham, R. R., G. W. Gee, and J. L. Downs, 1987. *An Experimental Plan for the Field Lysimeter Test Facility (FLTF)*. PNL-6351, Pacific Northwest Laboratory, Richland, Washington.

Kirkham, R. R., G. W. Gee, and T. L. Jones, 1984. "Weighing Lysimeters for Long-Term Water Balance Investigations at Remote Sites." *Soil Sci. Soc. Am. J.* 48:1205-1207.

Kneizys, F. X., E. P. Shettle, W. O. Gallery, J. H. Chetwynd, L. W. Abreu, J. E. A. Selby, S. A. Clough, and R. W. Fern, 1983. *Atmospheric Transmittance/Radiance: Computer Code LOWTRAN 6.* AFGL-TR-83-0187, U.S. Air Force Geophysics Laboratory, Hansom Air Force Base, Massachusetts.

Kohsiek, W., H. A. R. De Bruin, H. The, and B. Van Den Hurk, 1993. "Estimation of the Sensible Heat Flux of a Semi-Arid Area Using Surface Radiative Temperature Measurements." *Boundary Layer Meteor.* 63:213-230.

Kustas, W. P., B. J. Choudhury, M. S. Moran, R. J. Reginato, R. D. Jackson, L. W. Gay, and H. L. Weaver, 1989. "Determination of Sensible Heat Flux Over Sparse Canopy Using Thermal Infrared Data." *Agric. For. Meteor.* 44:197-216.

Kustas, W. P., 1990. "Estimates of Evapotranspiration with a One- and Two-Layer Model of Heat Transfer Over Partial Canopy Cover." *J. Appl. Meteor.* 29:204-715.

Kustas, W. P., and C. S. T. Daughtry, 1990. "Estimation of the Soil Heat Flux/Net Radiation from Spectral Data." *Agric. For. Meteor.* 49:205-223.

Kustas, W. P., D. C. Goodwirch, M. S. Moran, S. A. Amer, L. B. Bach, J. H. Blanford, A. Chehbouni, H. Classeen, W. E. Clements, P. C. Doraiswamy, P. Dubois, T. R. Clarke, C. S. T. Daughtry, D. I. Gellman, T. A. Grant, L. E. Hipps, A. R. Heute, K. S. Humes, T. J. Jackson, T. O. Keefer, W. D. Nichols, R. Parry, E. M. Perry, R. T. Pinker, P. J. Pinter, Jr., J. Qi, A. C. Riggs, T. J. Schmugge, A. M. Shutko, D. I. Stannard, E. Swiatek, J. D. van Leeuwen, J. van Zyl, A. Vidal, J. Washburne, and M. A. Weltz, 1991. "An Interdisciplinary Field Study of the Energy and Water Fluxers in the Atmosphere -- Biosphere System over Semiarid Rangelands: Description and Some Preliminary Results." *Bulletin American Meteor. Society 72*(11):1683-1705.

Link, S. O., G. M. Petrie, L. G. McWethy, R. R. Kirkham, and L. E. Rogers, 1992. "Landscape Ecological Studies: Net Radiation and the Relationship Among Surface Temperature, Normalized Difference Vegetation Index, and Elevation on the Arid Lands Ecology Reserve." In *Part 2: Environmental Sciences*, PNL-8000, Part 2 of *Pacific Northwest Laboratory Annual Report for 1991 to the DOE Office of Energy Research*, pp. 128-132. Pacific Northwest Laboratory, Richland, Washington.

Marek, T. H., A. D. Schneider, T. A. Howell, and L. L. Ebeling, 1988. "Design and Construction of Large Weighing Monolithic Lysimeters." *Trans. of ASAE* 31:477-484.

Markham, B. L., and J. L. Barker, 1986. "Landsat MSS and TM Post-Calibration Dynamic Ranges, Exoatmospheric Reflectances and At-Satellite Temperatures." *EOSAT Landsat Tech. Notes* Aug.:3-8.

McMillen, R. T., 1986. *A Basic Program for Eddy Correlation in Non-Simple Terrain,* NOAA Tech. Memo. ERL ARL-147, Silver Spring, Maryland.

Mercer, J. W., P. S. C. Rao, and I. W. Marine, eds., 1983. *Role of the Unsaturated Zone in Radioactive and Hazardous Waste Disposal*, Ann Arbor Publishing, Ann Arbor, Michigan.

Monteith, J. L., 1963. "Gas Exchange in Plant Communities." *Environmental Control of Plant Growth*, ed. L. T. Evans, pp. 95-112. Academic Press, New York.

Monteith, J. L., 1964. "Evaporation and Environment." In *The State and Movement of Water in Living Organisms* from 19th Symp. Soc. Exp. Biol., pp. 205-234. Academic Press, New York.

Monteith, J. L., 1975. *Principles of Environmental Physics*. Edward Arnold, London. 241 pp.

Moran, M. S., R. D. Jackson, L. H. Raymond, L. W. Gay, and P. N. Slater, 1989. "Mapping Surface Energy Balance Components by Combining Landsat Thematic Mapper and Ground-Based Meteorological Data." *Remote Sens. Environ.* 30:77-87.

Nichols, W. D., 1992. "Energy Budgets and Resistances to Energy Transport in Sparsely Vegetated Rangeland." *Agric. For. Meteor.* 60:221-247.

Oliver, S. A., H. R. Oliver, J. S. Wallace, and A. M. Roberts, 1987. "Soil Heat Flux and Temperature Variation with Vegetation, Soil Type, and Climate." *Agric. For. Meteor.* 39:257-269.

Penman, H. L., 1948. "Natural Evapotranspiration from Open Water, Bare Soil and Grass." *Proc. R. Soc. London Ser. A.* 193:120-145.

Phillips, S. J., A. C. Campbell, M. D. Campbell, G. W. Gee, H. H. Hoober, and K. L. Schwarzmiller, 1979. *A Field Test Facility for Monitoring Water/Radionuclide Transport Through Partially Saturated Geologic Media: Design, Construction, and Preliminary Description*. PNL-3226, Pacific Northwest Laboratory, Richland, Washington.

Reece, C. F., 1991. *Sparse Plant Community Effects on Soil Water Balance of an Arid Site.* Ph.D·Thesis, Washington State University, Pullman, Washington.

Rickard, W. H., L. E. Rogers, B. E. Vaughan, and S. F. Liebetrau, 1988. "Shrub-Steppe Balance and Change in a Semi-Arid Terrestrial Ecosystem." Series: *Developments in Agricultural and Managed Forest Ecology*, Vol. 20, Elsevier Science Pub., New York.

Roberts, D. A., M. O. Smith, and J. B. Adams, 1993. "Green Vegetation, Nonphotosynthetic Vegetation, and Soils in AVIRIS Data." *Remote Sens. Environ.* 44:255-269.

Rosenberg, N. J., B. L. Blad, and S. B. Verma, 1983. *Microclimate the Biological Environment*. John Wiley & Sons, New York.

Rouse, J. W., R. H. Haas, J. A. Schell, D. W. Deering, and J. C. Harlan, 1974. *Monitoring the Vernal Advancement and Retrogradation (Greenwave Effect) of Natural Vegetation*. NASA/Goddard Space Flight Center, Type III Final Report, Greenbelt, Maryland.

Sharma, M. L., ed., 1984. *Evapotranspiration from Plant Communities*. Elsevier Science Pub., New York.

Shuttleworth, W. J., and R. J. Gurney, 1990. "The Theoretical Relationship between Foliage Temperature and Canopy Resistance in Sparse Crops." *Q.J.R. Met. Soc.* 116:497-519.

Shuttleworth, W. J., and J. S. Wallace, 1985. "Evaporation from Sparse Crops-and Energy Combination Theory." *Q.J.R. Met. Soc.* 111:839-855.

Smith, M. O., S. Ustin, J. B. Adams, and A. R. Gillespie, 1990. "Vegetation in deserts: I. A Regional Measure of Abundance from Multispectral Images." *Remote Sens. Environ.* 31:1-26.

Stone, W. A., J. M. Thorp, O. P. Gifford, and D. J. Hoitink, 1983. *Climatological Summary for the Hanford Area*. PNL-4622, Pacific Northwest Laboratory, Richland, Washington.

U.S. Department of Energy (DOE), 1987. *Final Environmental Impact Statement, Disposal of Hanford Defense High Level, Transuranic and Tank Waste, Hanford Site, Richland, Washington*. DOE/EIS-0113, Vol. 1, U.S. Department of Energy, Washington, D.C.

Van Hylckama, T. E. A., 1968. "Water Level Fluctuation in Evapotranspirometers." *Water Resour. Res.* 4:761-768.

Wukelic, G. E., D. E. Gibbons, L. M. Martucci, and H. P. Foote, 1989. "Radiometric Calibration of Landsat Thematic Mapper Thermal Band." *Remote Sens. Environ.* 28:339-347.

Appendix A

Neutron Probe Sample Data Set and Calculations

The following calibration equation was used:

$$\text{Raw counts} * 0.000942 - 1.68 = \text{percent moisture}$$

To calculate cm of water in the soil,

$$\text{percent moisture} * \text{depth interval (cm)} = \text{cm of } H_2O$$

The three tables that follow (Tables A.1 through A.3) represent raw and processed data for the sagebrush site on March 23, 1989.

This example data set is extracted from a database of a currently inactive program referred to as Dynamics of Arid Lands (for further information on this database, contact Dr. Glendon Gee, Pacific Northwest Laboratory, Richland, Washington). Portions of the data set have been reported in Gee et al. (1991)

TABLE A.1. Raw Neutron Probe Data for Sagebrush Site on 23-Mar-89.

Neutron Probe Data for the ALE Site on March 23, 1989

0	1 Stat Data	2 Standard Counts	3 Depth cm	4 HOLE 20	5 HOLE 19	6 HOLE 22	7 HOLE 16	8 HOLE 13	9 HOLE 7N	10 HOLE 7S
1 ID Code->	SN3489	1962	-30	18002	19916	20928	21491	19104	19563	17734
2 Artificial STD->		2012	-45	16527	20571	21275	21981	19591	19118	17010
3 MSF->	1993.05	1981	-80	10226	14418	16193	11982	10745	10683	10348
4 STD Dev->	54.61	1897	-125	11051	9783	12296	9154	9955	11548	11077
5 Probe:		2138	-175	11646	10525	10660	9467	11814		
6 503_DR		1988	-225	10241	10391	11249	9432	9396		
7 H30103489		1979	-275	9504		10512	8791	9015		
8 Time:		2014								
9 15 sec.		2022								
10 Taken by:		2008								
11 MJ Harris		1875								
12 Entered by:		2041								
13 D Felmy		1991								
14 by Hand		2018								
15 Processed by:		1990								
16 ALENP_1		1956								
17 Slope:		1958								
18 0.000942		1978								
19 Offset:		2001								
20 -1.680000		2052								

0	11 HOLE 4	12 ASB3_S	13 ASB4_N
1 ID Code->	19927	19411	18400
2 Artificial STD->	20100	16137	15211
3 MSF->	12704	10238	9745
4 STD Dev->	9742	10901	10395
5 Probe:	10502		
6 503_DR	10616		
7 H30103489	9204		
8 Time:			
9 15 sec.			
10 Taken by:			
11 MJ Harris			
12 Entered by:			
13 D Felmy			
14 by Hand			
15 Processed by:			
16 ALENP_1			
17 Slope:			
18 0.000942			
19 Offset:			
20 -1.680000			

TABLE A.2. Soil Water Content (%) for Sagebrush Site on 23-Mar-89.

Neutron Probe Data for the ALE Site on March 23, 1989

0	1 Stat Data	2 Standard Counts	3 Depth cm	4 HOLE 20	5 HOLE 19	6 HOLE 22	7 HOLE 16	8 HOLE 13	9 HOLE 7N	10 HOLE 7S
1 ID Code->	SN3489	1962	-30	15.29	17.09	18.04	18.57	16.32	16.76	15.03
2 Artificial STD->		2012	-45	13.90	17.71	18.37	19.03	16.78	16.34	14.35
3 MSF->	1993.05	1981	-80	7.96	11.91	13.58	9.61	8.45	8.39	8.07
4 STD Dev->	54.61	1897	-125	8.73	7.54	9.91	6.95	7.70	9.20	8.76
5 Probe:		2138	-175	9.30	8.24	8.37	7.24	9.45		
6 503_DR		1988	-225	7.97	8.11	8.92	7.21	7.17		
7 H30103489		1979	-275	7.28		8.23	6.60	6.82		
8 Time:		2014								
9 15 sec.		2022								
10 Taken by:		2008								
11 MJ Harris		1875								
12 Entered by:		2041								
13 D Felmy		1991								
14 by Hand		2018								
15 Processed by:		1990								
16 ALENP_1		1956								
17 Slope:		1958								
18 0.000942		1978								
19 Offset:		2001								
20 -1.680000		2052								

0 Note: 3 ring binder 07-APR-89 MJ Kanyid	11 HOLE 4	12 ASB3_S	13 ASB4_N	14 ROWMEAN OF PLOT WELLS	15 STANDARD DEV PLOT WELLS	16 ROWMEAN OF WL WELLS	17 STANDARD DEV WL WELLS
1 ID Code->	17.10	16.61	15.66	16.78	1.224	16.14	0.672
2 Artificial STD->	17.26	13.53	12.65	16.72	1.815	13.09	0.622
3 MSF->	10.29	7.97	7.50	9.78	2.043	7.74	0.332
4 STD Dev->	7.50	8.59	8.12	8.29	1.014	8.35	0.332
5 Probe:	8.22			8.47	0.811		
6 503_DR	8.32			7.95	0.672		
7 H30103489	6.99			7.18	0.635		
8 Time:							

TABLE A.3. Soil Moisture Storage (cm) for Sagebrush Site on 23-Mar-89.

Neutron Probe Data for the ALE Site on March 23, 1989

0	1 Stat Data	2 Standard Counts	3 Depth cm	4 HOLE 20	5 HOLE 19	6 HOLE 22	7 HOLE 16	8 HOLE 13	9 HOLE 7N	10 HOLE 7S
1 ID Code>	SN3489	1962	-30	4.59	5.13	5.41	5.57	2.68	5.03	4.51
2 Artificial STD->		2012	-45	2.19	2.61	2.73	2.82	-2.86	2.48	2.20
3 MSF->	1993.05	1981	-80	3.83	5.18	5.59	5.01	0.30	4.33	3.92
4 STD Dev->	54.61	1897	-125	3.76	4.38	5.29	3.73	0.72	3.96	3.79
5 Probe:		2138	-175	4.51	3.95	4.57	3.55	0.25		
6 503_DR		1988	-225	4.32	4.09	4.32	3.61	0.03		
7 H30103489		1979	-275	3.81		4.29	3.45			
8 Time:		2014								
9 15 sec.		2022								
10 Taken by:		2008								
11 MJ Harris		1875								
12 Entered by:		2041								
13 D Felmy		1991								
14 by Hand		2018								
15 Processed by:		1990								
16 ALENP_1		1956								
17 Slope:		1958								
18 0.000942		1978								
19 Offset:		2001								
20 -1.680000		2052								

0	11 HOLE 4	12 ASB3_S	13 ASB4_N	14 ROWMEAN OF PLOT WELLS	15 STANDARD DEV PLOT WELLS	16 ROWMEAN OF WL WELLS	17 STANDARD DEV WL WELLS
1 ID Code->	5.13	4.98	4.70	5.03	0.366	4.84	0.198
2 Artificial STD->	2.58	2.26	2.12	2.51	0.227	2.19	0.099
3 MSF->	4.82	3.76	3.53	4.64	0.619	3.64	0.163
4 STD Dev->	4.00	3.73	3.51	4.07	0.546	3.62	0.156
5 Probe:	3.93			4.13	0.393		
6 503_DR	4.14			4.11	0.262		
7 H30103489	3.83			3.78	0.336		
8 Time:							
9 15 sec.							
10 Taken by:							

Appendix B

Calculations of Sun Angle, Atmospheric Corrections to Landsat, NDVI, $R_S\uparrow$, and R_N

The following material is a printout of a Mathcad program. No editing or formatting has been done.

Appendix B Calculations fo sun angle, atmospheric corrections to Landsat, NDVI, Rs up, and Rn

This Mathcad program determines sun angle for day and time, then applies atmospheric correction to landsat data set (modified from program by Dan Gibbons and Guy McWethy personal comm.) to determine SWR reflected, then calculates radiation buget to determine Rn, finally the normalized vegetation index is calculated.

Day of year $JULDAY := 128$ Time of Day (approx Sat. overflight) $XHH := 10$

Site location $LONG := 119.5$ $LAT := 45.5$
Time zone offset $XMIN := 12$

Calculate solar declination angle

alternate equation

$$DECL := 23.45 \cdot \sin\left[\left[\left(\frac{360}{365}\right) \cdot (284 + JULDAY)\right] \cdot deg\right]$$

$$ndecl := -23.5 \cdot \cos\left(\left(360 \cdot \frac{JULDAY + 10}{365.25} \cdot deg\right)\right)$$

$DECL = 16.969$

$ndecl = 16.909$

Calculation of zenith angle **********

$$ZA := \left[\left(\frac{360}{365}\right) \cdot JULDAY - 1\right] \cdot deg$$

$$XE := 229.18 \cdot (.000075 + .001868 \cdot \cos(ZA) - .032077 \cdot \sin(ZA) - .014615 \cdot \cos(2.0 \cdot ZA) - .04089 \cdot \sin(2.0 \cdot ZA))$$

$$XS := XHH + \left[\frac{XMIN + 4.0 \cdot (120.0 - LONG) + XE}{60}\right]$$

$XS = 10.295$

$W := \sin(DECL \cdot deg)$
$W = 0.292$

$W1 := \sin\left(LAT \cdot \frac{\pi}{180}\right)$ $W2 := \cos(LAT \cdot deg)$ $W3 := \cos(DECL \cdot deg)$ $W4 := 15 \cdot (12 - XS)$

$W1 = 0.713$ $W2 = 0.701$ $W3 = 0.956$ $W4 = 25.57$

$\cos(W4 \cdot deg) = 0.902$

$THETA := acos((W \cdot W1 + W2 \cdot \cos(W4 \cdot deg) \cdot W3))$

$THETA = 35.62 \cdot deg$

Results

8-May-89=35.62

1-Jun-89=31.537

exoatomospheric irradiance mW/sq.cm.

$$xatmirr := \begin{bmatrix} 195.8 \\ 182.8 \\ 155.9 \\ 104.5 \\ 21.93 \\ 10 \\ 7.457 \end{bmatrix}$$

TM4 Band Gains mW/sq.cm. Sr. microm

$$GainTM4 := \begin{bmatrix} .060235 \\ .11749 \\ .08059 \\ .08145 \\ .01081 \\ 1000 \\ .005698 \end{bmatrix}$$

TM4 Band Offsets

$$OffsetTM4 := \begin{bmatrix} -.15 \\ -.28 \\ -.12 \\ -.15 \\ -.037 \\ 1000 \\ -.0151 \end{bmatrix}$$

Band Atmospheric Transmittance

$$trans := \begin{bmatrix} .875 \\ .919 \\ .951 \\ .942 \\ .895 \\ .832 \\ .924 \end{bmatrix}$$

Band Atmospheric Radiance mW/sq.cm. Sr. microm.

$$pathrad := \begin{bmatrix} 2.737 \\ 1.436 \\ .638 \\ .133 \\ .002 \\ .106 \\ .001 \end{bmatrix}$$

TM Band Width

$$HPB := \begin{bmatrix} .07 \\ .0813 \\ .0668 \\ .1281 \\ .2107 \\ 0 \\ .2518 \end{bmatrix}$$

Find surface irradiance correcting for solar angle, atm. transmission, atm radiance **********

$j := 0..6$

$$RADD_j := \left[\left[\left(\frac{xatmirr_j}{\pi}\right)\cdot\left(trans_j\right)^{\left[1+\left(\frac{1}{\cos(THETA)}\right)\right]} + .72\cdot pathrad_j\right]\cdot\cos(THETA)\right]$$

Atm. background correction in DN's

$$B_j := \frac{pathrad_j - OffsetTM4_j}{GainTM4_j}$$

Expected DN's at 100 % reflectance

$$XM_j := \frac{RADD_j}{GainTM4_j}$$

$$\frac{1}{\cos(THETA)} = 1.23$$

$$\sec(THETA) = 1.23$$

Example given

$DN := 255$ calculated maximun reflectance for TM4 band 2 (note arrays indices begin with 0)

$$DNL := \frac{DN - B_1}{XM_1}$$

$DNL = 0.706$

These DN values were obtain by inclosing a region representative of each field site and determining the mean value for that group of pixels. .

DN := READPRN(dnmay8) Site := 0..7 bn := 0..6 8 sites by 7 bands

$$DN = \begin{bmatrix} 96.97 & 106.86 & 104.41 & 110.52 & 105.61 & 90.56 & 99.42 & 94.79 \\ 37.69 & 43.5 & 42.77 & 47.56 & 44.19 & 36.7 & 42.39 & 40.41 \\ 47.83 & 55.06 & 52.72 & 62.63 & 55.55 & 43.33 & 48.92 & 45.17 \\ 56.07 & 54.9 & 58.18 & 69.72 & 63.97 & 72.15 & 63.36 & 77.29 \\ 107.8 & 82.93 & 95.77 & 113.98 & 108.77 & 93.11 & 101.25 & 107.12 \\ 193.59 & 192.56 & 181.27 & 179.81 & 176.67 & 176.4 & 152.07 & 155.75 \\ 63.3 & 49.86 & 58.32 & 68.18 & 63.13 & 43.36 & 46.64 & 46.87 \end{bmatrix}$$

Band width

$$HPB := \begin{bmatrix} .07 \\ .0813 \\ .0668 \\ .1281 \\ .2107 \\ 0 \\ .2518 \end{bmatrix}$$

Calculate surface reflectance **********

$$T1_{bn} := xatmirr_{bn} \cdot \left(trans_{bn}\right)^{sec(THETA)}$$

$$T2_{bn} := .72 \cdot pathrad_{bn} \cdot \pi$$

$$radcorr := \cos(THETA) \cdot (T1 + T2)$$

$$radcorr = \begin{bmatrix} 140.088 \\ 136.573 \\ 120.309 \\ 79.173 \\ 15.557 \\ 6.678 \\ 5.502 \end{bmatrix}$$

$$DNL_{bn,Site} := \frac{DN_{bn,Site} - B_{bn}}{XM_{bn}} \qquad \frac{THETA}{deg} = 35.62$$

Calculation of temperature and using standard formula
****

$K_1 := 67.162$ $K_2 := 1284.3$ $\tau := .832$ Transmission

$R_a := .106$ Radiance

$$R_{\lambda_{Site}} := .0056322 \cdot DN_{5,Site} + .1238$$

$$R_{c_{Site}} := \frac{R_{\lambda_{Site}} - R_a}{1.0 \cdot \tau} - \left(\frac{1}{\tau} - 1\right) \cdot .12$$

Temperature uncorrected

$$T_{u_{Site}} := \frac{K_2}{\ln\left[\left(\frac{K_1}{R_{\lambda_{Site}}}\right) + 1\right]}$$

$T_{u_{Site}} - 273$

45.607
45.235
41.1
40.557
39.38
39.279
29.793
31.273

Temperature corrected for atmospheric effects

$$T_{c_{Site}} := \frac{K_2}{\ln\left[\left(\frac{K_1}{R_{c_{Site}}}\right) + 1\right]}$$

$T_{c_{Site}} - 273$

51.47
51.041
46.253
45.622
44.257
44.139
33.075
34.807

BREB station air and wet bulb temperatures used to estimate incoming long wave radiation

$$AirWet := \begin{bmatrix} 23.81 & 13.72 \\ 24.84 & 13.95 \\ 24 & 14 \\ 22.82 & 13.75 \\ 23.01 & 14.3 \\ 24.13 & 14.32 \\ 24 & 14 \\ 24 & 14 \end{bmatrix}$$

Grass /
BWTF
Met. Station
Ale grass /
Alesage /
Low Sniv /
Up Sniv
Up Sniv2

$$EA_{sat_{Site}} := \exp\left(52.57633 - \frac{6790.4985}{AirWet_{Site,1} + 273} - 5.02808 \cdot \ln\left(AirWet_{Site,1} + 273\right)\right)$$

$$EA_{Site} := EA_{sat_{Site}} - .00066 \cdot \left[\left[1 + .00115 \cdot \left(AirWet_{Site,1} + 273\right)\right] \cdot 101.1 \cdot \left(AirWet_{Site,0} - AirWet_{Site,1}\right)\right]$$

$$EA_{sat} = \begin{bmatrix} 1.555083503 \\ 1.578508593 \\ 1.583641816 \\ 1.558121529 \\ 1.614750122 \\ 1.616842954 \\ 1.583641816 \\ 1.583641816 \end{bmatrix} \qquad EA = \begin{bmatrix} 0.66 \\ 0.612 \\ 0.696 \\ 0.753 \\ 0.842 \\ 0.746 \\ 0.696 \\ 0.696 \end{bmatrix}$$

$$\varepsilon_{a_{Site}} := 1.24 \cdot \left(\frac{EA_{Site}}{AirWet_{Site,0}}\right)^{\frac{1}{7}}$$

Atmospheric emissivity

$\varepsilon_{a_{Site}}$
0.743
0.731
0.748
0.762
0.773
0.755
0.748
0.748

Calculation of reflected Short wave radiation **********

$$SWR_{out_{Site}} := 2.54 \cdot \sum_{bn=1}^{6} radcorr_{bn} \cdot DNL_{bn,Site} \cdot HPB_{bn}$$

$radcorr_{bn}$	$radcorr_{bn} \cdot HPB_{bn}$
140.088	9.806
136.573	11.103
120.309	8.037
79.173	10.142
15.557	3.278
6.678	0
5.502	1.385

$SWR_{out_{Site}} \cdot 10$

111.589	Grass
111.915	BWTF
116.808	Met. Station
140.365	Ale grass
127.614	Alesage
117.494	Low Sniv
119.021	Up Sniv
129.218	Up Sniv2

$$SWR_{in} := \frac{\frac{808.57 + 819.04 + 814.13}{3}}{10}$$

$$SWR_{in} = 81.391$$

Long wave radiation out **********

$$LWR_{out_{Site}} := 5.6697 \cdot 10^{-9} \cdot \left(T_{c_{Site}}\right)^4$$

$$LWR2_{out_{Site}} := 5.6697 \cdot 10^{-9} \cdot \left(T_{u_{Site}}\right)^4$$

Difference in LWR out from atmospheric W/m2 corrected band 6

Long wave radiation in

$$LWR_{in_{Site}} := \varepsilon_{a_{Site}} \cdot \left[5.6697 \cdot 10^{-9} \cdot \left(AirWet_{Site,0} + 273\right)^4\right]$$

$$\left(LWR_{out} - LWR2_{out}\right) \cdot 10 = \begin{bmatrix} 44.208 \\ 43.608 \\ 37.113 \\ 36.284 \\ 34.51 \\ 34.358 \\ 21 \\ 22.979 \end{bmatrix}$$

Net Radiation calculated with constant SWR in

$$Rnet_{Site} := SWR_{in} - SWR_{out_{Site}} + LWR_{in_{Site}} - LWR_{out_{Site}}$$

$SWR_{out_{Site}} \cdot 10$	$LWR_{out_{Site}} \cdot 10$	$LWR_{in_{Site}} \cdot 10$	$Rnet_{Site} \cdot 10$	
112	628	327	401	Grass
112	625	326	403	BWTF
117	589	330	438	Met. Station
140	584	331	420	Ale grass
128	574	336	448	Alesage
117	574	333	456	Low Sniv
119	498	330	527	Up Sniv
129	509	330	506	Up Sniv2

Calculation of Normalized Difference Vegitation Index **********

from raw DN values

$$NDVI_{DN_{Site}} := \frac{DN_{3,Site} - DN_{2,Site}}{DN_{3,Site} + DN_{2,Site}}$$

Background values from Columbia River removed

$D3 := 23.64$ $D4 := 13.42$

$$NDVI_{BG_{Site}} := \frac{\left(DN_{3,Site} - D4\right) - \left(DN_{2,Site} - D3\right)}{\left(DN_{3,Site} - D4\right) + \left(DN_{2,Site} - D4\right)}$$

ratio radiance

$$NDVI_{c_{Site}} := \frac{\left(DNL_{3,Site} \cdot radcorr_3 \cdot HPB_3\right) - \left(DNL_{2,Site} \cdot radcorr_2 \cdot HPB_2\right)}{\left(DNL_{3,Site} \cdot radcorr_3 \cdot HPB_3\right) + \left(DNL_{2,Site} \cdot radcorr_2 \cdot HPB_2\right)}$$

ratioed reflectance

$$NDVI2_{Site} := \frac{\left(DNL_{3,Site}\right) - \left(DNL_{2,Site}\right)}{\left(DNL_{3,Site}\right) + \left(DNL_{2,Site}\right)}$$

$NDVI_{DN_{Site}}$	$NDVI_{BG_{Site}}$	$NDVI_{c_{Site}}$	$NDVI2_{Site}$	
0.079	0.24	0.456	0.36	Grass
-0.001	0.121	0.376	0.272	BWTF
0.049	0.187	0.424	0.324	Met. Station
0.054	0.164	0.418	0.317	Ale grass
0.07	0.201	0.439	0.341	Alesage
0.25	0.44	0.597	0.517	Low Sniv
0.129	0.289	0.496	0.403	Up Sniv
0.262	0.443	0.603	0.524	Up Sniv2

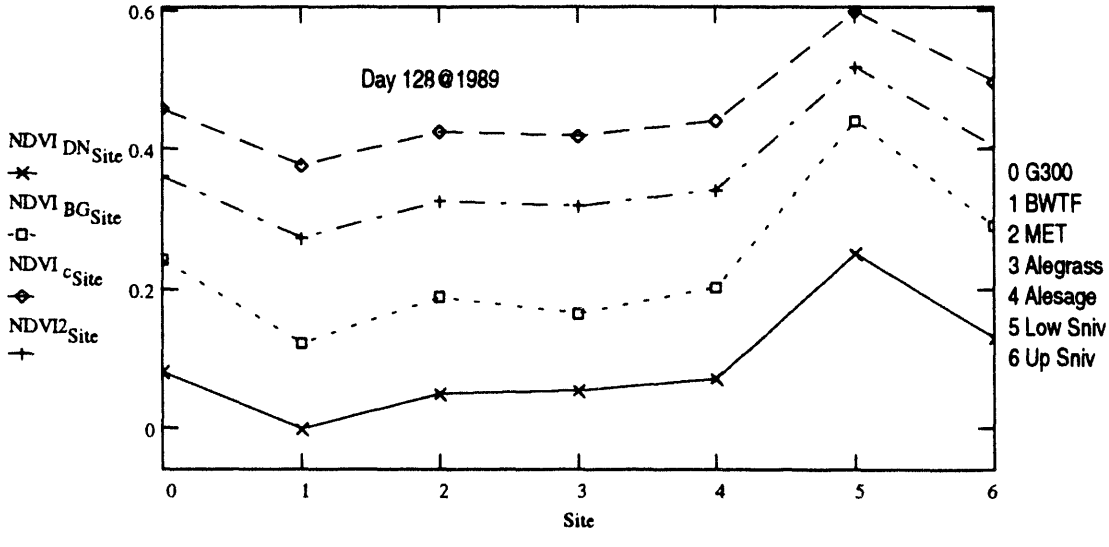

$\mathrm{corr}(NDVI2, NDVI_{DN}) = 0.998$ $\quad$ $\mathrm{mean}(NDVI2 - NDVI_{DN}) = 0.271$

$\mathrm{corr}(NDVI2, NDVI_{BG}) = 0.999$ $\quad$ $\mathrm{mean}(NDVI2 - NDVI_{BG}) = 0.122$

$\mathrm{corr}(NDVI2, NDVI_{c}) = 1.000$ $\quad$ $\mathrm{mean}(NDVI2 - NDVI_{c}) = -0.094$

Appendix C

Calculations of Aerodynamic Resistance for Bunchgrass in 1988

The following material is a printout of a Mathcad program. No editing or formatting has been done.

Appendix C Calculations of resistance (ra) for bunchgrass using 1988 data

This Mathcad program calibrates two sensible heat transport equations

Constants

$\rho := 1.164$ $C_p := 1010$ $\rho \cdot C_p = 1.176 \cdot 10^3$ $i := 0..36$ $k := .4$ $TOL := .00001$ $z := 2$

Read in data

$AG := READPRN(ag88le)$ Data at end of this appendix

Array labels
0 day.time 1 DAY 2 TIME 3 1CM 4 AIR SHELTER 5 AIR DRY BULB 6 2M U 7 IR TEMP
8 AVAIL ENERGY 9 LATENT 10 SENSIBLE

Estimate an appropriate surface radiometric temperature by compositing 1 cm soil and IR thermometer

$dt_i := \left[\left(AG_{i,3} \cdot .53 + AG_{i,7} \cdot .47\right) - AG_{i,5}\right]$ $TC1_i := AG_{i,3}$ 1 cm Soil $IR_i := AG_{i,7}$ Everest IR

$mean(TC1) = 28.274$ $mean(IR) = 25.223$

$mean(dt) = 12.103$

Solve for resistance from measured temperatures and H=Rn-G-E with E from lysimeters

$$R_{lys_i} := \frac{(dt_i) \cdot \rho \cdot C_p}{AG_{i,10}}$$

$mean(R_{lys}) = 82.747$

Method used by Moran et al. 1989 in alfalfa, wheat and cotton at Maricopa Ag. Cen. Phoenix, Az.
Assign vectors from array AG

$AG3_i := AG_{i,10}$ $\quad AG6_i := AG_{i,6}$ $\quad AG8_i := AG_{i,8}$ $\quad AG5_i := AG_{i,5}$

$x_i := dt_i$ $\quad AG8_i := AG_{i,8}$

$$G(AG6, AG5, dt, \eta) := \left[\left[\frac{\ln\left[\frac{\left(z-\eta\cdot\frac{2}{3}\right)}{\left(\frac{\eta}{8}\right)}\right]}{k}\right]^2 \cdot \left[\frac{1-15\cdot\left[\left(\frac{9.8}{AG5+273}\right)\cdot((-dt))\cdot\frac{z-\eta\cdot\frac{2}{3}}{(AG6\cdot.44)^2}\right]}{\left[1+75\cdot k^2\cdot\frac{\left[\frac{z-\eta\cdot\frac{2}{3}+\frac{\eta}{8}}{\left(\frac{\eta}{8}\right)}\right]^{.5}}{\ln\left[\frac{z-\eta\cdot\frac{2}{3}+\frac{\eta}{8}}{\left(\frac{\eta}{8}\right)}\right]^2}\cdot\left[\left[-\left[\left(\frac{9.8}{AG5+273}\right)\cdot((-dt))\cdot\frac{z-\eta\cdot\frac{2}{3}}{(AG6\cdot.44)^2}\right]\right]\right]^{.5}\right]}\right]^{-1}}{AG6\cdot.44}\right]$$

sensible measured - sensible estimated

$c := 0..36$

Initial guess

$$SSE(\eta) := \sum_c \left(AG3_c - \frac{\rho\cdot C_p\cdot dt_c}{G(AG6_c, AG5_c, dt_c, \eta)}\right)^2$$

Given $\quad \eta := .04$

$SSE(\eta) = 0 \quad 1 = 1$

$\eta := Minerr(\eta)$ $\quad \frac{SSE(\eta)}{37-2} = 1.028\cdot 10^4$

$\eta = 0.086$

Calculate Richardson number **from above** $h := .086$ $d_o := \frac{2}{3}\cdot h$ $z_{om} := \frac{h}{8}$

$$RI_i := \left(\frac{9.8}{AG_{i,5} + 273}\right)\cdot\left(\left(-dt_i\right)\right)\cdot\frac{z - d_o}{\left(AG_{i,6}\cdot .44\right)^2}$$

$d_o = 0.057$ $z_{om} = 0.011$

$mean(RI) = -0.28$ $stdev(RI) = 0.176$

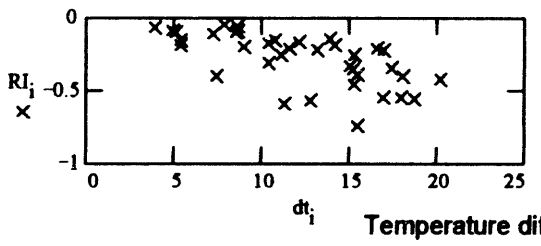

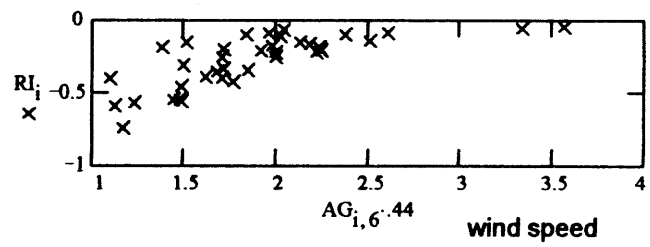

$A1_i := G\left(AG6_i, AG5_i, dt_i, \eta\right)$ $mean(A1) = 79.847$

modified similar to Kustas 1990 with added KB and fraction of available energy term
solve for gamma as part of the KB term and beta as an adjustment for available energy

$$F(AG6, AG8, RI, dt, \beta, \gamma) := \left[\left[\frac{\ln\left[\frac{(z - d_o)}{z_{om}}\right]}{k}\right]\cdot\left[\frac{\ln\left[\frac{(z - d_o)}{z_{om}}\right]}{k} + (\gamma\cdot(AG6\cdot .44)\cdot(dt))\right]\cdot\frac{\left[\frac{1 - 15\cdot RI}{\left[1 + 75\cdot k^2\cdot\frac{\left(\frac{z - d_o + z_{om}}{z_{om}}\right)^{.5}}{\ln\left(\frac{z - d_o + z_{om}}{z_{om}}\right)^2}\cdot((-RI))^{.5}\right]}\right]^{-1}}{AG6\cdot .44} - \beta\cdot AG8\right]$$

$h = 0.086$

$c := 0..36$

$$SSE(\beta,\gamma) := \sum_c \left(AG3_c - \frac{\rho \cdot C_p \cdot dt_c}{F(AG6_c, AG8_c, RI_c, dt_c, \beta, \gamma)} \right)^2$$

Initial guess

$\beta := .21$ $\gamma := 1.06$

Given

$SSE(\beta,\gamma) = 0$ $1 = 1$

$\begin{pmatrix} \beta \\ \gamma \end{pmatrix} := \text{Minerr}(\beta,\gamma)$ $\frac{SSE(\beta,\gamma)}{37-2} = 2.801 \cdot 10^3$ $\gamma = 0.516$

$\beta = 0.198$

$B1_i := F(AG6_i, AG8_i, RI_i, dt_i, \beta, \gamma)$

$\text{mean}(B1) = 81.802$

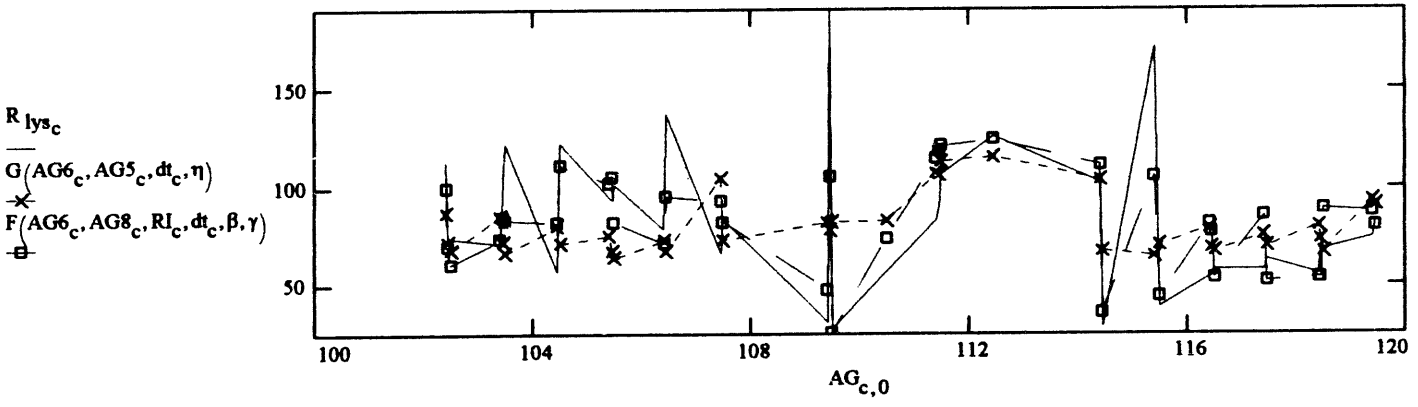

Sensible heat flux

as proposed by Moran et al.

$$H_{\eta_c} := \frac{\rho \cdot C_p \cdot (dt_c)}{G(AG6_c, AG5_c, dt_c, \eta)}$$

$\text{corr}(v, H_\eta) = 0.526$

with KB and fraction of availble energy

$$Hn_c := \frac{\rho \cdot C_p \cdot (dt_c)}{F(AG6_c, AG8_c, RI_c, dt_c, \beta, \gamma)}$$

$\text{corr}(v, Hn) = 0.889$

Sensible heat vector from source matrix AG

$v_i := AG_{i,10}$

$$H_{lys_i} := \frac{\rho \cdot C_p \cdot (dt_i)}{R_{lys_i}}$$ **Represents 1:1 line**

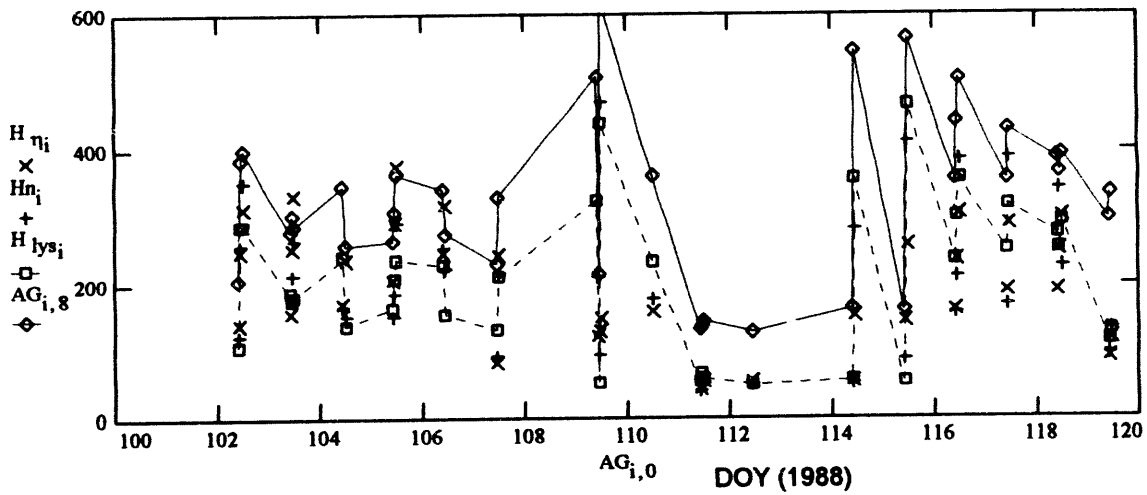

Equations to estimate sensible heat flux given air,wind speed, radiometric temperature, Rn,and Gt

$$HG(AG6, AG5, dt, \eta) := \frac{\rho \cdot C_p \cdot (dt)}{G(AG6, AG5, dt, \eta)}$$

$$Ri(Air, AG6, dt) := \left(\frac{9.8}{Air + 273}\right) \cdot ((-\alpha i)) \cdot \frac{z - d_o}{(AG6 \cdot .44)^2}$$

$$HF(AG6, AG8, RI, dt, \beta, \gamma) := \frac{\rho \cdot C_p \cdot (dt)}{F(AG6, AG8, RI, dt, \beta, \gamma)}$$

Array sd contains
Air,Wind speed,IR,Rn,Gt
at time of overflights
entered into array

Air,Wind speed,IR,Rn,Gt

$$sd := \begin{bmatrix} 16.33 & 2.3 & 38.42 & 517 & 136 & 0 & 0 & 0 & 0 \\ 22.82 & 3.55 & 48.25 & 450 & 113 & 0 & 0 & 0 & 0 \\ 26.89 & 4.5 & 46.29 & 473 & 120 & 0 & 0 & 0 & 0 \\ 26.01 & 3.9 & 51.47 & 452 & 165 & 0 & 0 & 0 & 0 \\ 27.25 & 6 & 49 & 468 & 182 & 0 & 0 & 0 & 0 \\ 22.32 & 5 & 44.14 & 506 & 61 & 0 & 0 & 0 & 0 \\ 26.63 & .6 & 45.5 & 547 & 81 & 0 & 0 & 0 & 0 \end{bmatrix}$$

$k := 0..6$

$$sd_{k,5} := F\left[sd_{k,1}, sd_{k,3} - sd_{k,4}, Ri\left[sd_{k,0}, sd_{k,1}, \left(sd_{k,2} - sd_{k,0}\right)\right], \left(sd_{k,2} - sd_{k,0}\right), \beta, \gamma\right]$$

$$sd_{k,6} := HF\left[sd_{k,1}, sd_{k,3} - sd_{k,4}, Ri\left[sd_{k,0}, sd_{k,1}, \left(sd_{k,2} - sd_{k,0}\right)\right], \left(sd_{k,2} - sd_{k,0}\right), 0, \gamma\right]$$

$$sd_{k,7} := G\left[sd_{k,1}, sd_{k,0}, \left(sd_{k,2} - sd_{k,0}\right), \eta\right]$$

$$sd_{k,8} := HG\left[sd_{k,1}, sd_{k,0}, \left(sd_{k,2} - sd_{k,0}\right), \eta\right]$$

$$sd = \begin{array}{c} \begin{array}{ccccccccc} Air & U & Ts & Rn & Gt & & & & \end{array} \\ \begin{bmatrix} 16.33 & 2.3 & 38.42 & 517 & 136 & 39.295 & 226.319 & 60.672 & 428.04 \\ 22.82 & 3.55 & 48.25 & 450 & 113 & 81.755 & 201.33 & 57.501 & 519.93 \\ 26.89 & 4.5 & 46.29 & 473 & 120 & 94.106 & 139.057 & 64.82 & 351.856 \\ 26.01 & 3.9 & 51.47 & 452 & 165 & 101.16 & 189.444 & 57.655 & 519.149 \\ 27.25 & 6 & 49 & 468 & 182 & 136.827 & 132.168 & 58.862 & 434.407 \\ 22.32 & 5 & 44.14 & 506 & 61 & 87.617 & 145.964 & 60.351 & 425.054 \\ 26.63 & 0.6 & 45.5 & 547 & 81 & -16.032 & 290.919 & 63.553 & 349.068 \end{bmatrix} \end{array}$$

8-May-86 294 AG

8-May-89 188 to 223 AG
1-Jun-89 274 to 300 AG

8-May-89 156 to 176 G300

1-Jun-89 NA G300

8-May-89 246 to 265 LS
1-Jun-89 236 to 258 LS

Data from file ag88le.prn

0 note 1/24/93	1 DAY	2 TIME	3 1CM	4 AIR TEMP	5 AIR min	6 U 2m	7 IR	8 Avail	9 E	10 H
1 102.42	102	1000	26.63	17.40	13.65	3.39	20.99	206.55	98.41	108.14
2 102.46	102	1100	32.01	20.66	16.35	3.81	31.04	385.19	98.41	286.78
3 102.50	102	1200	35.00	22.58	17.58	3.36	36.20	398.72	112.47	286.25
4 103.42	103	1000	28.49	19.90	15.41	2.56	24.68	277.71	91.38	186.32
5 103.46	103	1100	34.23	22.37	17.36	3.69	31.22	301.69	126.53	175.16
6 103.50	103	1200	37.76	23.70	17.92	3.37	35.34	286.23	105.43	180.80
7 104.46	104	1100	28.95	21.68	18.17	4.36	30.61	344.58	105.44	239.14
8 104.50	104	1200	34.16	23.10	19.79	5.08	33.82	256.47	119.50	136.97
9 105.42	105	1000	32.17	19.87	16.82	4.53	27.53	262.80	98.41	164.39
10 105.46	105	1100	35.68	20.91	17.75	5.10	32.78	307.35	98.41	208.95
11 105.50	105	1200	39.28	22.55	18.61	4.02	38.33	362.26	126.54	235.73
12 106.42	106	1000	33.52	20.58	15.98	3.37	28.65	341.24	112.47	228.77
13 106.46	106	1100	38.03	21.47	17.42	3.88	32.54	274.24	119.50	154.74
14 106.50	106	1200	39.92	24.18	18.85	2.78	39.91	414.78	98.41	316.37
15 107.46	107	1100	23.38	19.54	16.18	2.49	23.78	230.27	98.41	131.86
16 107.50	107	1200	32.93	22.34	18.07	3.90	33.23	329.84	119.50	210.33
17 109.42	109	1000	22.94	15.57	12.06	5.40	17.96	507.24	182.77	324.47
18 109.46	109	1100	23.55	15.82	12.47	5.93	18.31	215.00	161.68	53.32
19 109.50	109	1200	25.49	16.61	13.94	4.50	23.02	623.12	182.77	440.35
20 110.50	110	1200	25.81	17.88	14.35	3.88	25.14	359.32	126.53	232.79
21 111.42	111	1000	18.08	16.56	13.97	4.64	17.69	133.10	77.33	55.77
22 111.46	111	1100	19.77	17.18	14.44	4.18	19.31	137.42	70.29	67.12
23 111.50	111	1200	20.51	17.69	14.90	3.43	19.94	143.61	84.35	59.26
24 112.46	112	1100	17.68	13.80	11.64	3.14	16.17	127.39	77.32	50.07
25 114.42	114	1000	16.08	13.51	10.93	4.45	15.59	162.21	105.44	56.76
26 114.46	114	1100	22.69	15.68	13.03	7.59	20.46	545.04	189.80	355.24
27 115.42	115	1000	20.85	11.12	9.03	8.10	12.49	159.71	105.44	54.27
28 115.46	115	1100	20.29	11.98	10.30	4.69	19.29	471.82	84.35	387.47
29 115.50	115	1200	26.13	13.76	11.11	4.53	26.62	563.12	98.41	464.71
30 116.42	116	1000	24.57	13.34	10.08	4.84	16.66	355.63	119.49	236.14
31 116.46	116	1100	28.30	14.78	11.51	5.69	22.04	441.33	140.59	300.74
32 116.50	116	1200	31.44	15.88	12.33	4.20	27.79	503.80	147.62	356.18
33 117.42	117	1000	28.58	15.01	12.32	4.97	19.83	354.02	105.44	248.58
34 117.46	117	1100	32.59	17.17	13.08	3.28	27.04	429.88	112.48	317.40
35 117.50	117	1200	35.40	18.88	14.74	2.39	32.63	466.54	105.44	361.10
36 118.42	118	1000	29.54	17.76	13.89	2.79	23.47	385.36	112.47	272.89
37 118.46	118	1100	33.02	19.31	15.31	2.66	28.16	364.60	112.48	252.12
38 118.50	118	1200	35.03	20.85	16.78	5.04	32.19	392.19	98.41	293.78
39 119.42	119	1000	24.22	17.49	14.87	4.60	19.62	297.03	182.78	114.25
40 119.46	119	1100	27.08	19.53	16.17	3.91	23.04	332.52	203.86	128.66

Appendix D

Calculations of Aerodynamic Resistance for Sagebrush in 1988

The following material is a printout of a Mathcad program. No editing or formatting has been done.

Appendix D Calculations of resistance (ra) for sagebrush 1988

This Mathcad program calibrates a sensible heat transport equation to an Alesage 1988 data set

Constants

$\rho = 1.164$ $C_p = 1010$ $i = 0..59$ $k := .4$ $z := 2$

calculation tolerance

$TOL := .00001$

Read in data

$AS := READPRN(as88comp)$

Array labels data printed at end of this appendix

0 Daytime
1 Day
2 Time
3 Temp soil 1 cm
4 Air temperature shelter
5 Dry Bulb aspirated pyschrometer
6 2 meter wind speed
7 Infrared thermometer
8 Available energy (Rn-Gt)
9 ,10,11 not used
12 Lysimeter measured latent heat flux
13 Available energy - latent heat flux (lys) - Gt
14 not used

Estimate an appropriate surface radiometric temperature by compositing 1 cm soil and IR thermometer

$TC1_i := AS_{i,3}$ 1 cm Soil

$IR_i := AS_{i,7}$ Everrest IR

$dt_i := \left[\left(AS_{i,3}\cdot 1 + AS_{i,7}\cdot .12\right) - \left(AS_{i,5}\right)\right]$

$mean(IR) = 15.576$

$mean(TC1) = 23.963$

$mean(dt) = 10.41$

Solve for resistance from measured temperatures and H=Rn-G-E with E from lysimeters

$R_{lys.a_i} := \frac{(dt_i)\cdot\rho\cdot C_p}{AS_{i,13}}$

$mean(R_{lys.a}) = 67.84$

Assign vectors from array AS

$AS6_i := AS_{i,6}$ $AS8_i := AS_{i,8}$

$x_i := dt_i$ $AS5_i := AS_{i,5}$ $AS3_i := AS_{i,13}$

Method used by Moran et al. 1989 in alfalfa, wheat and cotton at Maricopa Ag. Cen. Phoenix, Az.

This equation is solved for η which represents canopy height

$$G(AS6, AS5, dt, \eta) := \left[\left[\frac{\ln\left[\frac{\left(z-\eta\cdot\frac{2}{3}\right)}{\left(\frac{\eta}{8}\right)}\right]}{k}\right]\cdot\left[\frac{\ln\left[\frac{\left(z-\eta\cdot\frac{2}{3}\right)}{\left(\frac{\eta}{8}\right)}\right]}{k}\right]\cdot\left[\frac{1-15\cdot\left[\left(\frac{9.8}{AS5+273}\right)\cdot((-dt))\cdot\frac{z-\eta\cdot\frac{2}{3}}{(AS6\cdot.44)^2}\right]}{\left[1+75\cdot k^2\cdot\frac{\left[\frac{z-\eta\cdot\frac{2}{3}+\frac{\eta}{8}}{\left(\frac{\eta}{8}\right)}\right]^5}{\ln\left[\frac{z-\eta\cdot\frac{2}{3}+\frac{\eta}{8}}{\left(\frac{\eta}{8}\right)}\right]^2}\cdot\left[\left[-\left[\left(\frac{9.8}{AS5+273}\right)\cdot((-dt))\cdot\frac{z-\eta\cdot\frac{2}{3}}{(AS6\cdot.44)^2}\right]\right]\right]^5\right]}{AS6\cdot.44}\right]^{-1}\right]$$

$n := \text{length}(AS6) - 1$

$n = 59$

$c := 0..n$

$$SSE(\eta) := \sum_c \left(AS3_c - \frac{\rho\cdot C_p\cdot dt_c}{G(AS6_c, AS5_c, dt_c, \eta)}\right)^2$$

Initial guess

$\eta := 1.06$

Given

$SSE(\eta) = 0 \qquad 1 = 1$

$\eta := \text{Minerr}(\eta)$

$$\frac{SSE(\eta)}{n-2} = 2.609\cdot 10^3$$

$\eta = 0.122$ **canopy height**

$h := .122$

$d_o := \frac{2}{3}\cdot h \qquad z_{om} := \frac{h}{8}$

$d_o = 0.081 \qquad z_{om} = 0.015$

Calculate Richardson number for next equation

$$RI_i := \left(\frac{9.8}{AS_{i,5}+273}\right)\cdot((-dt_i))\cdot\frac{z-d_o}{(AS_{i,6}\cdot.44)^2}$$

$\text{mean}(RI) = -0.29 \qquad \text{stdev}(RI) = 0.202$

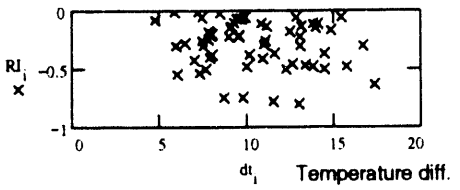

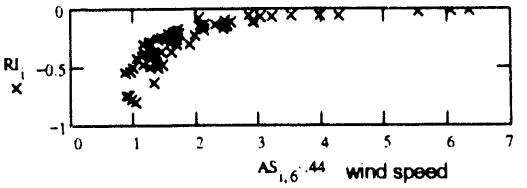

Equation modified similar to Kustas 1990 with added KB = $(\gamma\cdot(AS6\cdot.44)\cdot(dt))$
also a term Γ
to adjust the resistance
in responce to the available energy

$$F(AS6, AS8, RI, dt, \beta, \gamma) := \left[\frac{\ln\left[\frac{(z-d_o)}{z_{om}}\right]}{k}\right]\cdot\left[\frac{\ln\left[\frac{(z-d_o)}{z_{om}}\right]}{k} + (\gamma\cdot(AS6\cdot.44)\cdot(dt))\right]\cdot\frac{\left[\frac{1-15\cdot RI}{1+75\cdot k^2\cdot\frac{\left[\frac{z-\eta\cdot\frac{2}{3}+\frac{\eta}{8}}{\left(\frac{\eta}{8}\right)}\right]^5}{\ln\left[\frac{z-\eta\cdot\frac{2}{3}+\frac{\eta}{8}}{\left(\frac{\eta}{8}\right)}\right]^2}\cdot((-RI))^5}\right]^1}{AS6\cdot.44} - \beta\cdot AS8$$

$c := 0..n$

$$SSE(\beta,\gamma) := \sum_c\left(AS3_c - \frac{\rho\cdot C_p\cdot dt_c}{F(AS6_c, AS8_c, RI_c, dt_c, \beta, \gamma)}\right)^2$$

Initial guess

$\beta := .01$ $\gamma := .17$

Given

$SSE(\beta,\gamma) = 0$ $1 = 1$

$$\begin{pmatrix}\beta\\ \gamma\end{pmatrix} := Minerr(\beta,\gamma)$$

$\gamma = 0.117$ $\frac{SSE(\beta,\gamma)}{n-2} = 2.135\cdot 10^3$

$\beta = 0.041$

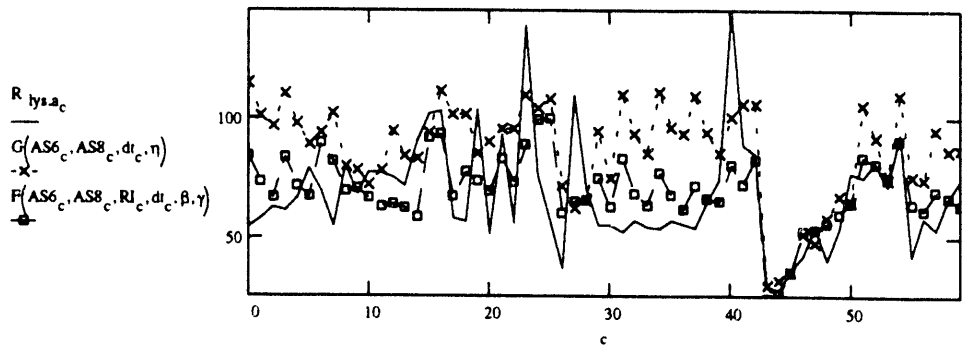

$$H_{lys_i} := \frac{\rho \cdot C_p \cdot (dt_i)}{R_{lys.a_i}}$$

$$H_{\eta_c} := \frac{\rho \cdot C_p \cdot (dt_c)}{G(AS6_c, AS5_c, dt_c, \eta)}$$

solved for canopy height

$$Hn_c := \frac{\rho \cdot C_p \cdot (dt_c)}{F(AS6_c, AS8_c, RI_c, dt_c, \beta, \gamma)}$$

with KB and fraction of availble energy

Sensible heat vector from source matrix AS

$$v_i := AS_{i,13}$$

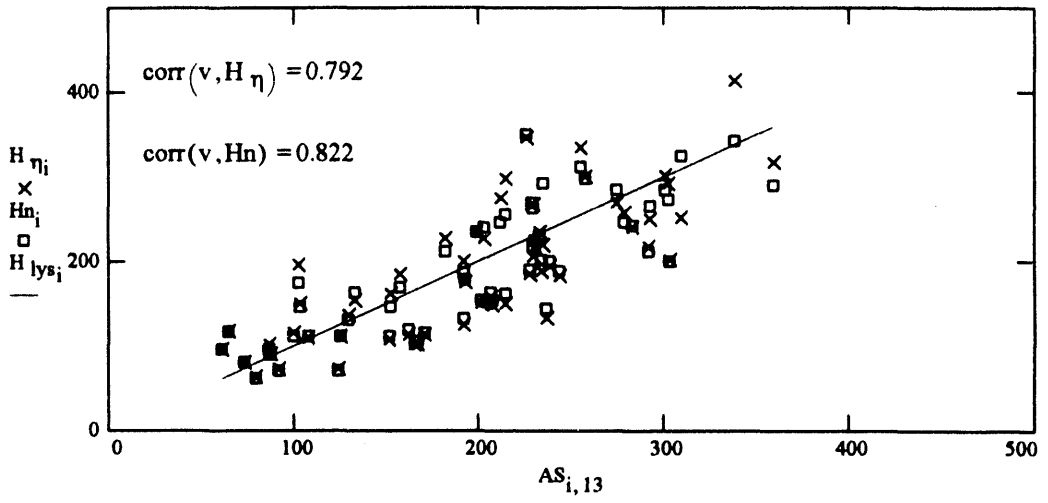

Equations to estimate sensible heat flux given air,wind speed, radiometric temperature, Rn,and Gt

$$HF(AS6, AS8, RI, dt, \beta, \gamma) := \frac{\rho \cdot C_p \cdot (dt)}{F(AS6, AS8, RI, dt, \beta, \gamma)}$$

$$RI_i := \left(\frac{9.8}{AS_{i,5} + 273}\right) \cdot ((-dt_i)) \cdot \frac{z - d_o}{(AS_{i,6} \cdot .44)^2}$$

$$Ri(Air, AS6, dt) := \left(\frac{9.8}{Air + 273}\right) \cdot ((-dt)) \cdot \frac{z - d_o}{(AS6 \cdot .44)^2}$$

Air,Wind speed,IR,Rn,Gt from on site data during satellite overflights

$$sd = \begin{pmatrix} 16.91 & 2.5 & 36.9 & 556 & 135 & 0 & 0 \\ 23.02 & 2.6 & 45.8 & 486 & 190 & 0 & 0 \\ 26.6 & 3.8 & 45.17 & 497 & 197 & 0 & 0 \end{pmatrix}$$

Equation using U,Air temperature, Surface - Air temperature, estimated plant height

$$HG(AS6, AS5, dt, \eta) := \frac{\rho \cdot C_p \cdot (dt)}{G(AS6, AS5, dt, \eta)}$$

$k := 0..2$ Apply both sensible heat flux equations to array containing observations at time of satellite overflights

$$sd_{k,5} := HF\left[sd_{k,1} \cdot .44, sd_{k,0}, Ri\left[sd_{k,0}, sd_{k,1}, (sd_{k,2} - sd_{k,0})\right], (sd_{k,2} - sd_{k,0}), \beta, \gamma\right]$$

$$sd_{k,6} := HG\left[sd_{k,1} \cdot .44, sd_{k,0}, (sd_{k,2} - sd_{k,0}), \eta\right]$$

Pedicted Measured

$$sd = \begin{pmatrix} 16.91 & 2.5 & 36.9 & 556 & 135 & 175.449 & 449.792 \\ 23.02 & 2.6 & 45.8 & 486 & 190 & 208.466 & 541.875 \\ 26.6 & 3.8 & 45.17 & 497 & 197 & 150.352 & 387.504 \end{pmatrix}$$

Alesage 8-May-86 372
Alesage 8-May-89 174 to 213
Alesage 1-Jun-89 228 to 247

Sensitivity analysis for a 10 percent error in each component individually and combined

$HF(2, 40, Ri(40, 2, 10), 10, 0, \gamma) = 135.753 \ \frac{W}{m^2}$

$Baseline := HF(2, 40, Ri(40, 2, 10), 10, 0, \gamma)$

$Baseline = 135.753$

increment windspeed

$HF(2 + 2 \cdot .1, 40, Ri(40, 2, 10), 10, 0, \gamma) - Baseline = 12.413$

increment the difference between air and surface temperature

$HF(2, 40, Ri(40, 2, 10 + 10 \cdot .1), 10 + 10 \cdot .1, 0, \gamma) - Baseline = 19.718$

increment air temperature

$HF(2, 40 + 40 \cdot .1, Ri(40 + 40 \cdot .1, 2, 10), 10, 0, \gamma) - Baseline = -0.864$

decrement canopy height

$HF(2, 40, Ri(40, 2, 10), 10, 0, \gamma + \gamma \cdot .1) - Baseline = -1.057$

increment all terms by 10 percent

$HF(2 + 2 \cdot .1, 40 + 40 \cdot .1, Ri(40 + 40 \cdot .1, 2 + 2 \cdot .1, 10 + 10 \cdot .1), 10 + 10 \cdot .1, 0, \gamma + \gamma \cdot .1) - Baseline = 15.917$

Data from file as88comp.prn

0	1 Time Day	2 Day	3 Hour	4 1 cm soil	5 Air shelt	6 Air psychr	7 U 2 m	8 IR	9 Avail W/m2	10 Ri	11 N/A	12 N/A	13 E W/m2	14 H W/m2	15 ra obs
1	102.42	102.00	1000	21.46	17.25	15.72	2.26	15.55	243.06	-0.04	0.06	0.19	77.07	165.99	29.88
2	102.46	102.00	1100	26.48	20.24	18.61	3.01	18.86	304.70	-0.03	0.04	0.15	98.09	206.61	35.53
3	102.50	102.00	1200	30.21	22.37	20.51	2.83	21.16	328.31	-0.04	0.07	0.21	98.09	230.22	40.02
4	103.42	103.00	1000	24.43	20.90	18.79	2.57	18.52	242.81	-0.02	0.03	0.12	91.08	151.73	27.40
5	103.46	103.00	1100	29.24	22.98	20.83	2.96	20.87	291.49	-0.03	0.04	0.16	98.09	193.40	38.04
6	103.50	103.00	1200	32.89	24.29	22.28	3.07	22.38	282.78	-0.04	0.06	0.20	84.07	198.70	50.92
7	104.42	104.00	1000	22.47	20.70	20.02	4.64	18.84	150.01	-0.00	0.00	0.01	70.06	79.95	25.92
8	104.46	104.00	1100	26.57	22.59	21.16	3.52	21.05	262.41	-0.01	0.01	0.07	91.08	171.33	27.36
9	104.50	104.00	1200	32.56	24.84	22.86	4.83	22.75	294.88	-0.01	0.01	0.07	112.10	182.78	49.68
10	105.42	105.00	1000	28.21	21.37	19.36	5.23	18.69	275.94	-0.01	0.01	0.05	84.07	191.87	41.93
11	105.46	105.00	1100	31.75	22.13	20.25	5.61	20.14	310.15	-0.01	0.01	0.06	98.09	212.07	53.31
12	105.50	105.00	1200	35.81	24.24	21.87	4.29	22.56	332.22	-0.03	0.04	0.13	77.07	255.15	53.34
13	106.42	106.00	1000	28.59	20.09	17.86	2.33	18.88	302.02	-0.07	0.12	0.33	98.09	203.94	49.05
14	106.46	106.00	1100	33.34	22.16	20.14	3.30	20.66	314.06	-0.04	0.07	0.22	56.05	258.01	50.95
15	106.50	106.00	1200	36.63	24.26	22.12	2.99	23.31	331.66	-0.06	0.10	0.29	105.09	226.57	64.16
16	107.42	107.00	1000	22.56	18.54	17.01	2.87	16.18	72.85	-0.02	0.03	0.11	-14.01	86.86	54.43
17	107.46	107.00	1100	22.69	19.40	18.44	2.81	18.30	178.90	-0.02	0.02	0.09	105.09	73.81	52.36
18	107.50	107.00	1200	29.66	23.24	20.85	2.22	22.46	318.51	-0.06	0.10	0.28	84.07	234.44	32.17
19	109.42	109.00	1000	19.72	14.82	13.53	3.87	13.30	330.63	-0.01	0.01	0.07	168.15	162.48	35.44
20	109.46	109.00	1100	21.97	15.58	14.53	4.80	13.98	278.75	-0.01	0.01	0.06	175.15	103.59	72.56
21	109.50	109.00	1200	22.85	16.96	15.69	4.68	15.79	397.19	-0.01	0.01	0.06	189.17	208.02	33.32
22	110.46	110.00	1100	21.04	16.50	14.91	3.78	14.65	197.80	-0.01	0.01	0.07	98.09	99.71	53.56
23	110.50	110.00	1200	23.99	18.40	16.49	3.91	17.09	320.63	-0.02	0.02	0.08	119.10	201.53	32.61
24	112.50	112.00	1200	19.26	15.25	13.68	2.14	13.90	166.56	-0.04	0.06	0.20	105.09	61.47	76.66
25	113.46	113.00	1100	13.87	9.58	8.96	2.63	8.70	71.18	-0.03	0.04	0.14	-21.02	92.20	54.73
26	113.50	113.00	1200	14.18	9.80	9.24	1.95	8.84	75.44	-0.05	0.09	0.26	-49.04	124.48	41.39
27	114.46	114.00	1100	20.00	15.76	14.43	6.45	15.14	447.25	-0.00	0.00	0.02	210.19	237.06	21.05
28	114.50	114.00	1200	22.40	15.53	14.43	7.28	13.52	243.12	-0.01	0.00	0.02	140.12	103.00	78.50
29	115.42	115.00	1000	18.54	11.48	10.37	6.89	10.07	262.58	-0.01	0.00	0.03	105.09	157.49	52.74
30	115.46	115.00	1100	19.35	12.53	11.19	3.80	11.80	274.71	-0.02	0.03	0.11	70.06	204.65	39.20
31	115.50	115.00	1200	24.16	14.43	12.71	5.66	13.59	391.08	-0.01	0.01	0.06	112.10	278.98	41.00
32	116.42	116.00	1000	16.26	11.81	10.15	3.13	10.74	272.21	-0.02	0.02	0.10	105.09	167.12	31.31
33	116.46	116.00	1100	21.12	13.24	11.54	3.86	11.97	347.03	-0.02	0.03	0.12	119.10	227.92	40.65
34	116.50	116.00	1200	24.93	14.67	13.55	4.49	13.55	395.14	-0.02	0.03	0.11	112.10	283.04	42.62
35	117.42	117.00	1000	18.48	13.93	11.21	2.01	11.95	261.84	-0.05	0.08	0.25	70.06	191.78	27.87
36	117.46	117.00	1100	23.21	15.99	13.34	3.29	13.87	336.64	-0.03	0.04	0.15	98.09	238.56	35.61
37	117.50	117.00	1200	27.17	17.44	15.30	3.11	15.92	376.79	-0.04	0.07	0.22	84.07	292.71	39.10
38	118.42	118.00	1000	23.88	18.66	16.10	2.11	16.97	312.85	-0.05	0.09	0.26	98.09	214.77	28.61
39	118.46	118.00	1100	28.25	20.29	17.83	3.05	18.12	329.05	-0.04	0.06	0.19	98.09	230.96	40.53
40	118.50	118.00	1200	31.06	21.11	18.95	3.64	19.23	313.96	-0.03	0.05	0.16	84.07	229.89	50.89
41	119.42	119.00	1000	22.58	17.94	16.51	3.69	16.08	268.12	-0.02	0.02	0.07	203.18	64.94	84.14
42	119.46	119.00	1100	25.83	20.30	18.01	2.64	18.26	322.17	-0.03	0.05	0.18	189.17	133.00	48.91
43	119.50	119.00	1200	25.10	20.85	19.59	3.25	18.95	262.34	-0.02	0.02	0.09	154.14	108.21	46.17
44	120.42	120.00	1000	17.64	13.75	13.18	14.40	11.90	466.26	-0.00	0.00	0.00	231.20	235.05	19.42
45	120.46	120.00	1100	19.76	14.81	14.20	13.76	13.29	519.78	-0.00	0.00	0.00	210.19	309.60	18.80
46	120.50	120.00	1200	21.44	15.46	14.69	12.57	13.86	450.15	-0.00	0.00	0.00	175.15	274.99	25.56
47	121.46	121.00	1100	23.40	13.10	12.02	9.02	12.22	457.62	-0.01	0.00	0.02	98.09	359.54	33.69

VITA

Randy Kirkham was born on November 24, 1952 in Yakima, Washington. His degrees in Environmental Science BS (1976) and Soil Science MS (1979) were obtained from Washington State University. Mr. Kirkham has worked as a scientist at Pacific Northwest Laboratory in Richland, Washington, since 1980. He has participated in hydrologic and atmospheric studies related to hazardous waste isolation and global climate warming. Mr. Kirkham holds a patent for a fiber optic moisture sensor and shares a patent for a optical oil/water sensor. The optical oil/water sensor has been further recognized by the receipt of an R&D 100 award (1991) from R&D Magazine for developing one of the 100 most significant technical products of the year and a technology transfer award from the Federal Laboratory Consortion.

Distribution

OFFSITE

2 DOE/Office of Scientific and Technical Information

J. B. Adams
University of Washington
College of Geological Sciences
Seattle, WA 98105

F. Barnes
Los Alamos National Laboratory
P.O. Box 1663
Los Alamos, NM 87545

G. S. Campbell
Washington State University
Pullman, WA 99164

T. L. Jones
New Mexico State University
Agricultural Experiment Station
Box 3BF
Las Cruces, NM 88003

S. Tomlinson
U.S. Geological Survey
1201 Pacific Ave., Suite 600
Tacoma, WA 98402

S. W. Tyler
Desert Research Institute
P.O. Box 60220
Reno, NV 89506

4 University of Washington
College of Forestry, AR-10
Seattle, WA 98105
Attn: T. W. Cundy
L. J. Fritschen
F. E. Greulich
P. Schiess

ONSITE

DOE Richland Operations Office

R. K. Stewart	A5-19

7 Westinghouse Hanford Company

D. S. Landeen	H4-14
M. J. Lauterbach	H6-01
H. E. McGuire	B3-63
M. R. Sackschewsky	H4-14
J. C. Sonnichsen	H4-14
J. A. Voogd	R4-03
N. R. Wing	H4-14

31 Pacific Northwest Laboratory

D. E. Beaver	K6-84
L. L. Cadwell	P7-54
M. D. Campbell	K6-77
J. C. Doran	K6-11
J. L. Downs	P7-54
M. J. Fayer	K6-77
M. G. Foley	K6-84
G. W. Gee	K6-77
M. J. Graham	K6-78
J. M. Hubbe	K6-11
R. R. Kirkham (5)	K6-77
S. O. Link	P7-54
K. L. Manke	K6-86
E. M. Perry	K6-84
G. M. Petrie	K6-84
L. E. Rogers	P7-54
W. J. Shaw	K6-11
C. D. Whiteman	K6-11
M. S. Wigmosta	K6-77
G. E. Wukelic	K6-84
Publishing Coordination	
Technical Report Files (5)	

Routing

R. M. Ecker
M. J. Graham
D. M. Irving
C. S. Sloane
P. C. Hays (last)

DATE
FILMED
4/19/94

END